UNIVERSITY OF CALIFORNIA
SANTA CRUZ

THE DESIGN, CONSTURCTION, AND EVALUATION OF CRUX: A TENSEGRITY-INSPIRED COMPLIANT ROBOTIC UPPER-EXTREMITY EXOSUIT

A dissertation submitted in partial satisfaction
of the requirements for the degree of

DOCTOR OF PHILOSOPHY

in

COMPUTER ENGINEERING
with an emphasis in ROBOTICS AND CONTROL

by

Steven R. Lessard

September 2018

The Dissertation of Steven R. Lessard is approved:

_____
Professor Mircea Teodorescu, chair

_____
Professor Sri Kurniawan

_____
Professor Patrick E. Mantey

_____
Adrian Agogino, Ph.D.

_____
Lori Kletzer
Vice Provost and Dean of Graduate Studies

Table of Contents

List of Figures

List of Tables

Abstract

THE DESIGN, CONSTRUCTION, AND EVALUATION OF CRUX: A TENSEGRITY-INSPIRED COMPLIANT ROBOTIC UPPER-EXTREMITY EXOSUIT

Steven R Lessard

Stroke is a disease that directly affects millions of people each year globally. Stroke therapy is challenging; survivors of the disease often must complete challenging exercises in the hopes of regaining some of their lost mobility and flexibility. Due to the limitations of visiting expert physical therapists and completing impactful rehabilitation outside of their therapist's office, this rehabilitation infrequently completely restores a survivor's quality of life to what it was pre-stroke. One potential solution to this issue is an augmentative exosuit. Exosuits, unlike other traditional exoskeletons, are primarily composed of soft materials and feature flexibility and compliance at a structural level. In this thesis, we describe the inspiration, research, design, implementation, and user testing of one such exosuit for the upper-extremities, CRUX. This exosuit exemplifies the paradigms of tensegrity robotics through its use of a novel hybrid soft-rigid structure to augment the upper-extremities of those who wear it. The design of CRUX emphasizes a harmonious human-robot interface that augments users sufficiently for potential applications in Graded Motor Imagery and mirror therapy. As a result, CRUX may be able to assist physical therapists in providing stroke survivors and other people with upper-extremity impairment with better rehabilitation.

Acknowledgments

Thank you to my co-authors and colleagues, who have helped me produce, correct, and re-correct numerous experiments, calculations, and papers. Thank you to my committee, Prof. Sri Kurniawan, Prof. Patrick Mantey, and Adrian Agogino, PhD who have taken the time to review my thesis and provide corrections and advice. Thank you to my advisor, Prof. Mircea Teodorescu who has taught me a lot in 4 years, least of all how to be an excellent researcher. Lastly, thank you to my wonderful family, including my sister Kate, my brother Joe, my sister-in-law to be Amelia, my mother Jennifer, and my father Philip. None of this would have been possible without their help and for that reason among many others, I love you guys so much. Thank you everyone.

Chapter 1

INTRODUCTION

1.1 Motivation

A core challenge of human exosuit design is creating an apparatus that promotes and augments human motion - a very unnatural accomplishment - while maintaining an intuitive and natural interface with the user. To combat this paradox, many researchers have employed idioms derived directly from biology. This bio-inspiration has led to the discovery of novel technologies that not only enhance the scientific field's understanding of the mechanisms that provide the foundation for our own bodies, but also how those techniques can be applied to modern engineering problems.

The application of these techniques, however, is itself a difficult problem. Biological joints and limbs exhibit a strange hybrid of soft and rigid materials which yield a body that functions at times unpredictably yet efficiently. Replicating the observed success of human joints and limbs, even partially, can improve the field of robotics and solve problems related to human augmentation.

Solving these problems and creating a better human exosuit has enormous implications for many industries, including medicine, physical therapy, military, and industrial work. Exoskeletons and exosuits can promote ergonomic movement, which can rehabilitate people with disabilities and prevent accidents and strains. In addition, scenarios which require greater strength and endurance from the user, such

as carrying a load for extended periods of time, could also be solved through an augmentative exosuit.

1.2 Goals

The goals of my dissertation are the following:

1. **Understand how bio-inspiration can yield new designs for structurally compliant, flexible, and lightweight robots**

   Tensegrity robots, particularly manipulators, demonstrate structural properties that give them attributes similar to their biological counterparts. Understanding these attributes (compliance, flexibility, and low-weight) can elucidate how to fundamentally design wearable robots to harmonize with the human body better.

2. **Build an upper-limb structurally compliant exosuit**

   The construction of an upper-limb exosuit should exemplify compliance inherently at the structural level, creating a user-interface which simultaneously augments the user's actions while not significantly interfering with the user's workspace. This task requires a novel design for conforming the entire robot to the morphology and function of the human body such that the robot maintains a steady position throughout usage.

3. **Test the exosuit on relevant demographics, record the efficacy of the exosuit, and identify trends**

   The constructed exosuit should prove capable of augmenting people who are physically impaired. Specifically, the exosuit should follow instruction according to a physical therapist or a practiced physical therapy technique, such as mirror therapy. The efficacy of the exosuit can be determined by measuring the ability of the exosuit's controller to follow these instructions,the exosuit's ability to flex and remain compliant, and the ability of the exosuit to augment the user and decrease metabolic impact. These tests should be repeated multiple times on impaired users and unimpaired users both in a lab and in the field to understand the impact of the new technology.

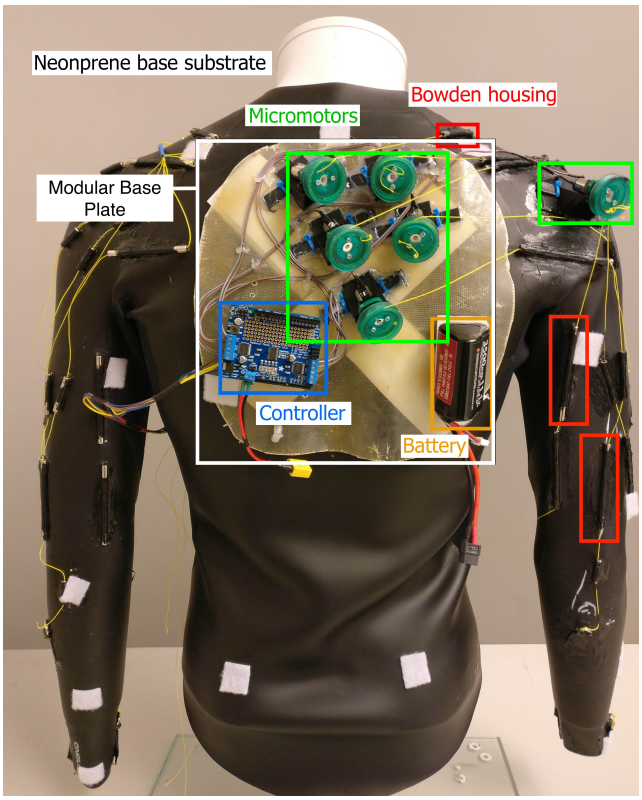

Figure 1.1: CRUX: a soft, lightweight ($1.3kg$), flexible, robotic exosuit for upper-extremity augmentation. This exosuit was designed for the purpose of assisting patients undergoing physical therapy.

Chapter 2

LITERATURE REVIEW

2.1 Human Anatomy and Physiology

2.1.1 Musculoskeletal System

The human body can be described as a hybrid soft-rigid organization, comprised of multiple distinct systems of varying mechanical and morphological properties. The structure of the human body is principally defined by the relatively rigid skeletal system. The bones that assemble this skeletal system are nestled amongst a network of different types of fibrous tissue. One of these types of fibrous tissue is muscular tissue. Muscles are responsible for moving the body itself. When muscles contract, they create a tensile force that pulls on a part of the body to move that region. The combination of many muscles contracting creates complex movement. A consequence of this complex movement is the equally complex morphology of not just the muscles on the macro scale, but of the muscles fibers which constitute the overall muscles as well [1, 2]. This movement can be characterized by the range of motion or workspace of the individual as well as the redundancy of their movement within that full workspace. This redundant movement results in a dexterous workspace which is a subset of the total reachable workspace of the human. Humans who are more flexible therefore have larger workspaces, both dexterous and reachable.

At the center of this force generation in skeletal muscle activity are antagonistic pairs. An antagonistic pair is two coupled muscles or muscle groups, one agonist

and its relative antagonist. These muscles or muscle groups pull opposite to one other. When an agonist muscle contracts and shortens, its corresponding antagonistic muscle lengthens inversely proportionally. This phenomenon can be quantified by examining the net torque produced by the muscles about the joint that they share. Agonist and antagonist muscles regulate this torque together with respect to gravity such that the joint as a whole is stabilized in the reference frame of the body [3]. The end result of this cooperation is antagonistic muscle pairs working at a linear rate despite the non-linear properties inherent to the muscles themselves [4].

Bio-mechanical Simulation

Some software has extended these principles and allowed programmers to simulate the complex kinematics and dynamics of the human body [5]. AnimatLab, one example of such a simulator, operates by modeling Hill's muscle model [6]. Hill's muscle model uses a function to describe skeletal muscle state with regards to kinematics, tension, and thermodynamics (Equations 2.1 and 2.2).

$$(v + b)(F + a) = b(F_0 + a) \tag{2.1}$$

$$b = \frac{a \cdot v_0}{F_0} \tag{2.2}$$

In this equation, F is the tension force exerted by the muscle, F_0 is the maximum generated tension force by that muscle, v is the velocity of contraction, v_0 is the maximum contraction velocity of the muscle (i.e. when $F = 0$), and a is the coefficient of shortening heat. b is the relationship between the maximum tension force and velocity due to added heat in the muscle. One important conclusion derived from these equations is that F is inversely proportional to v. This theory matches empirical results obtained near muscle-resting length [6]. Because of this, one can solve for tension force knowing the velocity (or vice-versa) if they also know the shortening heat coefficient.

Other bio-mechanics simulators include OpenSim, a Stanford based open-source

project [7]. This simulator excels in providing real-time analysis of any chosen musculo-skeletal component in the human body and additionally illustrating the simulated phenomenon in 3D (Figure 2.1).

OpenSim Simulation

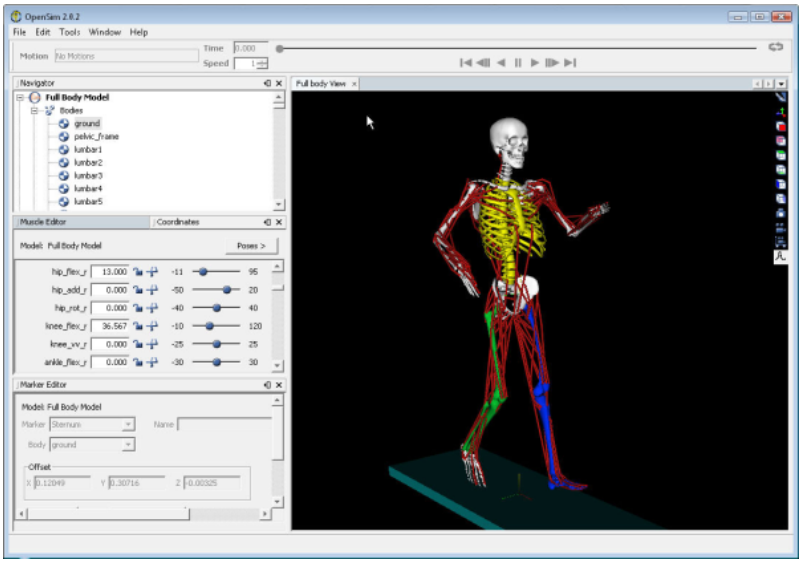

Figure 2.1: An example of an OpenSim program running. An OpenSim programmer can control the musculoskeletal system of a human body and analyze its kinematics and dynamics in real time.

The harmony between muscular tissue, especially in antagonistic pairs found in the upper-extremity, allows humans fine motor control of their complicated bodies.

2.1.2 Connective Tissue

The active role played by muscles is not the only fibrous tissue function in the human body however. Both the skeletal and muscular systems are linked via connective tissue, like cartilage, ligaments, tendons, and fascia. This connective tissue serves as an elastic medium to cushion external stresses applied to the body as a whole. The compliance afforded by the connective tissue allows humans to resist and absorb impacts that would otherwise damage their body. This passive role in the human body contrasts with the active role of the muscles, demonstrating the necessity of both types of tension-based elements in the human body. Without either, the human body would be neither controllable nor structurally compliant and flexible.

Human motion can be further characterized by the constraints regarding the

integumentary system. The primary organ of this system, the skin, acts as an enveloping tension member that serves as both a protector and a foundation for the rest of the human body. All human organs and processes are housed partially, if not entirely, within this system. Although the skin is flexible and elastic, there exist lines along the body which do not change in length as the body moves normally.

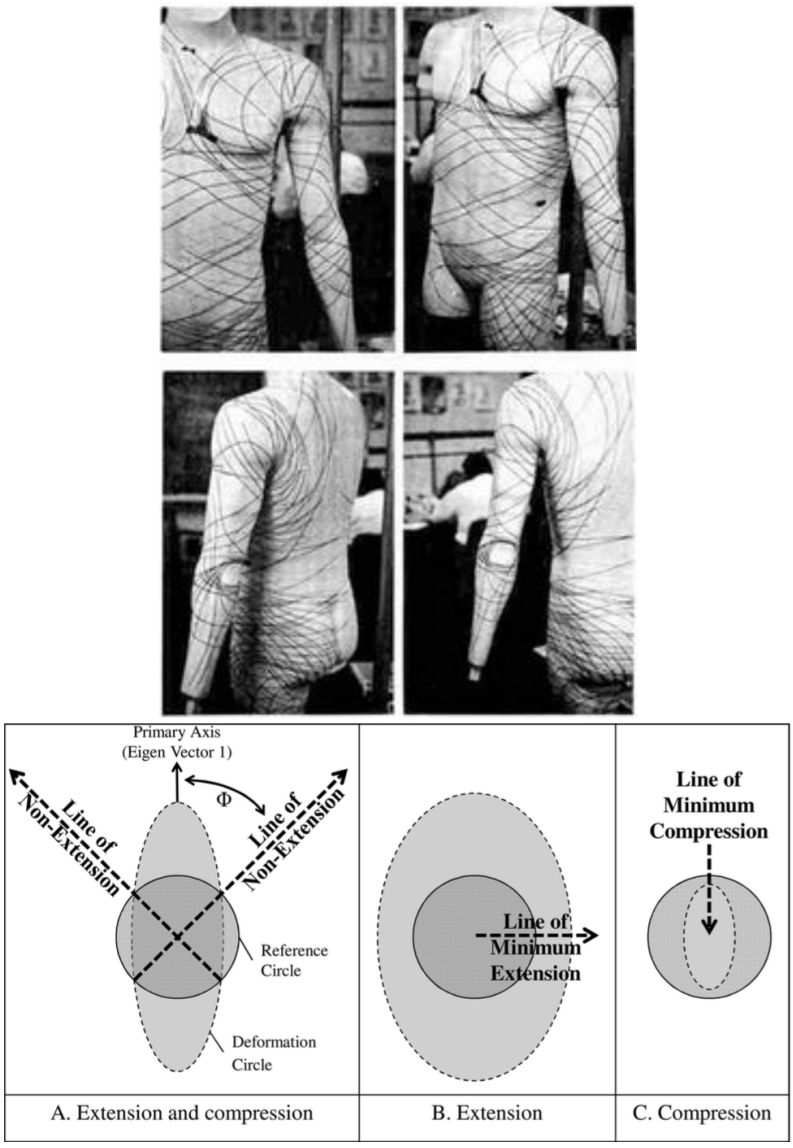

Figure 2.2: The quantitative definition of the lines of non-extension, demonstrated by Wessendorf and Neuman [8]. Earlier definitions without the use of motion capture were constructed initially by Arthur Iberall et al. [9].

These lines of non-extension (Figure 2.2) are useful for understanding the implicit strain field analysis of the body's surface and provide invaluable insight when

designing wearable technology that must obey the strains underwent by a dynamic human body [8].

In many ways, the human body operates similar to some cable-driven robots. Bones serve as an analog to the structure of the robot, which is in turn actuated by muscles. These muscles act like a cable-driven actuation system, providing tensile forces as opposed to compressive forces. Muscular forces in the human body are often routed through passive tension members, tendons, which do not actuate themselves, rather they transmit the force produced by a separate component. In tension based robots, the passive cables which also serve this function are sometimes referred to as tendons, just like their biological counterparts. Bio-inspired robotics have re-used multiple other idioms observed in nature and used those to engineer new technological applications. One of the most important lessons garnered from biology is the production of soft robots. Soft robots exhibit flexibility and structural compliance not found in traditional robots.

2.2 Flexibility and Compliance in Robotics

One important trade-off in the design of robots is mechanical compliance. Mechanical compliance is the measure of how well an object absorbs and distributes applied mechanical stress via elastic deformation. This means that robots which are mechanically compliant can robustly handle external and unpredictable stresses. This compliance can be enabled at many stages in the design process when constructing robots.

Anthropomimetic robots, those which can simulate human motion, have been designed because of desirable human-like properties, including compliance. Anthrob, a cable-driven robotic arm, is widely regarded as seminal research on bio-mimetic limbs [10]. Solid bones are woven together with a matrix of cables which are pulled using on-robot motors. Similarly, Kenshiro integrates tensile elements layered on top of a solid, jointed metal full-body skeleton like muscles [11]. Kenshiro has not just a large reachable workspace, but a large dexterous workspace as well due to the large redundancy in its tension system (Figure 2.3). This design philosophy can be

observed in other humanoids [12] and in humans as well [13].

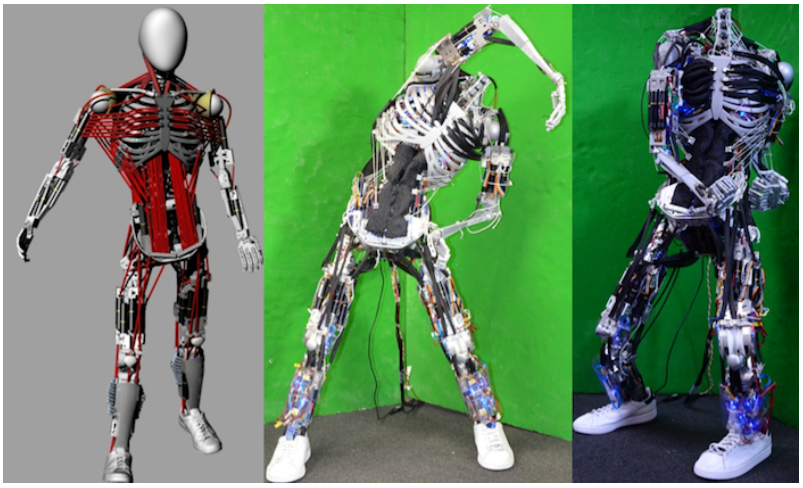

Figure 2.3: Kenshiro, an anthropomorphic robot designed with a large dexterous workspace akin to human range of motion [11].

In addition to the construction and implementation of humanoid and bio-mimetic human robotic limbs, significant theory on bio-mimetic motion has been developed through the studies of how humans themselves function as well as how the robots with which we emulate humans behave. To study human movement, Zanchettin et al. studied the kinematics of participants' arms as they performed a series of tasks [14]. These findings were then used to formulate precise mathematical models of human arms, for future robotic manipulators. The mathematical representation of cable-driven robotics, a crux of modern humanoid robots, has been shown to be expresssable through a tensile adjacency matrix [15]. Together, these contributions illustrate the merging of the field's understanding of human and humanoid motion.

Actuator compliance, as exemplified by models including series elastic actuators [16, 17], McKibben pneumatic muscles [18], and dielectric elastomers [19], is a property that enables mechanical flexibility within the actuators of the robot, often located within the joints for robotic arms. Compliance by control involves an agent autonomously sensing an applied stress, causing the controlled robot (for example) to quickly react to sensed impedances, mitigating any strain on the manipulator [20].

In contrast to these two methods, compliance in a given robot can also be applied

when designing its structure. Both homogeneous and heterogeneous compositions of materials can achieve this goal. Examples of homogeneous soft robots include textile based and plastic based applications [21, 22]. The inherent flexibility in soft materials, such as plastics and textiles, makes them excellent candidates for structural compliance [23]. Some robots, like the autonomous octopus developed by Wehner et al., can be produced entirely from soft materials and use techniques like monopropellant fuel supply and microfluidic logic to ensure every component involved in the manufacture is flexible [24]. Other robots make use of soft materials for specific components on robots. Gecko-inspired gripping devices approach a common problem in robotics using flexible gripper devices [25, 26]. Bio-inspired robotic fish have been produced that can swim through an undulatory motion induced by bilateral dielectric elastomer actuators on either side of a body [27]. One class of examples of structurally compliant heterogeneous robots is tensegrity structures. Unlike their homogeneous counterparts, these robots integrate both soft and hard materials to create their flexible, yet robust structures.

2.3 Tensegrity Structures

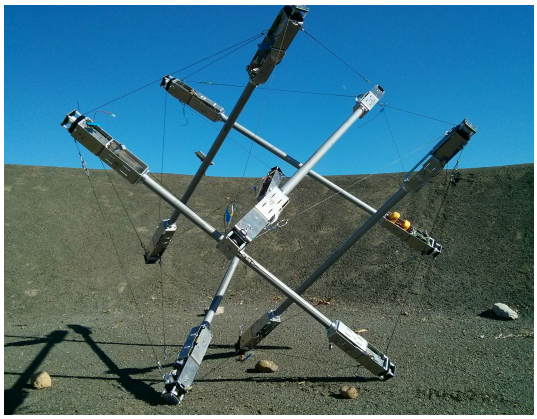

Figure 2.4: SUPERball, an example of a tensegrity robot. The structure of this robot is composed of two primary elements: compression elements (rods) and tension elements (cables).

Tensegrity structures (Figure 2.4) are hybrid soft-rigid structures that feature compression elements suspended within a network of tension elements. In traditional

tensegrity structures, the compression elements are rods and the tension elements are cables. As a result, these structures tend to be spacious and consequently lightweight. Passive tensegrity structures, such as those designed by Tom Flemons, Stephen Levin, and Graham Scarr exemplify how these static models can functionally represent similar structures in body, such as individual joints, limbs and even full humanoids [28–30]. To achieve dynamic stability in an otherwise chaotic network, tensegrity structures often employ closed kinematic chains inspired by similar biological analogs [31]. The study of these passive structures has influenced many active tensegrity structures and robots.

Active tensegrity structures actuate by contracting and extending their cables to change the morphology of the whole system. Although individual cables in most active tensegrity robots can only contract and extend, the abundance of cables in a particular tensegrity lend the active structure many degrees of freedom. From this redundancy the structure becomes compliant and flexible. These properties in particular have made various active tensegrity robots capable of robust locomotion [32–37], manipulation [38–40], and even heat-shielding [41].

Because the kinematics and dynamics of compliant mechanisms, including tensegrities, can be difficult to simulate using conventional inverse kinematics, many tensegrity researchers use a common open-source simulator to design their tensegrity structures and robots. This simulator, NASA's Tensegrity Robotics Toolkit (NTRT), is based upon the open source Bullet physics engine[1]. NTRT can be used to simulate in real-time the effects of tensegrity structures as they interact with with rigid objects and terrains and even other tensegrities. Tensegrity objects can be created and combined to create a hierarchical models of robots or other structures. Controllers can be associated with particular tensegrity objects within simulation and employ any arbitrary control scheme, including open-loop controllers, impedance controllers, central pattern generators (CPG's), and machine learning policies. Because each simulation is deterministic, batch simulations can be run in parallel and compared to one another after execution. The result from designing tensegrity structures in

[1] Additional information about NTRT can be found at
`http://irg.arc.nasa.gov/tensegrity/NTRT`

NTRT is rapid and precise simulations.

2.4 Machine Learning for Soft Robots

The determinism and parallel simulation architecture of NTRT allows for the implementation of some machine learning algorithms, such as evolution and reinforcement learning. Algorithms can be applied on real robots after training within NTRT or can even be trained directly on the robots, when provided with the complementary hardware support.

2.4.1 Evolutionary Algorithms

An evolutionary algorithm optimizes the state or policy of a population of individuals over time according to a survival of the fittest metric [42]. Individuals are judged based upon the incarnation of their "genetic code", or phenotype, which can be described as a set of values. Between generations of individuals, this set of values can be mutated, producing a slightly different phenotype that has a change in that individual's fitness. The individuals with the best or most fit phenotype are selected by the algorithm to reproduce (have their genetic code duplicated, mutated slightly, and then run again). The precise techniques used to determine fitness and to evolve populations of individuals can be similar to those in nature.

This iterative approach to solving problems by generation has been used in conjunction with populations of robots to find novel solutions to otherwise complicated design challenges [43]. Evolutionary algorithms are particularly useful for mutating and optimizing tensegrity structures. The structure or control of a single species of tensegrity may be that tensegrity's genetic code and how well the tensegrity performs a particular task (such as locomotion or efficiently performing a function) can be judged by fitness metrics such as energy consumption, time required to perform that task, or accuracy.

2.4.2 Reinforcement Learning

Reinforcement learning is a sub-field of machine learning in which an agent performs actions with respect to its environment [44]. Each action the agent performs renders either a reward or punishment depending upon how favorably that action changes the state of the agent. As actions are performed, the agent remembers the consequences of actions and can over time make better choices.

Reinforcement learning is applicable to many problems within the realm of robotics. Because a persistent issue with robots, even mechanically compliant ones, is avoiding contact with harmful objects, including people, robots which can learn proper interfacing theoretically have an advantage. As a result, the decision to view problems in an agent-environment dynamic has produced unique and optimal solutions within the multi-robot domain [45].

2.5 Assitive Wearable Robots

The advances in both flexible and compliant robotic design as well as novel control algorithms apply to other fields, like wearable robots, as well. The field of prostheses and orthotics (including exoskeletons and exosuits) has very close ties to both biology and human-robot interaction, including compliance within robots. As the appropriate core-technologies advance, wearable robotic devices become increasingly relevant as a vector for rehabilitation and augmentation.

Traditional rigid exoskeletons have developed the field of human augmentation. For upper limb orthotics, several types of actuation strategies have been adopted, such as electric, hydraulic, and pneumatic hardware [46]. Cable-driven approaches, such as the EXO-UL7 exoskeleton and CAREX, use wall-mounted apparatuses (Figure 2.5) to control independent joints and support muscle movement [47, 48].

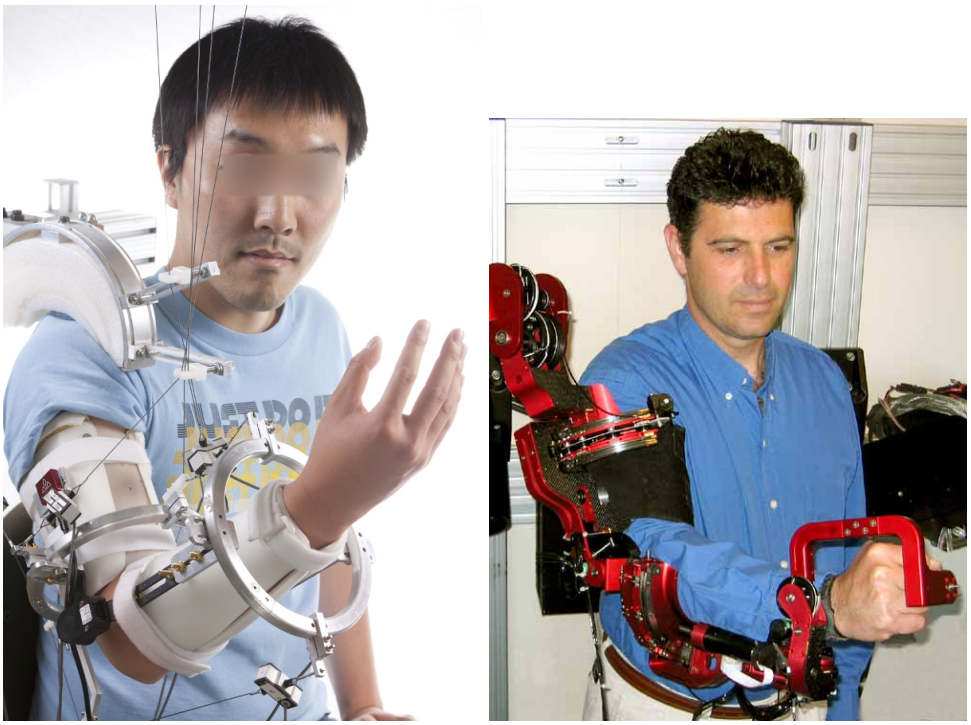

Figure 2.5: CAREX (2012) and the EXO-UL7 (2007): two examples of the state-of-the-art in upper-limb orthotic devices

This type of design allows motors and other heavy equipment to be off-loaded from the user. As a consequence, users of this device do not need to exert as much or any effort to support the assistive device itself. One downside of wall-mounting exoskeletons however, is the severe limitation in mobility. When tethered, users are still rigidly confined to a specific place (i.e the place of treatment) when using the exoskeleton. This hinders the user's temporal access to the device, which in turns affects how often the user can wear the exoskeleton. For time-sensitive applications, such as stroke therapy, the amount of treatment the user receives and how quickly they receive it significantly affects how well they recover [49, 50]. In these types of scenarios, a fully-compartmentalized exosuit that does not require a tether can provide accessibility that would otherwise be denied. The added autonomy may also have positive psychological effects on users as well, particularly those with previously-impaired mobility. Turner and Noah found that there was a correlation between physical disability and likelihood for depression [51], suggesting that physical disability has severe impacts on the morale of those who experience it.

An untethered exosuit could enable someone who is otherwise physically disabled to lead a higher quality of life through greater autonomy, provided the exosuit can operate intuitively and predictably enough for the user.

Additionally, rigid exoskeletons features structures and materials that impose inflexibility and constraint on their users. Metal chassis typically involve rigid linkages rigidly connected. Oftentimes these connections occur over portions of the human body that are meant to flex and change morphologically. As a result, these robot-induced impediments artificially inhibit users' ranges of motion, both reachable and dexterous. A robot that inhibits user movement not only fails to augment that movement, but can potentially injure that user as well. Long-term impediment can prevent muscles from exercising to their fullest extent and lose that range of motion over time [52].

2.5.1 Soft Exo Design

Soft exosuits provide a solution to bringing portable, flexible augmentation to users. These wearable robots feature a diverse array of actuators, materials, and strategies to achieve this goal.

Most exosuits use a cable-driven design. In a cable driven design, power from actuators is mechanically transferred through the exosuit to move users. One advantage of a cable driven design is that the cables themselves mimic human muscles. Both cables and muscles can only provide tension forces on the body of a human or a robot. As a result of this similarity, many researchers have cited similarities between the kinematics and dynamics of muscle fibers and cables as the foundation for their bio-inspired work [23].

Other actuators, such as shape-memory alloys and dielectric elastomers function kinematically and dynamically like muscles as well. Shape-memory alloys provide enormous tensile strength at the cost of efficiency. Dielectric elastomer actuators require a high amount of voltage to operate, but are able to conform to a lower profile, potentially useful for clothing and fabric applications. A third common actuator, the artificial muscle, uses pneumatic energy to reshape a bladder, which

can push and pull an end-effector either directly or indirectly. These exotic actuators yield alternative designs for exosuit creators, allowing for engineering trade-offs to be measured. One company, Superflex, has investigated the use of dielectric elastomers for a robotic exosuit of their own [53]. Roam robotics, a company also invested in compliant exosuits, has used pneumatic devices to actuate artificial muscles on candidate users [54]. Other fabric based and soft exosuits have integrated material compliance in their design to create flexible wearable devices for augmentation in the lower limbs [55, 56], the hands [57, 58], and the upper limbs [59–62].

2.5.2 Sensing on Wearable Robots

All intelligent robots require information to function. This information, typically gained through sensors, provides input to the robot's control function. Sensing accurately and precisely are necessary to inform the robotic agent of the exosuit user's own state and environment. In exosuits and other wearable robots, several sensors can be used.

Electromyography, the ability to sense muscle activity, is one common approach. When muscles in animals contract, an electrical signal is propagated by the nervous system. This signal, although fairly weak, can be measured through either implanted electrodes or surface electrodes. Although implanted electrodes provide a higher fidelity signal, surface electrodes are less invasive, less painful for the participant, and sometimes able to mesh with fabric. The electrode pads for surface electromyographs (EMG's) can be placed directly over the muscles to be sensed on the skin. Properly placed electrodes maximize the precision of the signal and provide a clear change in voltage when the muscle is flexed and when it is not. This signal can be abstracted as a Boolean variable with a characteristic rising curve indicating the beginning of a muscle contraction. EMGs have been used previously in some upper limb exoskeletons to update the impedance parameters necessary for control [63]. Embedding EMGs into an exosuit theoretically allows that suit to proprioceptively sense user intent (e.g. biceps flexion) just before occurring, allowing the worn robot to actuate and assist the predicted movement. This strategy suffers from several

drawbacks. First, surface EMGs are very delicate. Slight imprecision when they are initially placed and natural drift during usage prevents optimal readings. Perspiration and different body types can also influence EMG readings. These problems only amplify as more EMGs are used to measure the activity of each of the many muscles involved during an exercise.

Another form of on-robot sensing is stretch sensing. These types of sensors increase their resistance as their conductive medium (usually an alloy) is stretched. The stretch results in a longer length and a smaller cross-section. As a result, an electrical signal is produced that varies as the medium is pulled. One type of soft stretch sensor, developed by the Fabrication Laboratory at Purdue, uses eGaIn (a eutectic Indium-Gallium mixture) for their medium [64].

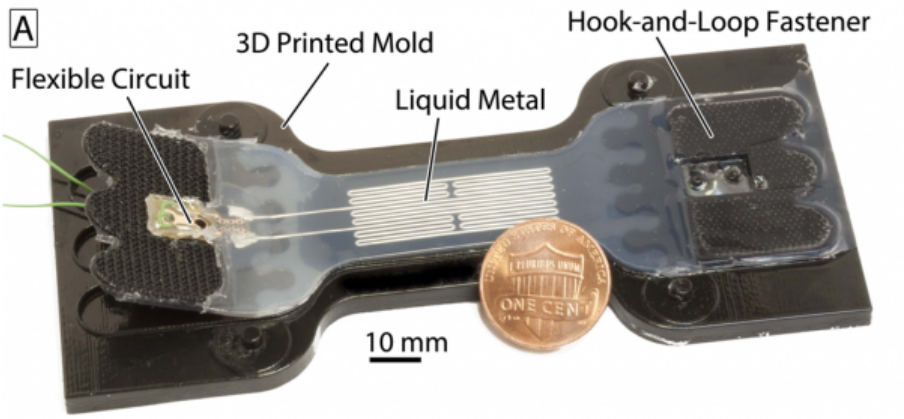

Figure 2.6: An eGaIn stretch sensor developed by the FabLab at Purdue [64].

This sensor has been designed for soft robots in particular, allowing the sensor itself to conform to curves as opposed to rigid surfaces. This makes the sensor a better candidate compared to rigid stretch sensors due to the flexibility and morphological changes expected in a mobile person and on a mobile robot. One exosuit, the biologically inspired Soft Exosuit from the Wyss Institute at Harvard University, employs hyper-elastic soft sensing at lower extremity joints [65]. Integrating both EMGs and stretch sensors has allowed this suit the ability to detect muscle change at both the electrical and morphological scale. One downside of stretch sensors is that they are delicate, much like their EMG counterparts. Due to this fact, they are difficult to manufacture reliably. These issues may resolve as this relatively young

technology improves.

Alternatively, a classic method of sensing tensile strain is load cells. Load cells provide relatively accurate measurements and can conform to very small spaces. Some models are also capable of on board processing of sensed data. Their price and rigidity, however, makes them difficult to integrate on top of flexible surfaces. Nonetheless, they are common in many exoskeletons and even some more flexible exosuits [66–68].

The final sensing strategy discussed here is inertial movement units (IMU's). IMUs are small devices that calculate pose data (i.e. pitch, roll, and yaw) through the use of several internal components, including gyroscopes and magnetoscopes. These sensors are relatively accurate, usually manufacturer guaranteed within tenths of a degree. Because pose data also generates predictable matrices, state estimation can be managed through simple linear algebra as well. One downside of these devices is that if they output Euler angles, precise pose can be lost due to a mathematical phenomenon called "gimbal lock". This issue can be resolved, however, if quaternions are used in lieu of Euler angles when calculating IMU pose.

2.6 Physical Therapy for Stroke Survivors and Upper-Extremity Impairment

According to the Center for Disease Control (CDC), Stroke affects over $800,000$ Americans every year [69, 70]. This number increases globally. Stroke survivors are often left impaired after their strokes, meaning that they lose function over some part of their body. A frequently reported outcome of this impairment is a loss in quality of life and a decrease in mobility. When left untreated, these issues plague survivors for the rest of their lives.

Physical therapists approach this problem through repeated sessions of rehabilitative exercise. One technique used by physical therapists is Graded Motor Imagery. Graded Motor Imagery is a type of training proctored by a physical therapist that assists patients in regaining muscular control over their body. Part of Graded Motor

Imagery is the use of mirror therapy, demonstrating bilaterally symmetrical movement of a user's limb through either an optical illusion with a mirror or through the therapist-guided kinesthetic feedback. The neurological response of this feedback as a user attempts to move their limb again can rehabilitate users and reduce both phantom pain and improve motor control after enough trials [71, 72]. A major factor in the outcome of this treatment is the number and duration of exercises performed [73]. Wearable technology can potentially assist in this regard, but only if it matches the flexibility expected by a physical therapist and is portable enough to be used outside of a single location.

Augmentative exosuits may be able to address this. These devices are designed fundamentally to remain sufficiently flexible throughout their use to provide users with unfettered range of motion as they exercise. Portable exosuits can then potentially give patients the ability to flexibly augment themselves according to prescribed exercise even outside of normal physical therapy sessions.

2.7 User Evaluation for Assistive Technology in Physical Therapy

The development of methods for analyzing the efficacy of physical therapy and any technology which augments it is critical. User evaluation ideally studies both the quantitative and qualitative methods to understand whether or not assistive technology is providing the help that it claims it can.

A survey study by LoPresti et al. identifies trends in the study of assistive technology for cognition (ATC). One of the largest contributors to rehabilitative success in patients, they found, was the ability of the patients to perform their exercises independently [74]. Independent support for both intrinsic and extrinsic tasks are likely to result in a healthier recovery for users of ATC.

ATC has also contemporaneously seen an increase in prevalence due to this fact throughout the United States. As the assistive technology improves in capability over time, so do the number of users and the number of targeted treatments [75].

An increasingly growing population is likely to demand more and stronger ATC.

In this thesis, we discuss the development and testing of one such ATC: an augmentative exosuit. This exosuit targets the upper-extremity of its user to provide them with motorized strength for use during bilaterally symmetrical exercise. In the subsequent chapters of this thesis, we outline our research and the process through which we design, implement, and test the exosuit.

Chapter 3

TENSEGRITY ROBOT MODELING

Traditional robots, composed of rigid parts and linkages, are prone to single-points of failure. The very rigidity which provides these robots with structure becomes their downfall when carrying loads. One solution to this problem, is more evenly distributing applied loads throughout the entire structure to dissipate forces. The human body, as described in the Literature Review chapter, achieves this through a hybrid tension-compression network. The observed strategy of the human body can be replicated in robots as well. Tension elements like springs and cables can substitute for active tension members (i.e. muscles) and passive tension members (i.e. connective tissue). The bio-inspired structures consequently formed are called tensegrity structures and the robots therewith derived are called tensegrity robots or 'tensegrities' for short.

The design of such robots, however is challenging. Non-linear kinematics and dynamics common to these tensegrities makes the prediction of their movement and response to external forces unpredictable. As a result, dedicated simulators such as NASA's Tensegrity Robotics Toolkit (NTRT) have arisen (Figure 3.1)).

3.1 Accurate Modeling of Tensegrity Robots

NTRT is based upon the Bullet Physics Engine (version 2.82) and programmed primarily through imperative programming languages like C++ and Python [76]. [1] The Bullet Physics Engine, like NTRT, is open-source. Originally a gaming engine, the Bullet Physics Engine excels at rendering complex terrains as well as the often complicated interactions subjects and objects may have with them. Another asset offered by Bullet is the ability to view simulations in 3D in real-time. This simulation environment uses a Cartesian mapping system to describe the geometrical shape of the tensegrity structure, Euler-Lagrange formulation to describe the dynamics and Hooke's law to predict the elastic forces developed inside the elastic cables [32, 77].

The force f_i applied by cable i to the elastic structure can be computed as:

$$f_i = \begin{cases} k_i(x_i - l_i) + b\dot{x_i} & x_i > l_i \\ 0 & x_i \leq l_i \end{cases} \tag{3.1}$$

where k_i is the spring stiffness, b_i is the linear damping, and l_i is the initial length of the cable and x_i is the length of the deformed flexible cable.

The length of each cable during the simulation is computed as:

$$x_i = ||\mathbf{p}_{i,0} - \mathbf{p}_{i,1}|| \tag{3.2}$$

where $\mathbf{p}_{i,0}$ and $\mathbf{p}_{i,1}$ represent the position vectors of the two ends of elastic cable i. These features are excellent for studying the intricate collisions and movement of tensegrity structures and robots.

NTRT functions by emulating two kinds of objects: compression elements and tension elements. Compression elements are objects whose dimensions do not change throughout the simulation. They are assigned mass and therefore can be acted upon by the simulated gravity. Tension elements are objects that are represented by a morphable line with two endpoints. By default, these tension elements function as

[1] Additional information about NTRT can be found at `http://irg.arc.nasa.gov/tensegrity/NTRT`.

springs according to Hooke's Law with a damping term (Equation 3.3).

$$F = -kX - bV \tag{3.3}$$

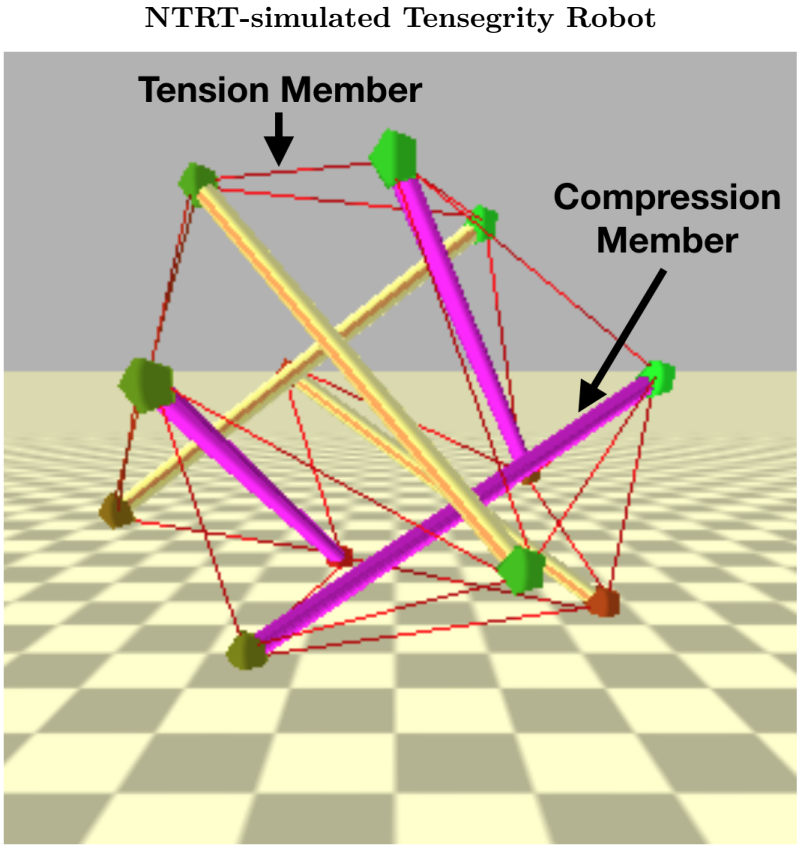

Figure 3.1: A simple 6-bar tensegrity structure simulated in NASA's Tensegrity Robotics Toolkit (NTRT). This structure features 6 distinct compression elements (the bars) and 24 distinct tension elements (the cables)[78].

Programs can specify cable lengths within the simulator using a controller. This controller is limited by the robot's own mechanics, which can be handcrafted to obey physical constraints including motor specifications and cable minimum and maximum lengths among others. These restrictions prevent inaccurate phenomena from occurring during simulations.

3.2 Controlling Tensegrity Robots through Genetic Algorithms

To begin our investigation into bio-inspired designs for tensegrity robots, we created a crater-escaping robot. In conjunction with NASA Ames Research Center's Dynamic Tensegrity Robotics Lab of the Intelligent Robotics Group, we studied a hypothetical example where one of their prototypes was trapped in an extraterrestrial ditch. This robot, based upon the real life SUPERball (Figure 2.4), was placed in a deep crevice in simulation. The crevice surrounded the robot in a radially symmetrical manner. The robot was half submerged within the crevice with only a few of its compression elements jutting out of the hole in which it resided (Figure 3.2). The robot's task was simply to escape the crater through its own movements and climb out.

We did not know the precise movements or order of movements that must be run in order to complete this task, so we developed a genetic algorithm to assist us. Genetic algorithms function by exhaustively testing multiple instances of a candidate solution space. This entire solution space is referred to as the "control policy pool" and each instance is referred to as a "control policy instance" or candidate solution. The collection of all tested control policy instances is the test population. Control policy instances are then tested iteratively and assigned a score based upon their achieved success. Control policy instances that solve a given task well are rewarded with higher scores than their less successful counterparts. In the first iteration of tests (i.e. those of the first generation of the test population), the control policy instances with the highest score have their specific "attributes" recorded for the next iteration of testing. In the second iteration of tests, the control policy instances from the first generation that were recorded have the values specific to their control policy instance replicated and mutated slightly. These mutated phenotypes in the second generation are tested and their scores compared to one another as well as the phenotypes from the first generation. The replication step for another generation of tests, also called "mutation", can be run again ad nauseum.

Crater Escape Algorithm

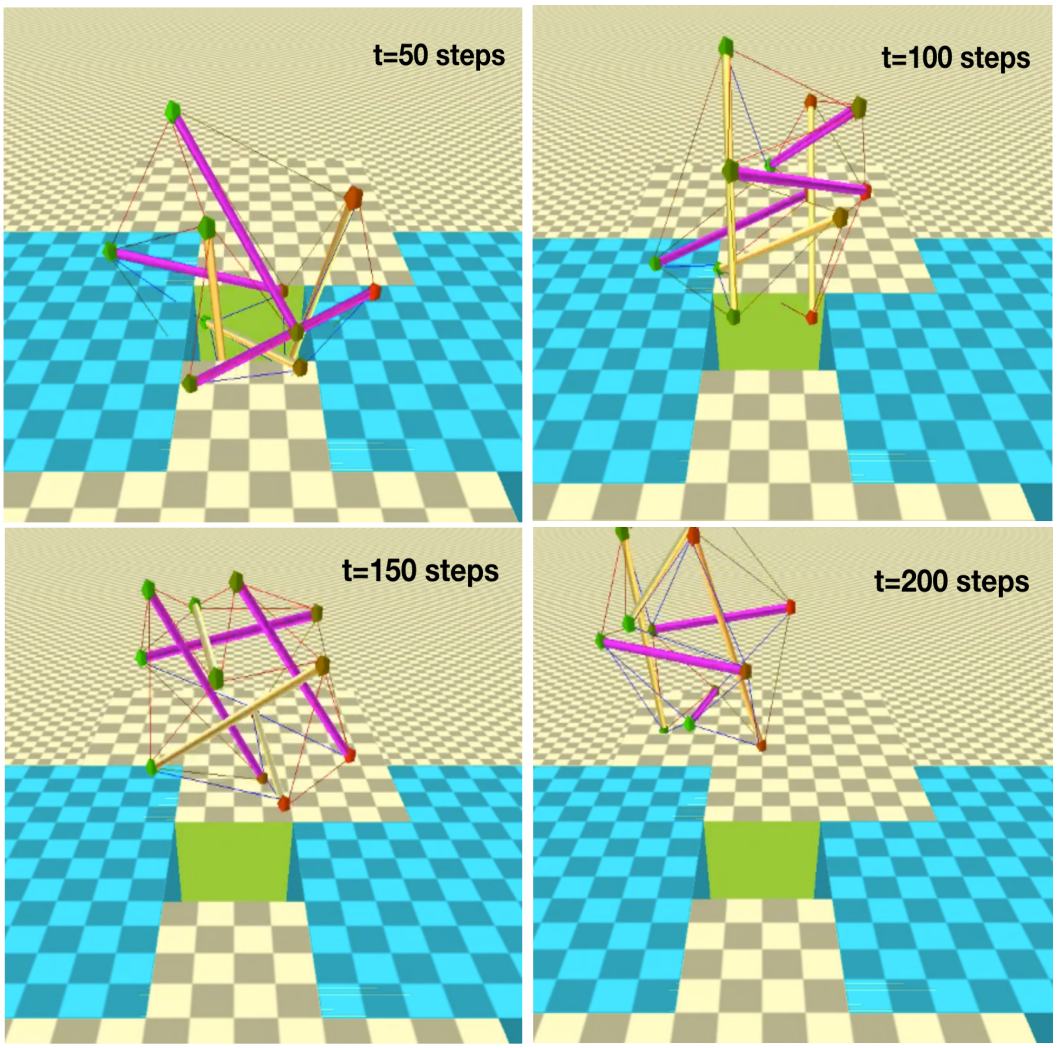

Figure 3.2: An instance of the crater escaping tensegrity robot actuating. This one instance of the robot was simulated and scored based upon whether or not the robot escaped the crater [78].

In the case of our algorithm, the control policy space of the candidate tensegrity robots is a 32-dimensional vector that describes the motor function of 8 triplets of cables in the robot. Each of these cable triplets form a triangular face on the exterior of the robot. The controller of this robot attempts to keep this triangle equilateral by moving all three cables in this face simultaneously according to the same sinusoidal function. This sinusoidal function, characterized by 4 constants, represents the lengths of these three cables with respect to time. The 4 constants are the amplitude (A), angular frequency (ω), angular frequency offset (φ), and DC offset (D) of the sine wave (Equation 3.4).

$$y = Asin(\omega t + \varphi) + D \tag{3.4}$$

The precise constants for each control policy instance are chosen to test the extremes of the simulated motors without exceeding their physical bounds. We uniformly sampled across the control policy space to produce our control policy instances, where the selection space can be described as "no movement produced" to "maximum allowable movement produced".

We run our genetic algorithm based upon a Multi-Level Monte Carlo method. This sequential Monte Carlo optimization operation excels at finding global extrema. For our application, this is particularly important since we know very little about the behavior and capabilities of this relatively new robot. The downside of this method is the computational time. Testing so many permutations makes each generation of control policy instances an expensive task. To mitigate this, we tested on a restricted subset of the control policy space. As opposed to testing unique sinusoids for each cable within the robot, we tested it on triplets of adjacent cables, thus reducing our test space by an order of 3.

Our results from the initial generation and the mutated generation can be seen in Figure 3.5 and Table 3.1. The scalar metric used to judge success for these trials was distance traveled from the origin. A robot which escaped the crater would move more than 25m away from the origin since the crater was located over 25m above the simulated ground. Robots that escaped would consequently fall of the precipice

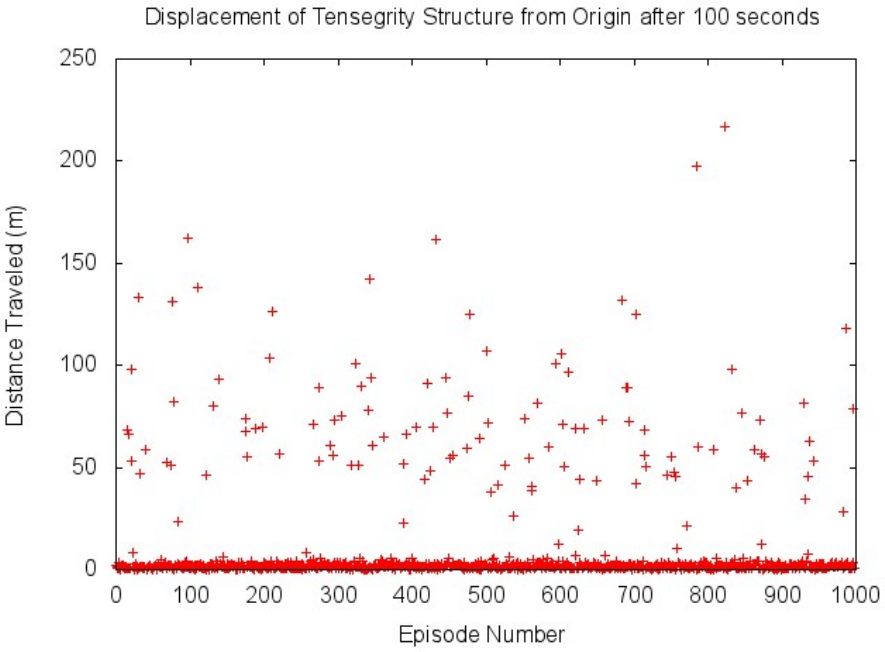

Figure 3.3: Initial Generation

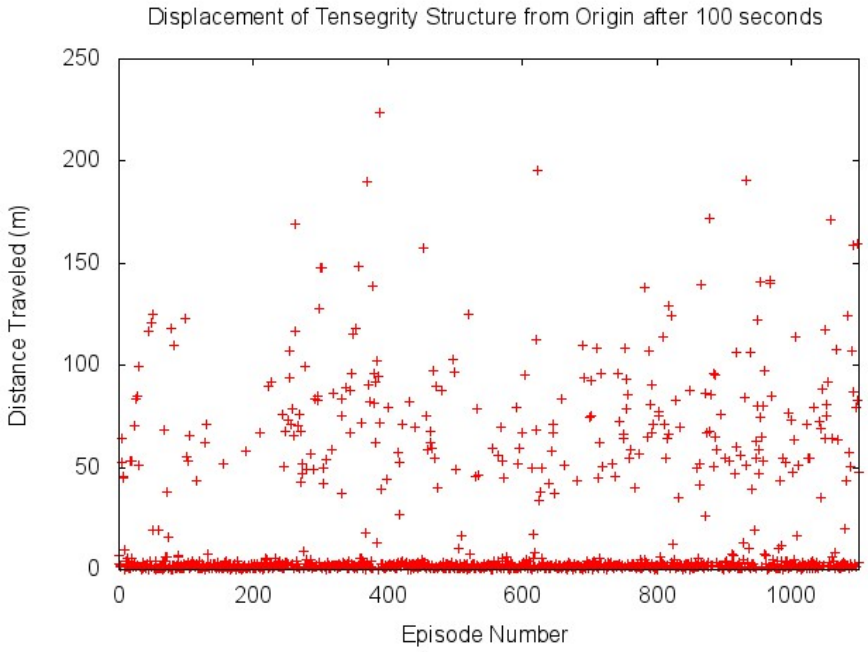

8

Figure 3.4: Mutated Generation

Figure 3.5: The initial and mutated generations of the multi-level Monte Carlo trials for the tensegrity rover escape algorithm. Each point represents the 32 parameters used to describe that robot's control policy. The child (mutated) generation (right) has a higher success rate than the parent (initial) generation (left) due to the improvements learned from the successes of the initial generation [78].

Table 3.1: Displacement (m) by Generation

Generation	**Minimum**	**Average**	**Maximum**	**% Escaped**
Initial	0.01	9.91	216.55	11.1
Mutated	0.05	20.53	223.59	24.0

and satisfy the success metric. To improve the gene pool of the mutated generation, we selected robots who were greater than 30m away from the origin, as we suspected they were able to escape more quickly.

We observe that over the course of the initial generation (Generation 0)'s 1000 trials, 11.1% of robots escaped the crater. Displacements ranged from 0.01 meters to 216.55 meters. The mean displacement traveled by the robot was 9.91 meters. The vast majority (88.9%) of the initial generation episodes featured a failed control policy (i.e. the robot did not escape the crater).

Generation 1 (the mutated generation produced from Generation 0's successful control policy instances) yielded a greater number of successes than Generation 0. This time, displacements ranged from 0.05 meters to 223.59 meters. The mean displacement traveled by the robot was 20.53 meters and 24.0% of episodes resulted in a successful escape. Although the majority (76.0%) of Generation 1 episodes still failed to escape, there was still a significant 22.9 percentage point improvement in success rate when compared to the initial generation (a 207% increase).

To further examine these promising results, we additionally decided to simulate under-actuated tensegrity structures as well. An extraterrestrial rover such as the one simulated in these trials could potentially fail to actuate motors and actively change cable lengths due to damage accumulated during a mission. In such scenarios, the robot will lose control capability. Another possibility is that a tensegrity rover may be designed before the mission to function with some cables unactuated. We ran three more sets of tests to examine the change in operational functionality as fewer cables can assist the robot in escaping (Figure 3.6).

Although fewer robots successfully escaped when under-actuated, some robots were still able to escape despite the artificial impediment. This means that these

Tensegrity Robot Escape Success as a Function of Cable Activity Level

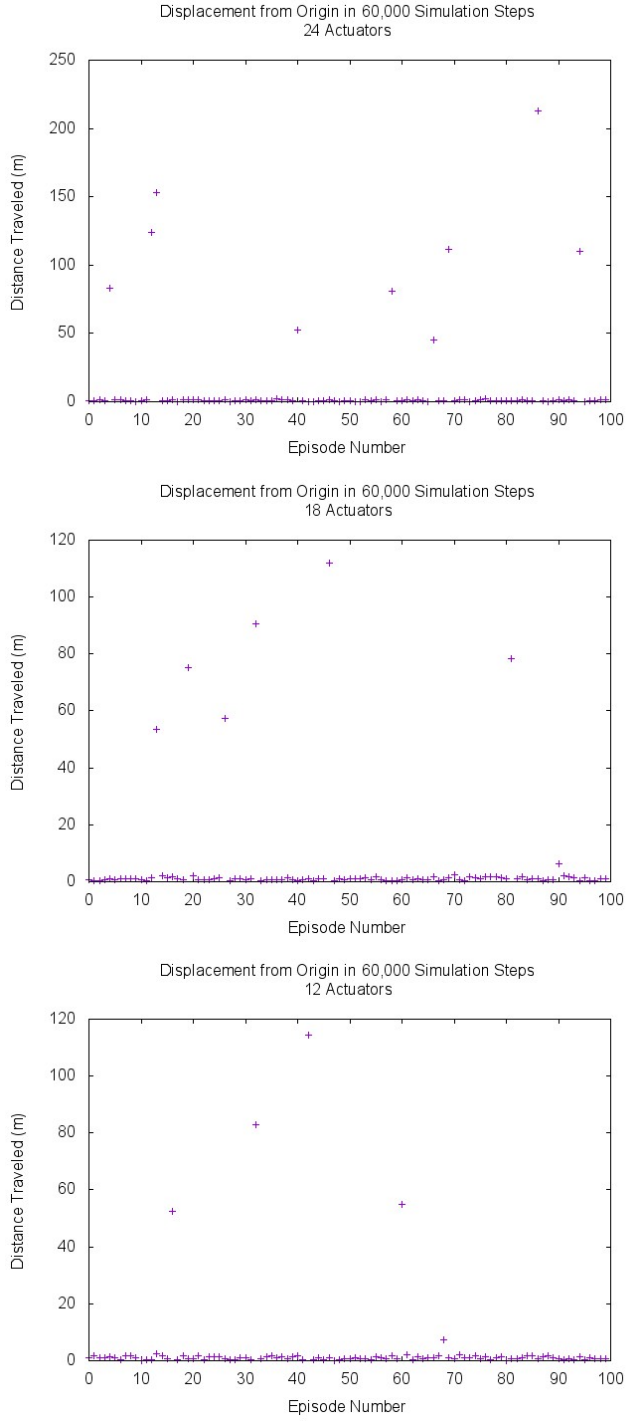

Figure 3.6: Distances traveled by 100 control policy instances mutated from Generation 1, with 100%, 75%, and 50% of their cables active [78]. The initial control policy instances for these trials were identically produced from the successful control policy instances of the mutated generation of tensegrity robots in Figure 3.5.

robots can successfully complete an escape even under sub-optimal settings. If tensegrity robots can still complete challenges even when under-actuated, future designs may not require complete actuation for the robot to function correctly.

From these experiments, we can see the improvement from the initial generation to the mutated generation [78]. One important insight from this is that tensegrity robots, especially those with many active components, can be controlled and taught how to complete a goal. One of the barriers to greater tensegrity usage in robots is finding a way to simulate and control them and these results elucidate one manner of doing so. These discoveries are important for designing other structurally compliant robots.

Chapter 4

HUMAN-INSPIRED TENSEGRITY MANIPULATORS

Understanding human upper-extremity anatomy and physiology is important for bio-inspired design, especially in tensegrity applications. Although experiments such as the genetic algorithm for crater escaping from before elucidate the potential impact for coupling machine learning with tensegrity robotic controllers, the design of bio-mimetic or even bio-inspired robotic joints require different insight. Tensegrity manipulators offer a potential method for interacting with objects in a compliant manner. Modern traditional robotic manipulators use various techniques such as impedance-based controllers, series-elastic actuators, or soft materials. However, very few manipulators are fundamentally compliant at the structural level. The advantage of this added feature would be reducing the necessary overhead associated with these other techniques. Having a structure which passively flexes according to external forces is potentially safer and more akin to human bio-mechanics. Structures that are more compliant can be more comfortable and mobile than their rigid counterparts, both which have been previously identified as important factors in device usage among prosthetic limb users [79, 80]. Designing tensegrity manipulators, whether for prosthetic use or industrial use, must therefore incorporate a

fundamentally comlpiant design at the structural level.

To create compliant tensegrity manipulators, we designed and tested multiple tensegrity joints, passive and active. These joints when acting alone or in concert with one another should produce meaningful actuation without sacrificing compliance and flexibility.

4.1 Prototype 1: Tensegrity Elbow

The first tensegrity joint constructed was an elbow. We chose to design an elbow first because it featured directional movement useful for general purpose applications as well as critical function for use in upper-limb movement.

Initially, we designed a passive model in NTRT (Figure 4.1). These prototypical designs are largely based upon those of the passive tensegrity elbows of Graham Scarr [30]. After observing these initial simulations, we constructed some passive prototypes to examine the interplay between 3D-printed PLA and simple tension members (Figure 4.2). In these designs, compression elements were 3D-printed out of polylactic acid (PLA) and strung together with the tension elements. All three of these passive prototypes can be manually hand-controlled to change the pitch of the manipulator's end-effector.

As the passive designs evolved between iterations, we discovered the value in not just thinning compression elements, but separating them as well. The value in using less printed material is that the structure as a whole is lighter, thus easier to move. Separated designs yield greater flexibility in the joint and can even add greater functionality than a natural elbow. The third passive design in particular totes two artificial tension members surrounding the suspended olecranon component symmetrically. As a result, three major compression elements constitute this robotic joint are the forearm bones, the humerus, and (detached) olecranon. Pulling these tension members changes the yaw of the end effector.

From these passive designs, we created a new design for an actively controlled tensegrity robotic elbow. We constructed an NTRT simulation of the elbow joint and provided it with a controller to modulate its pitch and yaw sinusoidally over

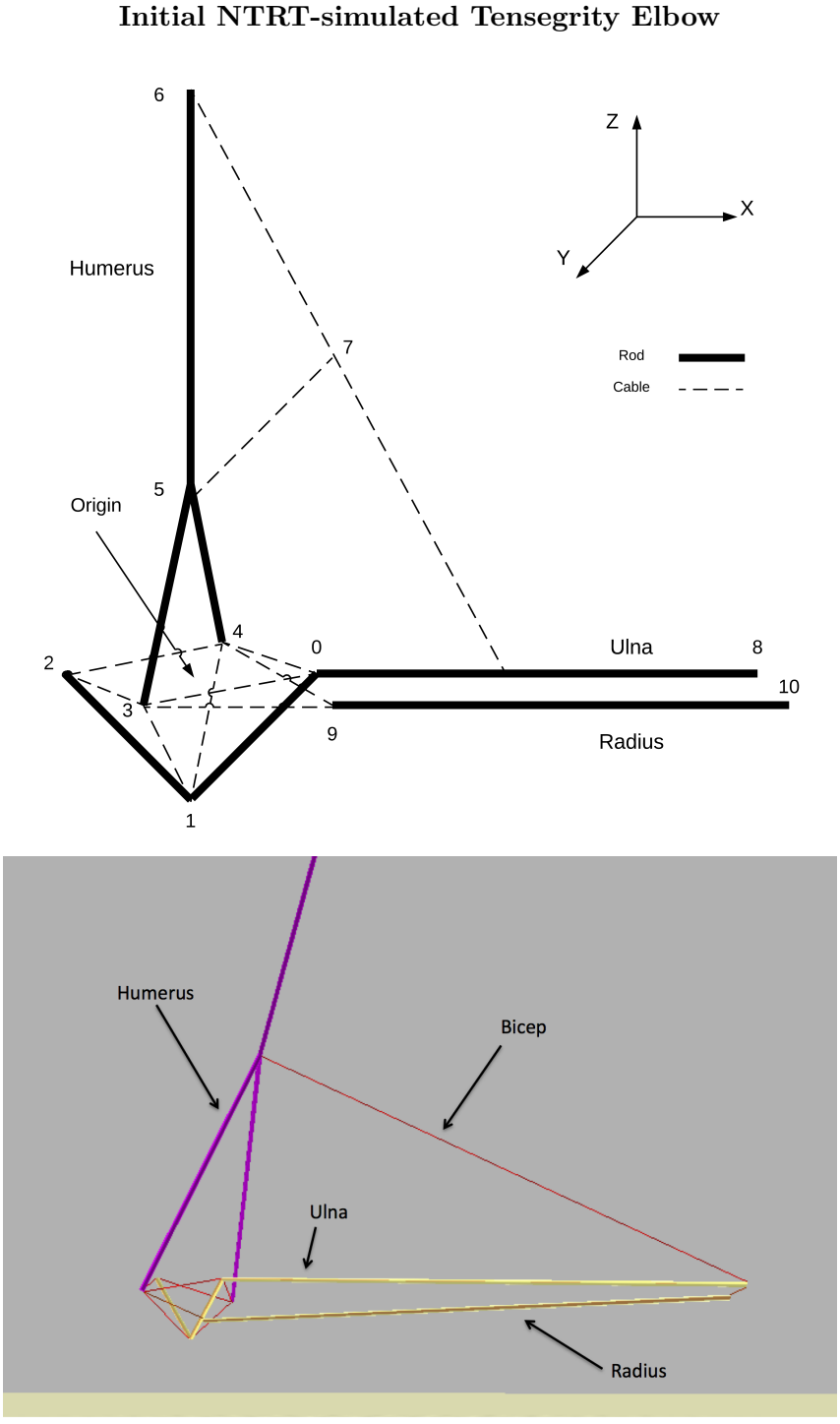

Figure 4.1: A tensegrity elbow simulated in NTRT. The NTRT model was based upon the passive schematic shown here. The bold colored cylinders are compression elements and the thinner red lines connected to their end points are the cables (tension elements) [38].

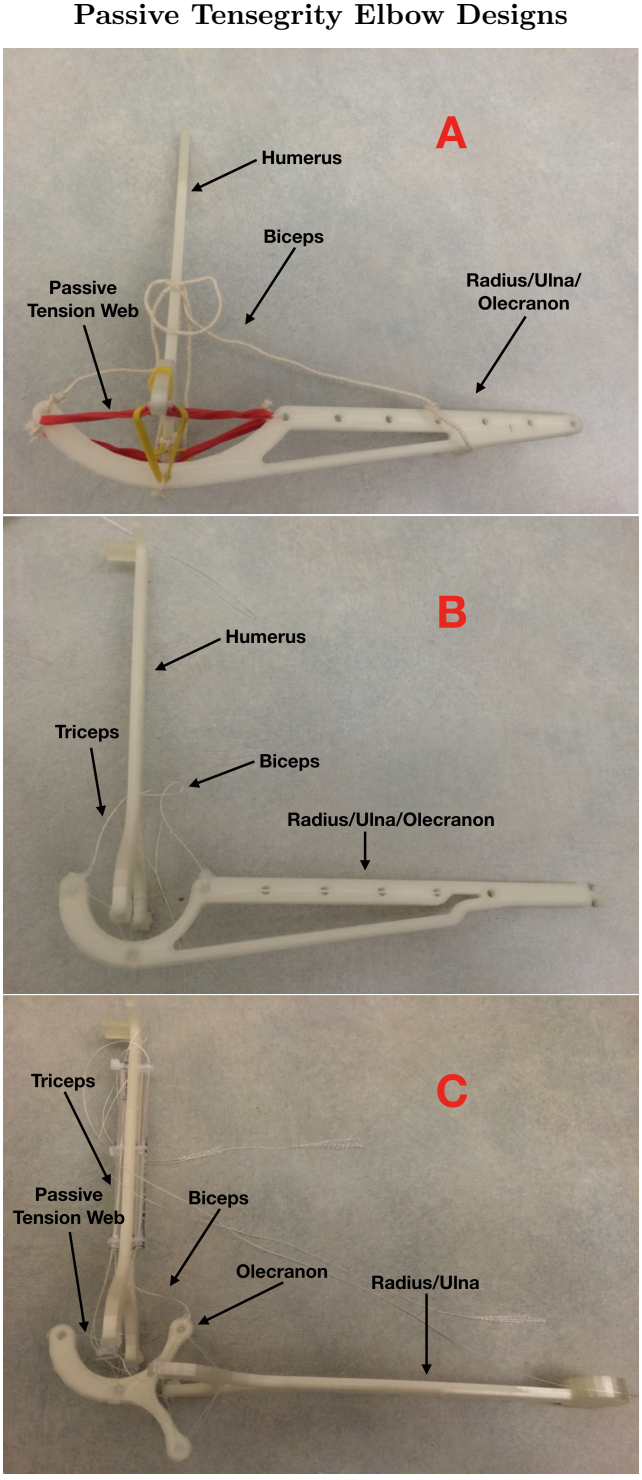

Figure 4.2: Three passive prototypes of a tensegrity elbow. These designs are heavily influenced by similar passive tensegrity designs of Graham Scarr [30]. The compression elements are composed of 3D-printed polylactic acid (PLA) and the tension elements range from twine to rubber bands to braided aramid cable [38].

Simulated Actively Controlled Tensegrity Elbow

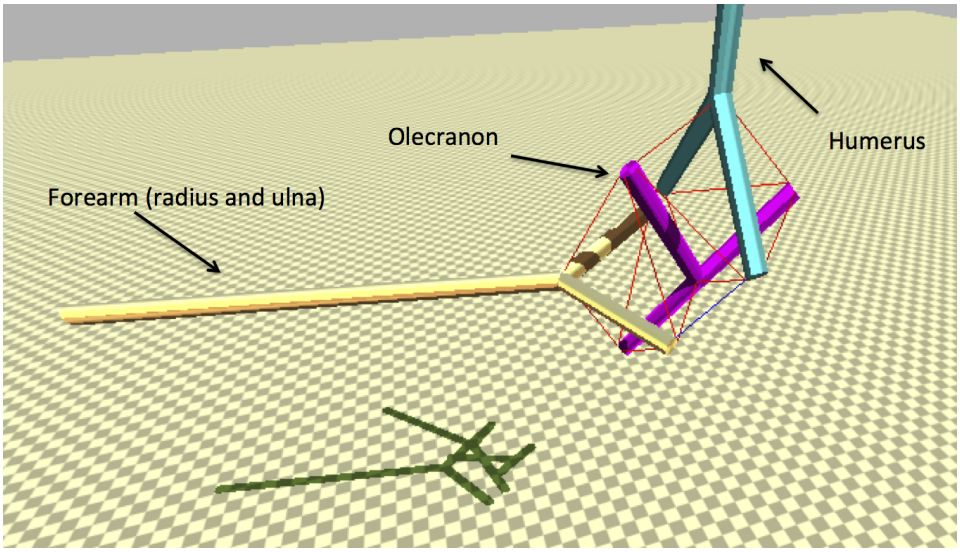

Figure 4.3: An actively-controlled tensegrity elbow constructed in NTRT. The bold colored rods are compression elements and the thinner red lines connected to their end points are the cables (tension elements). This robot can be actively controlled by changing its pitch and its yaw. All actively controlled cables are located locally within the joint itself [38].

Simulated Demonstration of Pitch Movement in a Tensegrity Elbow

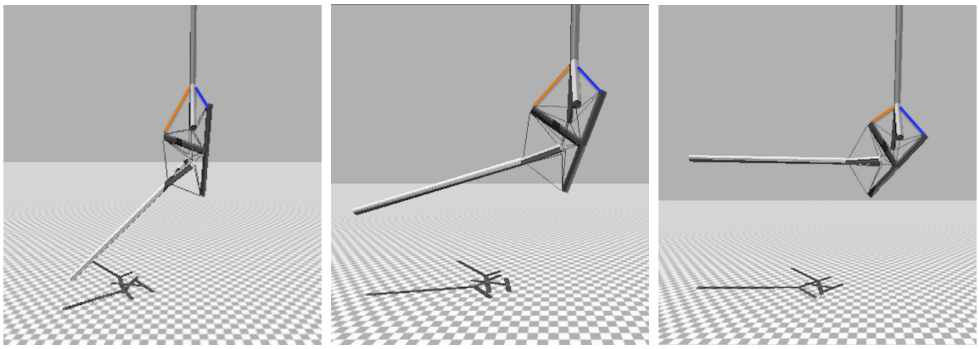

Figure 4.4: A simulated tensegrity elbow demonstrating pitch movement. Two cables (orange and blue), functioning akin to biceps and triceps, act as the antagonistic pair responsible for generating this movement [38].

Simulated Demonstration of Yaw Movement in a Tensegrity Elbow

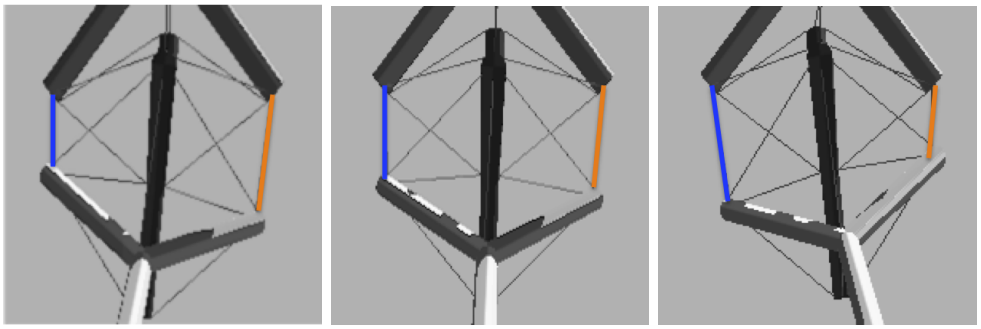

Figure 4.5: A simulated tensegrity elbow actuating side cables to demonstrate yaw movement. Unlike pitch movement, yaw movement is not naturally generated in the elbow, but instead in the shoulder in a physiologically accurate human arm. The antagonistic cable pair is highlighted blue and orange [38].

Table 4.1: Weight Constitution of the Active Prototype

PLA Arm (g)	Both Motors (g)	Combined
55.6	416.6	472.2

time as a demonstration (Figure 4.3). Isolated pitch movement can be observed in Figure 4.4. Isolated yaw movement can be observed in Figure 4.5. Additionally, we performed a movement analysis of the end-effector through space to identify the precision of control on the device (Figure 4.6).

This design was replicated in reality through a similar manufacturing method to the passive designs. This time, however, the robot was connected to an additional external chassis for the support of the manipulator arm and its off-loaded motors (Figure 4.7). The weight constitution of the elbow is recorded in Table 4.1. The focus of this separated design was the isolate the heaviest components of the functioning robot from the lightweight manipulator itself.

From the design, simulation, construction, and testing of this tensegrity elbow, we observed a number of interesting properties and traits of the robot. In addition to serving as a proof-of-concept for active bio-inspired designs, the tensegrity elbow multi-DoF movement in a single, compliant joint (Figure 4.8). The elbow demonstrates the ability to localize both pitch and yaw into one joint while maintaining compliance via a novel tension-based network [38]. Further analysis of the elbow yielded its reachable workspace in three dimensions (Figure 4.9). This workspace is

Simulated Range of Motion of Tensegrity Elbow End-Effector

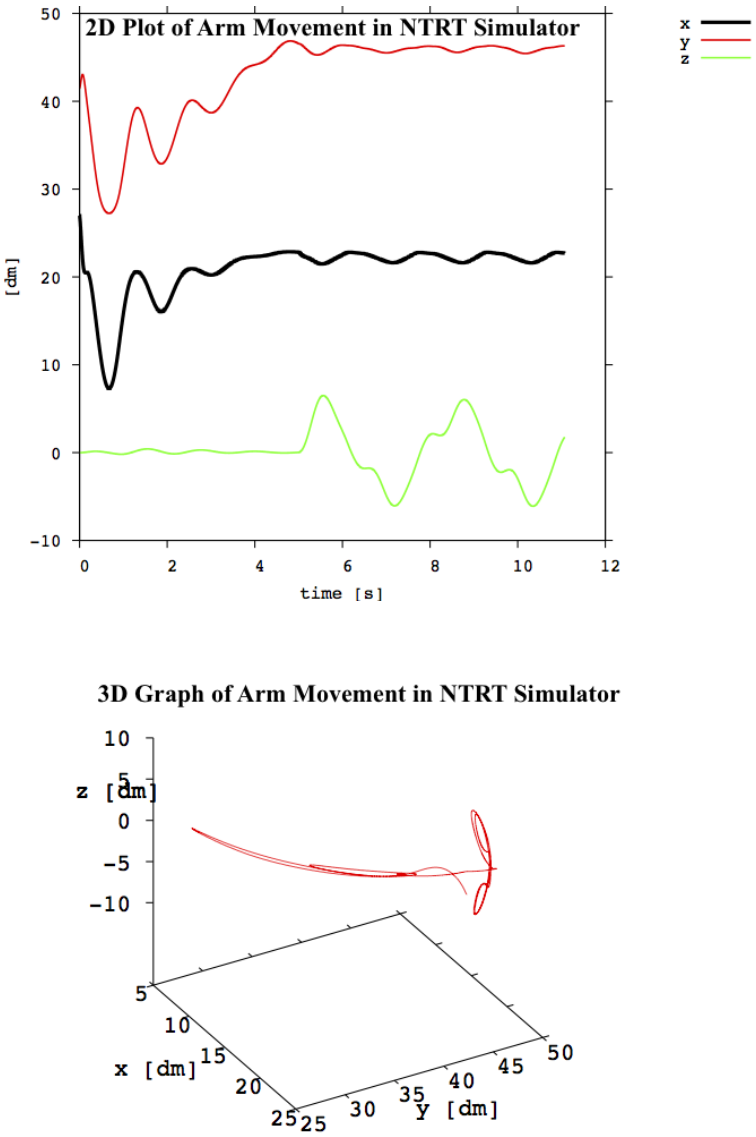

Figure 4.6: The movement of the end-effector on the simulated tensegrity arm. The path plotted illustrates the space swept out by isolated, independent movement of the joint along the pitch and yaw axes. Since the actuation of tension elements effect their neighboring tension elements easily, oscillations from their elasticity propagate quickly throughout the structure and are most apparent at the end of the lever arm during movement [38].

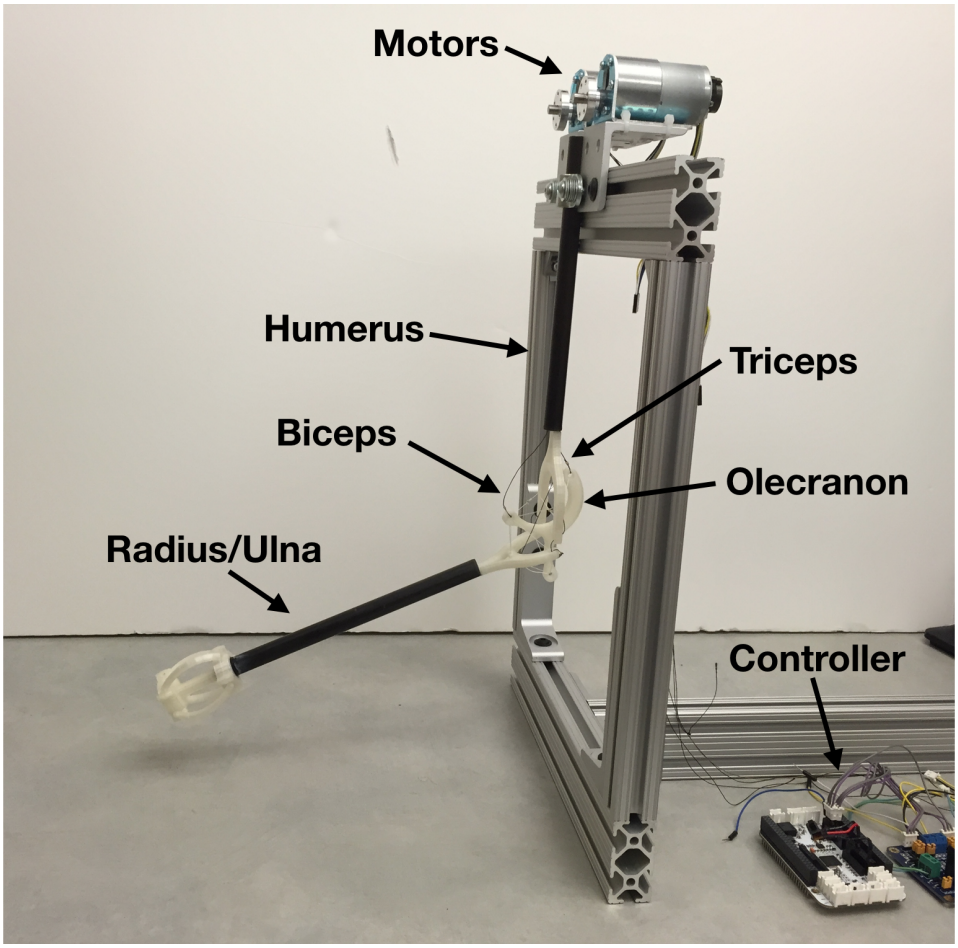

Figure 4.7: The physical prototype of our tensegrity elbow. Compression elements are composed of 3D-printed Polylactic Acid (PLA) and tension elements are composed of spectra braided fishing line. This model is actively controlled by motors seen mounted off of the robot and onto the chassis [38].

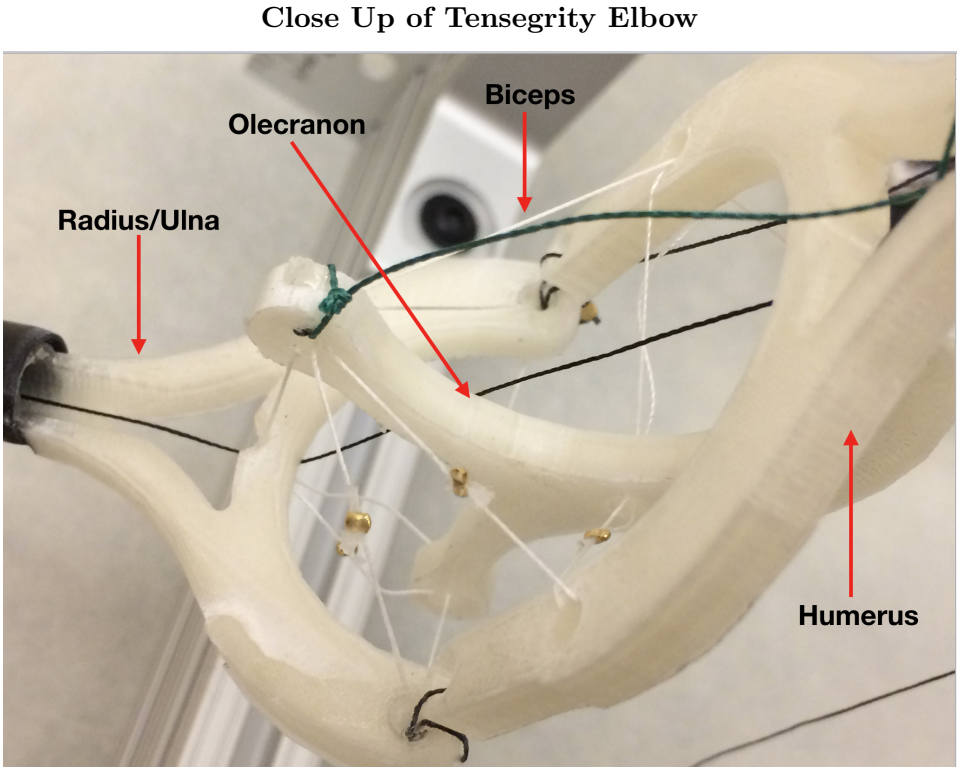

Figure 4.8: A close up shot of the light-weight, multi-axis compliant tensegrity joint. This joint can be actuated by offloaded motors to control the pitch and the yaw of the arm. These two degrees-of-freedom are achieved by two pairs of antagonistic tension elements (the dark colored thread). The active and passive tension members can also be tuned for stiffness, creating a variable level of flexibility within the joint [38].

an elliptical paraboloid, thus quadrilaterally symmetrical. The reason the workspace is symmetrical over two axes is because of the antagonistic cable actuation about the pitch and yaw axes. This workspace is proportionally larger than its biological analog; human elbows do not naturally rotate about the yaw axis. The functional addition of this capability in the manipulator has therefore yielded a bio-inspired multi-DoF manipulator joint that is functionally more robust than a bio-mimetic one.

4.2 Prototype 2: Tensegrity Shoulder

To extend the lessons learned from the constructed tensegrity elbow joint, we additionally constructed two tensegrity joints to be used in serial to the tensegrity elbow joint. These joints can potentially be used serially for the purpose of creating a full

Tensegrity Elbow Workspace

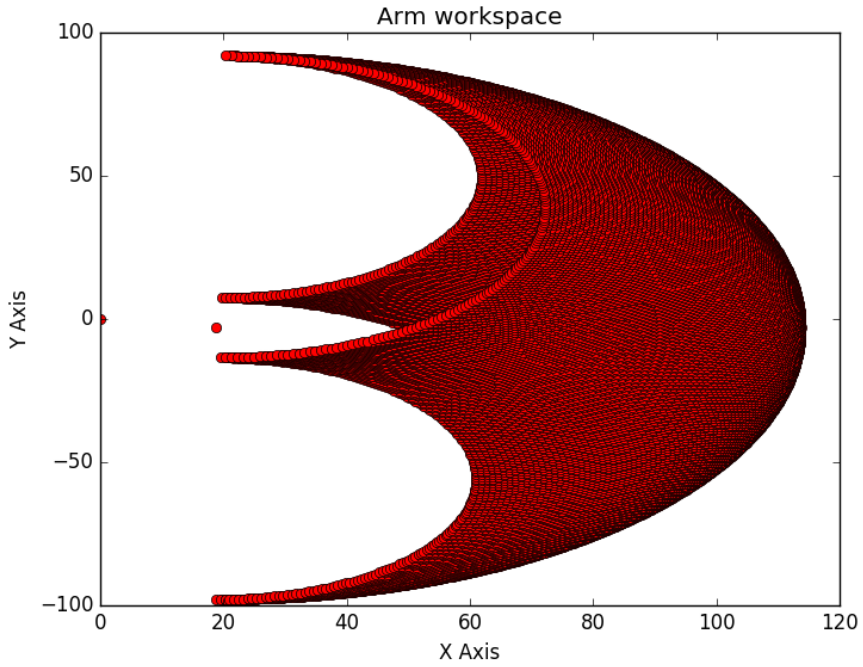

Figure 4.9: The workspace of the tensegrity elbow. This workspace demonstrates the ability of the tensegrity joint's end effector to reach within an elliptical paraboloid. This quadrilaterally-symmetrical workspace is a function of the two active-DoF in the robot: around the pitch axis and around the yaw axis.

upper-extremity or simply a more dexterous manipulator.

The two designs for the shoulder joint studied were a saddle joint (Figure 4.12) and a nested tetrahedrons joint (Figure 4.13). The saddle design was meant to be more bio-mimetic than the other design. Its primary focus was further extending the pitch of the manipulator as a whole while simultaneously adding to the range of motion around the yaw axis as well. The tetrahedrons joint, based upon the designs of the DuCTT robot [81], also incorporates further movement about the pitch axis. In lieu of further yaw flexibility however, the joint affords the manipulator vertical lift. As a result, two comparable manipulators can be designed to fit one of two purposes depending upon their chosen shoulder joint. Theoretically, manipulators can include both tensegrity shoulder joints into one arm for any arbitrary purpose. Both designs used the same elbow design from earlier research 4.14 [30, 38].

Another goal of these designs was to mimic their biological analogues to a reason-

able degree. Although true bio-mimetic design can be impractical, the development of bio-inspired devices still serve many purposes. Creating a structure similar to that of the human upper-extremity allows us to study future hybrid soft-rigid robots and potential human-interfacing designs (Figures 4.10, 4.11).

Skeletal Analogy for the Nested Tetrahedrons Tensegrity Manipulator

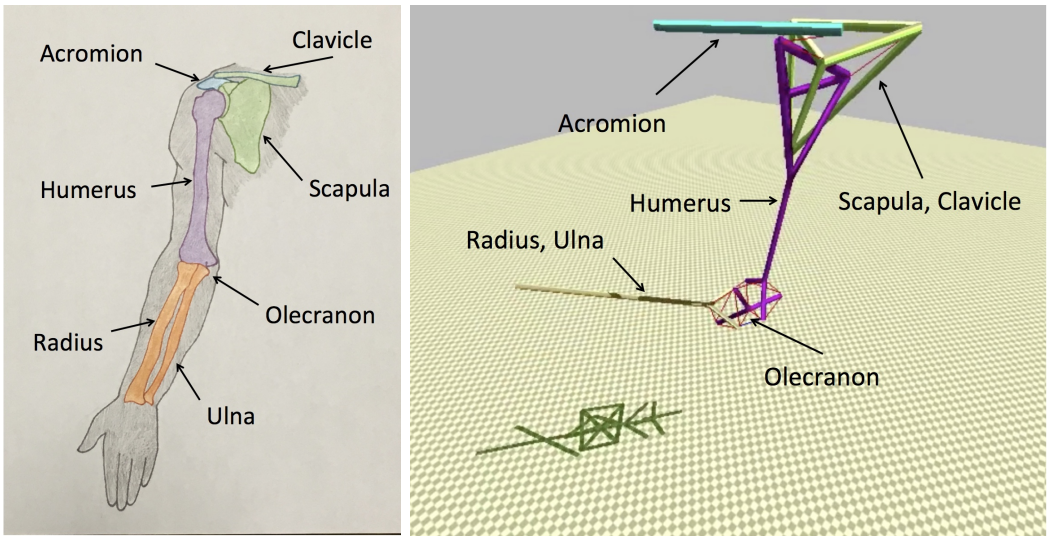

Figure 4.10: A mapping between the major compression elements of the human arm (left) and those of the simulated tensegrity manipulator models [82].

4.3 Simulation

We compared four designs against one another: a simple saddle model, a complex saddle model, a suspended tubercle model, and a tetrahedrons model (Figure 4.16). The goal of these simulations was to determine which shoulder geometries could theoretically provide the highest number of independent controllable degrees of freedom while maintaining structural compliance [82]. The implemented controllers for this examination can be described thus:

$$T = T_0 + K(L - L_0) + B(V - V_0) \tag{4.1}$$

where T is the tension set-point, To is a tension offset, K is the position displacement between the cable's length L, and V is the control input from sinusoidal input waves. The inspiration for these controllers came similar tensegrity research on CPG-

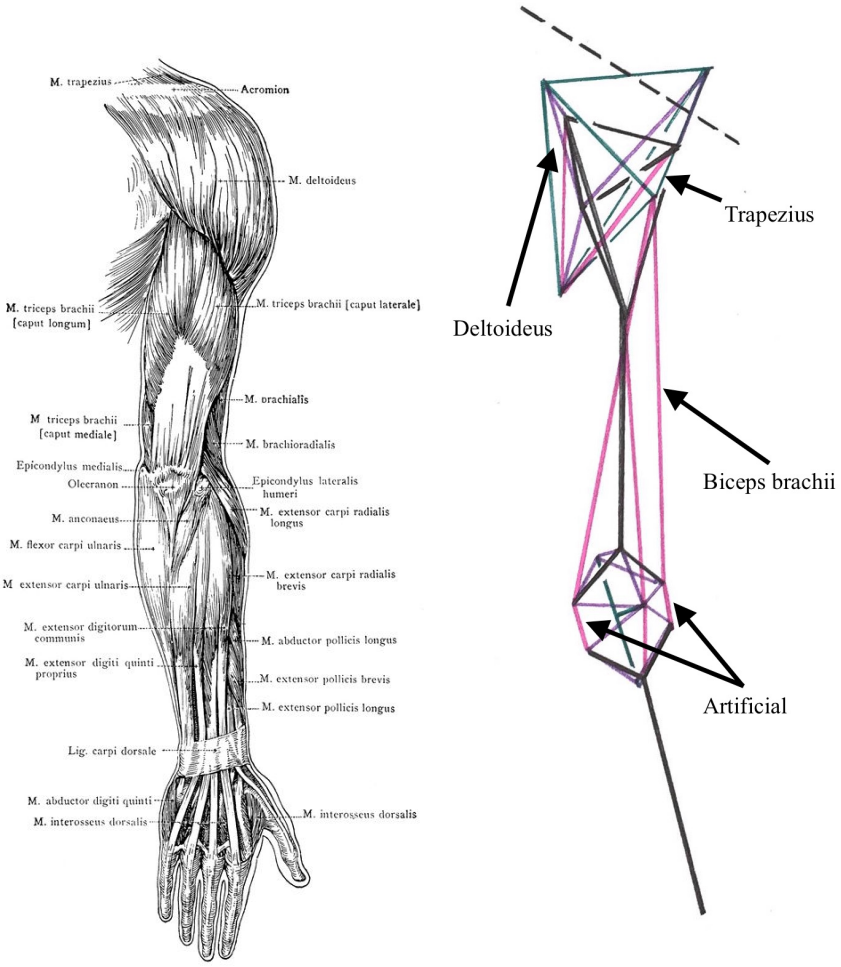

Figure 4.11: A comparison of upper-extremity muscles of the human arm (from Gray's Anatomy 41^{st} edition) and the proposed tetrahedrons tensegrity robotic manipulator. The cables (purple) indicated by the arrows are the tension members in the tetrahedrons prototype. Active cables serve an analogous role in bio-mimetic and bio-inspired robotics to muscles [39].

Saddle Shoulder Joint for a Tensegrity Manipulator

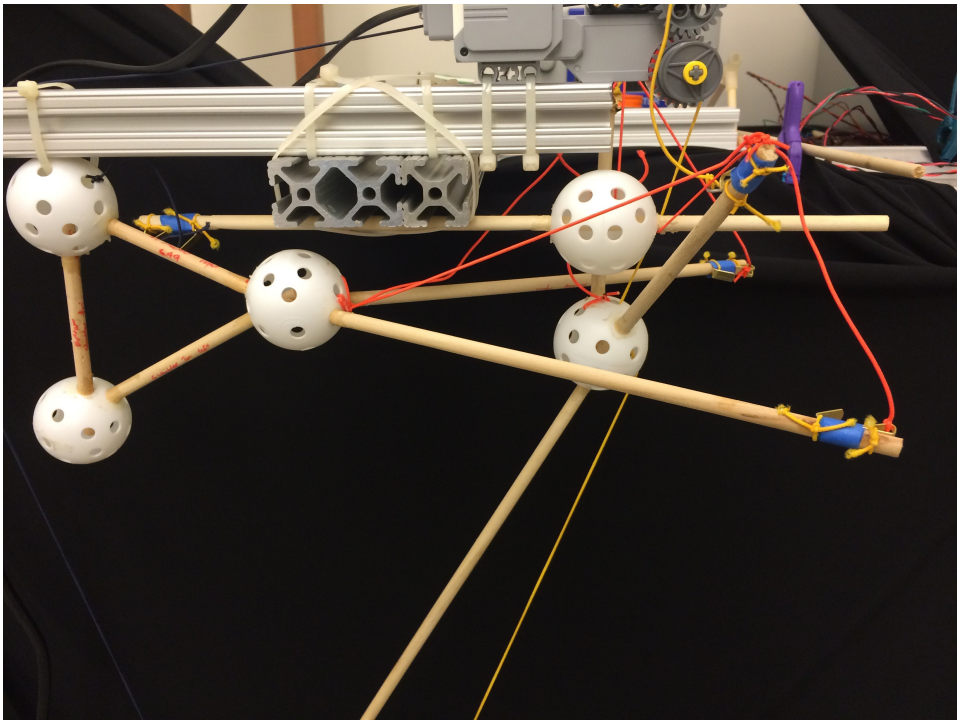

Figure 4.12: One design of a tensegrity shoulder featuring a Y-component that rests perpendicularly in tension between a single static shoulder component [39].

controlled locomotive spines [32, 83, 84]. The sinusoidal input waves, like those in the genetic algorithm, could theoretically be further refined through iterative learning. Their purpose in this experiment, however, was simply determining feasible range of motion of the tensegrity manipulators to select candidate designs for prototyping.

Each of the four proposed designs demonstrated one advantage over the others. The simple saddle model demonstrates a minimalist design that replicates the clavicle and scapula of the human arm for basic support of the rest of the manipulator.

The complex saddle extends the simple saddle model by connecting the suspended clavicle and scapula compression elements, dropping the newly-formed rigid component below the Y-shaped termination on the rest of the manipulator, and then adding an additional anchor above the entire manipulator. This last component is held in space by artificially setting its mass to 0, thus mimicking off-loaded foundation. The advantage of this model over its predecessor is that the shoulder joint itself appears to be easier to control. While the simple saddle model require two rigid components to support the rest of the manipulator, the complex model

Tetrahedrons Shoulder Joint for a Tensegrity Manipulator

Figure 4.13: One design of a tensegrity shoulder using two nested tetrahedrons as rigid units [39]. The designs of this shoulder were largely based upon the work done by Friesen et al. [81].

Elbow Joint for a Tensegrity Manipulator

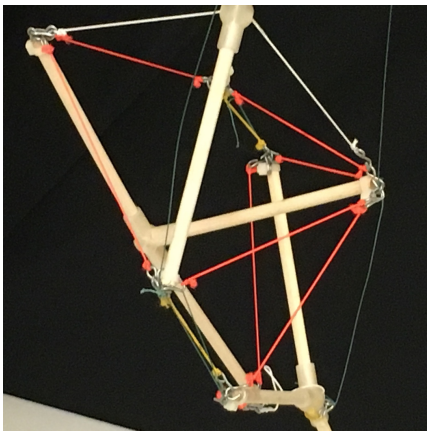

Figure 4.14: The tensegrity elbow based originally upon the passive tensegrity structure created by Graham Scarr [30]. It was replicated in a lighter weight manner for the combined multi-joint manipulator [39].

Map between Upper-Extremity Musculoskeletal System

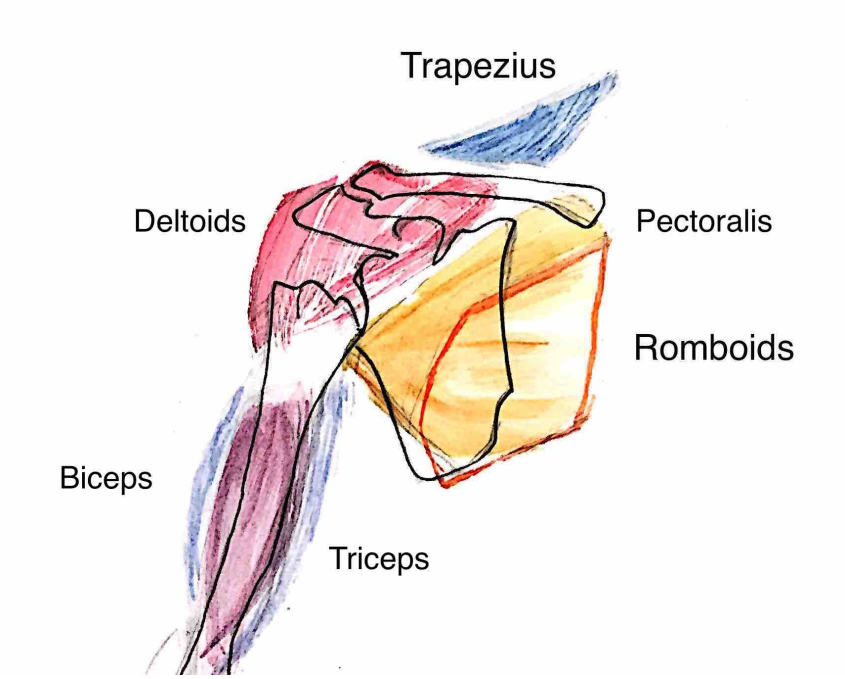

Figure 4.15: The schematic representations of the group of muscles (colored) in a human shoulder along with the involved bones (black outline) [82].

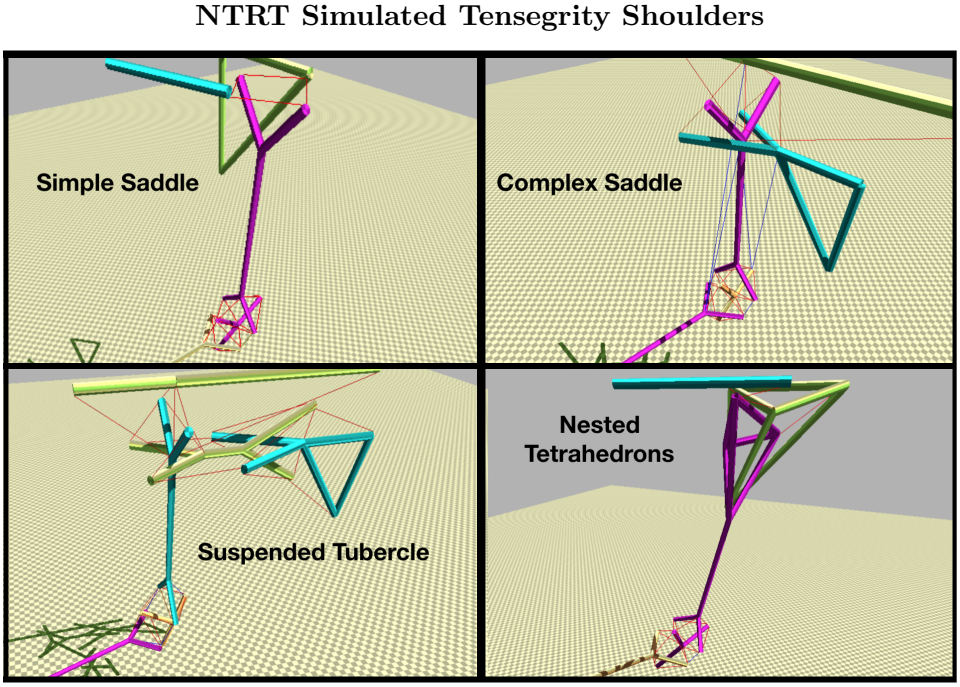

Figure 4.16: Four tensegrity shoulder designs simulated within NTRT. Thick, brightly colored rods are the simulated compression elements and the thinner lines connected to them are the simulated tension elements. Each design features a unique structure serving as the second joint within the tensegrity series that defines the respective manipulator. Each shoulder joint is located above the elbow joint (which is the same in each manipulator and derived from Lessard et al. [38].

localizes all movement into one rigid foundation. As a result, movement is localized away from the foundation itself, which is likely better for future modularity.

The suspended tubercle model features a clavicle bone (the yellow horizontal element in illustrated shoulder joint), a scapula (the horizontal turquoise element), an acromion (the yellow, double "Y" element) and a humerus head (the vertical turquoise element). This model affords the structure a lateral cushion greater than the others through its second joint. Such a design could prove useful in further studies, but we did not choose to prototype it due to its want of a single, multi-DoF joint. Multi-DoF joints are preferable as they localize more functionality in a smaller module. Theoretically, multi-DoF modules can be stitched together to recreate this cushion in future prototypes.

The final simulated model, the nested tetrahedrons model, was primarily based upon the DuCTT robot [81, 85]. In this design, two tetrahedrons are situated such that one is located above the other. The top tetrahedron serves as a foundation and actuation local to this joint is conducted through active tension members connecting this foundation to the bottom tetrahedron. This design was chosen for prototyping since it we found not only a rotational degree of freedom about which to actuate this joint, but a translational one as well. This lifting movement is loosely analogous to a shoulder shrug physiologically speaking.

4.4 Prototypes

The two chosen designs for prototyping were the complex saddle design and the nested tetrahedrons design (Figure 4.17). Each of the designs was planned for two, 2-DoF joints in serial, akin to the human arm. The differences between the two arms lie in the structure and function of their shoulder joints (Table 4.2).

Tensegrity Manipulator Prototypes

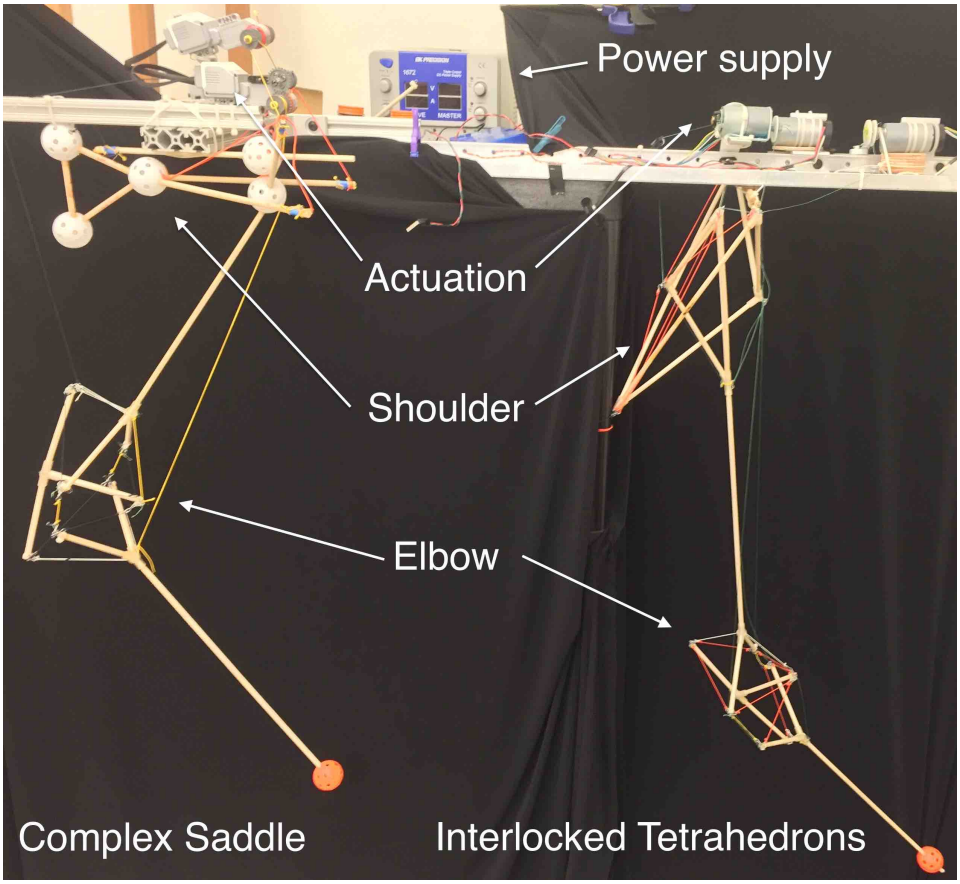

Figure 4.17: The complex saddle tensegrity manipulator (left) and the nested tetrahedrons manipulator (right) [39].

Table 4.2: Degrees of Freedom in Tensegrity Manipulators

Joint	Motion	Abstracted Biological Analog
Tetrahedrons Shoulder Joint		
Shoulder	Pitch	Forward shoulder raise
Shoulder	Lift	Shrug
Elbow	Pitch	Biceps curl
Elbow	Yaw	Artificial
Saddle Shoulder Joint		
Shoulder	Pitch	Forward shoulder raise
Shoulder	Yaw	Internal/External shoulder rotation
Elbow	Pitch	Biceps curl
Elbow	Yaw	Artificial

The rigid components of these structures are primarily wood, due to it's lightweight

Rigid Junctions for Rapid Prototyping

Figure 4.18: Rigid junctions created for connecting rigid components to one another in our tensegrity prototypes. These were crafted via 3D-printing [39].

property. A lightweight prototype requires less strong motors and less mechatronic overhead. Theoretically, different materials such as carbon fiber or plastics like the PLA used previously could be trivially substituted in. Wooden rods were fitted together to create non-cylindrical shapes using PLA junctions (Figure 4.18).

The tension elements of the tensegrity structures were the same as those used in the elbow experiments: braided Spectra cable. This material excels at lifting massive weights and is specially designed for mitigating friction caused by spinning the attached motors. Each compression element's end points were equipped with small hooks to which the tension members could attach their own hooks, allowing for replaceable components. Such a design is excellent in the event that a part needs upgrading and repair.

The motors used for both manipulators are located above the manipulator,

off-loaded from the robot. Although collocated on-structure motors are feasible, removing these motors from the manipulator allowed us to study the kinematics and dynamics of the robotic arms with minimal interference and payload.

4.5 Experimental Results and Discussion

To study the effect of the manipulators, both simulated and real results were observed and recorded [39]. Each model's specific dimensions, mass constitution, and flexibility was recorded (Tables 4.3, 4.4, 4.5, 4.6).

Table 4.3: Tetrahedrons Arm Measurements

Component	Mass (g)	Length (cm)
Forearm	10.1	58.6
Olecranon	6.0	24.0
Humerus	36.6	76.2
Shoulder Tetrahedron	24.8	36.1
Full Arm	77.5	149

Table 4.4: Saddle Arm Measurements

Component	Mass (g)	Length (cm)
Forearm	18.5	54.0
Olecranon	11.6	24.0
Humerus	23.2	53.0
Saddle Joint	36.1	54.0
Full Arm	89.4	104

Table 4.5: Flexibility Strain Limits

Movement	Range of Motion
Elbow Pitch	215 °
Elbow Inward Compression	2.6 cm
Elbow Yaw	40 °

Table 4.6: Tensegrity Joint Degree of Freedom Flexibility

Movement	Range of Motion	Standard Deviation
Elbow Pitch	36.33 °	5.03 °
Elbow Yaw (Left)	14.75 °	2.63 °
Elbow Yaw (Right)	12.00 °	1.414 °
Shoulder Pitch	21.00 °	0 °
Shoulder Lift	2.10 cm	0.368 cm

We also actuated a tensegrity manipulator to collide with a rigid object (Figure 4.21). In this demonstration, the tensegrity manipulator simply actuates around the pitch axis until it collides with the rigid object, the cardboard box. Normally, a lightweight robot should avoid collisions with more massive objects, but in this scenario, the manipulator was not damaged.

The quantitative results of sample trajectories were also used to track the exact movement and energy spent while actuating these manipulators (Figure 4.19, 4.20). Flexibility measurements were taken using a camera and video motion-tracking software by Kinovea (Figure 4.22).

4.6 Extended Analysis on Tensegrity Joints

The initial designs, prototyping, and testing of the tensegrity joints and manipulators established a scientific foundation for further study on the exotic properties of these structures and robots as a whole. A new version of the tensegrity elbow features the same geometry found in both prior iterations of the actively controlled tensegrity elbow, but now with tension and compression members that more easily connect to one another (Figure 4.23).

The new tension members were formed from injection-molds that were 3D-printed to fit their own 3D-printed compression elements. Additionally, the new material used for the tension elements was constructed out of a silicon rubber called Ecoflex. Since Ecoflex is liquid before fabrication, other materials, like the braided spectra mentioned at the start of this chapter can be embedded within the liquid for a stronger tension member. The trade-off for adding embedded materials is that they increase the rigidity of the tension member as a result.

As a result, tensegrity manipulators or even single joints could be pre-planned and modeled using CAD (Figures 4.24 and 4.25). This advanced planning allows for optimization that would have otherwise been imprecise. Quantitative analysis, like finite element analysis (FEA), can be applied to various parts of the structure to maximize their structural strength to mass ratio (Figure 4.26). Having stronger components as a result of this quantitative testing at the component level allows for an overall stronger design.

Additionally, further studies were conducted to examine the efficacy of these manipulators under different conditions. In Figure 4.27, we modulate the attachment point of one cable at the elbow to study how such details can affect the system as a whole. This particular analysis illuminates the effect of an attachment point changes the joint's ability to change pitch over time. So, selecting an attachment point of 10 or 12 cm above the bottom of the compression element will yield a faster change in pitch than a higher attachment point at 28 or 30 cm. Testing properties, like the attachment point, ahead of time affords tensegrity designers the ability to be plan at the precise component level when the initial purpose of the robot is decided.

Tensegrity Manipulator Trajectory Tracking in Simulation

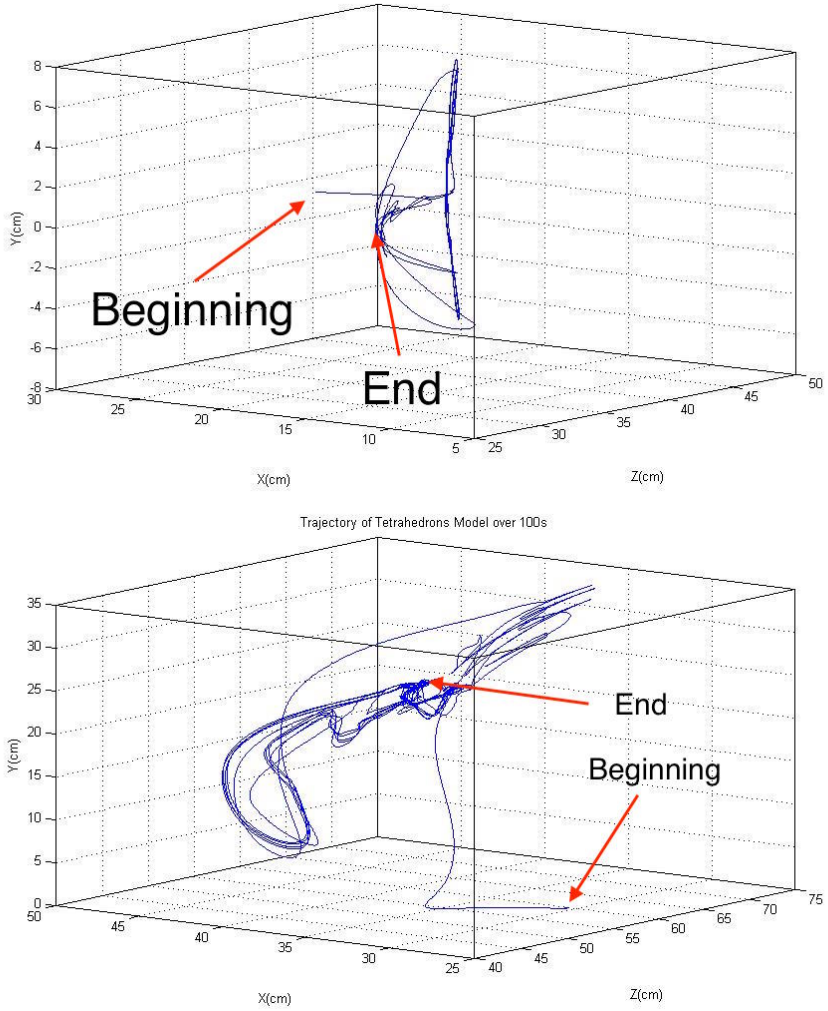

Figure 4.19: Trajectories of two of the shoulder designs within NTRT for a given control sequence. These trajectories were produced while the manipulator was given a simple control loop that instructed each actuator to operate sinusoidally, thus exercising the full range of each motor in parallel [39].

Tensegrity Manipulator Energy Expenditure in Simulation

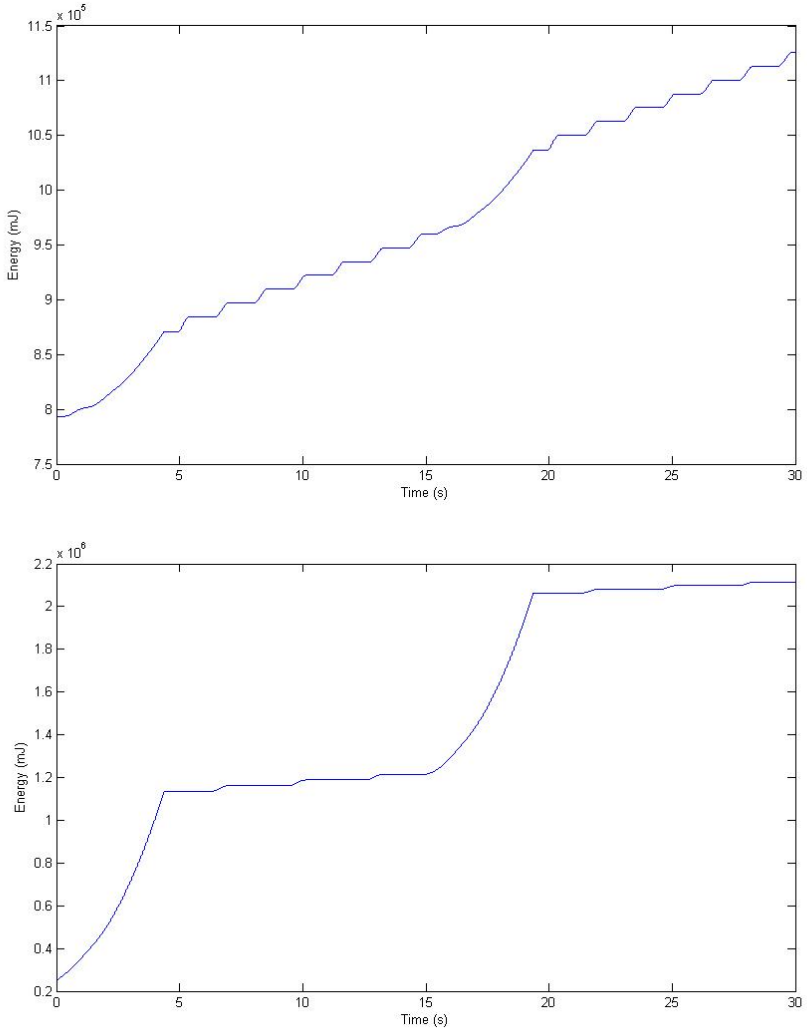

Figure 4.20: Energy spent actuating the two shoulder designs within NTRT for the control sequences in Figure 4.19. The energy spent in both cases monotonically increases since the robot can only consume energy in order to operate [39].

4.7 Reinforcement Learning

As previously discussed, the control of chaotic structures like tensegrities is challenging. Some strategies, like the multi-level Monte Carlo methods used for the tensegrity rover, can be employed to teach the robot to accomplish specific goals. For the tensegrity manipulators, we implemented a new machine learning strategy based upon reinforcement learning. Reinforcement learning is a field of machine learning where an agent learns behaviors through the accumulation of successes that yield rewards and failures that yield punishments. An agent can perform a series of actions in an environment. Whenever the agent performs an action in that environment, an interpreter will judge the outcome of that action and either reward or punish the agent.

In our case, the agent in question is the tensegrity manipulator and the state it is trying to control is its pitch, θ. Specifically, our test case is the manipulator attempting to maintain a constant pitch of 30° at all times. To achieve this, the robot can take one of three actions:

1. The motor spins forward to increase pitch
2. The motor spins backward to decrease pitch
3. The motor does not spin

As external disturbances from the environment, such as disgruntled PhD candidates, artificially change the pitch of the robot, the robot can perform an action to resume its desired state. So, if the sensed pitch (as read by the motor encoder) is interpreted as too high, the robot will want to spin its motor backward to decrease the pitch and compensate. The rate at which it does this, however, is the factor which must be learned by the robot. Decreasing too quickly may overshoot the target pitch and decreasing too slowly is not fast enough. Every time the robot performs an action for a step length of time, the interpreter will judge its performance. A reward is offered if the manipulator does not overshoot and that reward's size is increased if the manipulator reaches an acceptable threshold within 30°. There is a

punishment if the robot overshoots its target pitch. We demonstrate the ability of the robot to respond to external disturbances in Figure 4.28.

Here, we observe two disturbances performed one after another on the robot. After an initial period from $t = 0$ steps to $t = 40$ steps where the robot first reaches its target pitch, a disturbance is felt at $t = 70$ steps[1]. The robot compensates and actuates opposite the disturbance. After a relatively large overshoot, the robot changes the direction of its motor's spin and eventually reaches and remains at $\theta = 30^\circ$ at $t = 110$ steps. At $t = 120$ steps, another disturbance is felt. Although the disturbance is in the opposite direction, the robot responds more intelligently the second time and reaches its goal pitch more quickly than before. The first disturbance took the robot 40 steps to correct but the second disturbance required only 20 steps to correct. This result derives from the robot learning to spin its motor less quickly so that way it doesn't surpass the target pitch. Future learning may improve upon this achievement further.

[1] One step is $\frac{1}{30}$ of a second.

Tensegrity Manipulator End Effector Collision

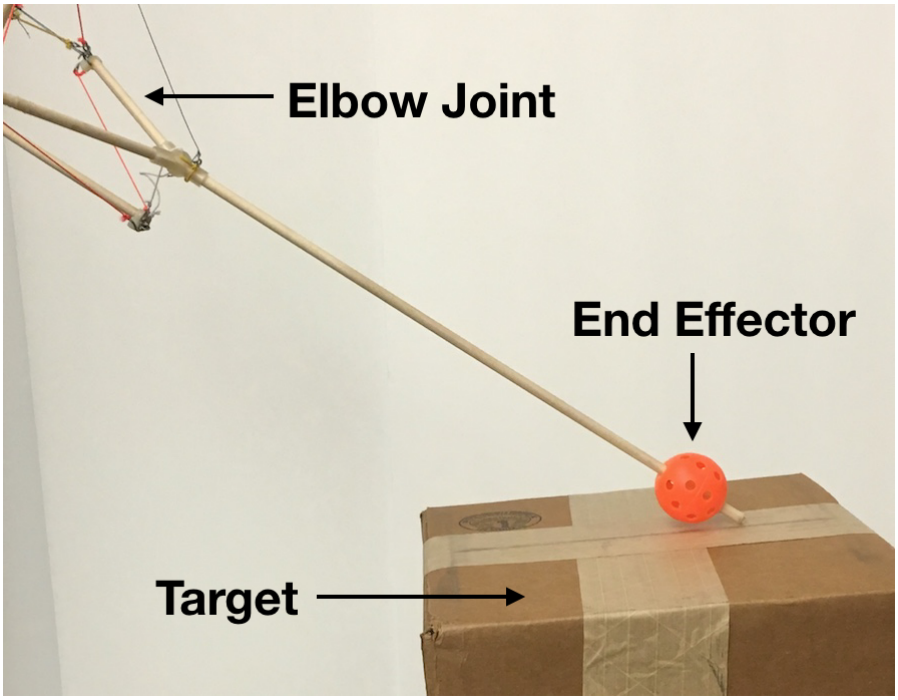

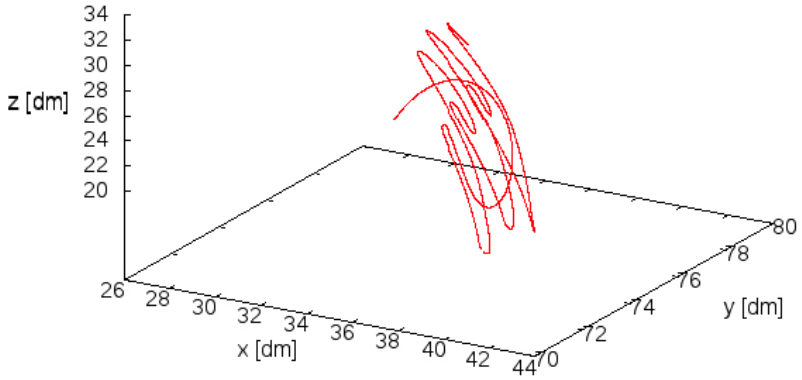

Figure 4.21: The trajectory of the end-effector on one of the tensegrity manipulators as it collides with a rigid object during pitch motion. The plot illustrates the elastic collision of the end-effector as it contacts a rigid target (the cardboard box). This demonstration underlines the important feature of tensegrity devices: their ability to passively distribute external forces like collisions without destroying the structure [39].

Tensegrity Manipulator Tracked Workspace

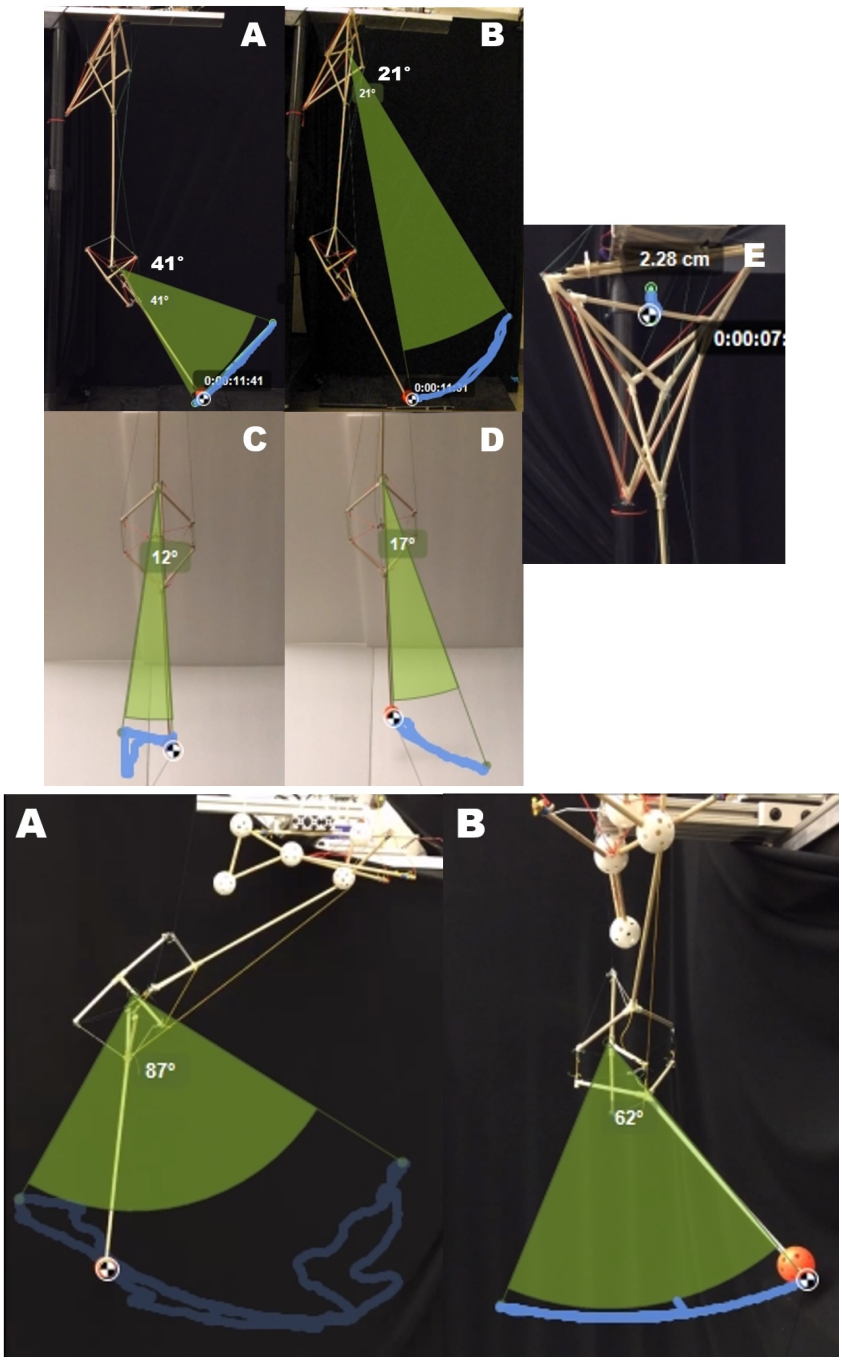

Figure 4.22: The tracked movement and range of motion of the tensegrity manipulators [39]. Movements were tracked using a camera and Kinovea software. Tetrahedrons Model: A: Shoulder Pitch, B: Elbow Pitch, C: Right Yaw, D: Left Yaw, E: Shoulder Lift
Saddle Joint: A: Elbow Pitch, B: Arm Yaw

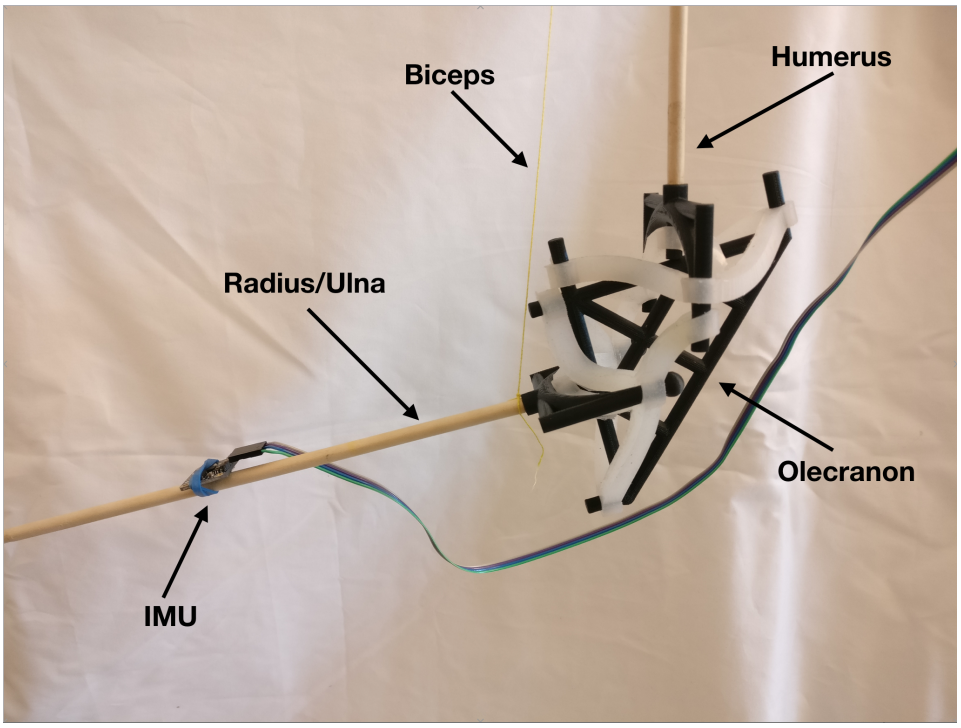

Figure 4.23: The third iteration of the tensegrity elbow. This iteration of the design uses Ecoflex passive tension elements for better shock absorption and a local IMU on the radius/ulna for collocated control algorithms.

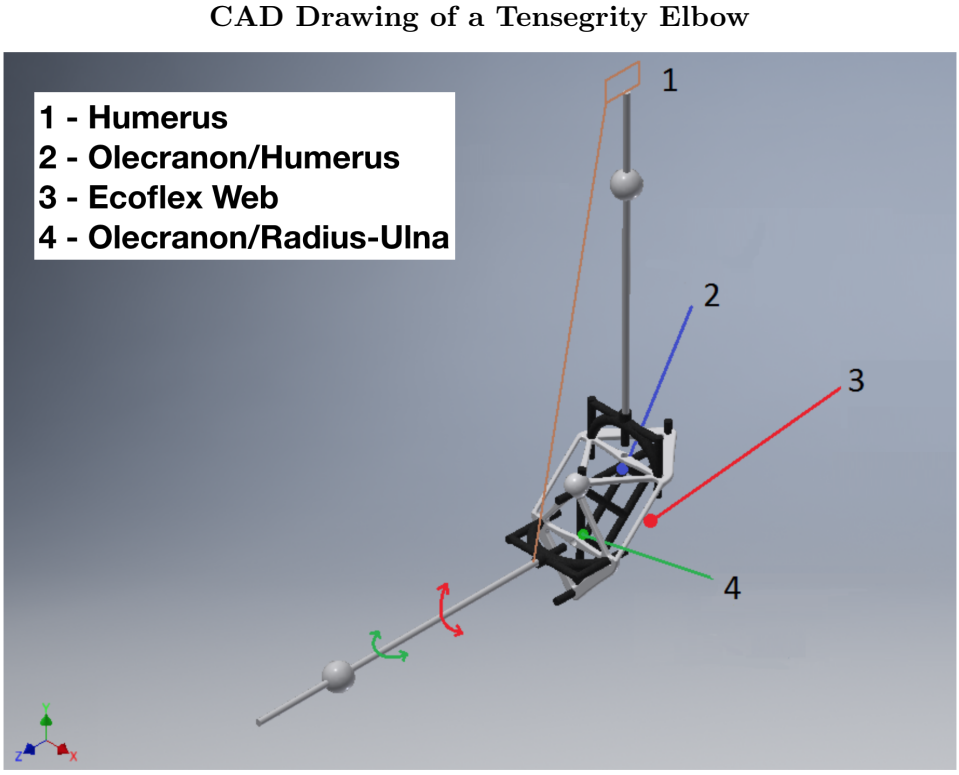

Figure 4.24: A tensegrity elbow modeled using CAD. A humeral compression element (1) anchors the robotic arm as it rotates about the pitch axis. The major connections (2 and 4) detail where the elbow joint bends to accommodate this movement. In this new prototype, Ecoflex silicone (3) provides a soft medium that complies and flexes as the robotic joint moves. Although NTRT is an excellent simulator for tensegrity manipulators, CAD drawings of tensegrity robots allows for them to be more easily exported for manufacturing, as is the case in the robot depicted in Figure 4.23.

CAD Drawing of a Tensegrity Manipulator

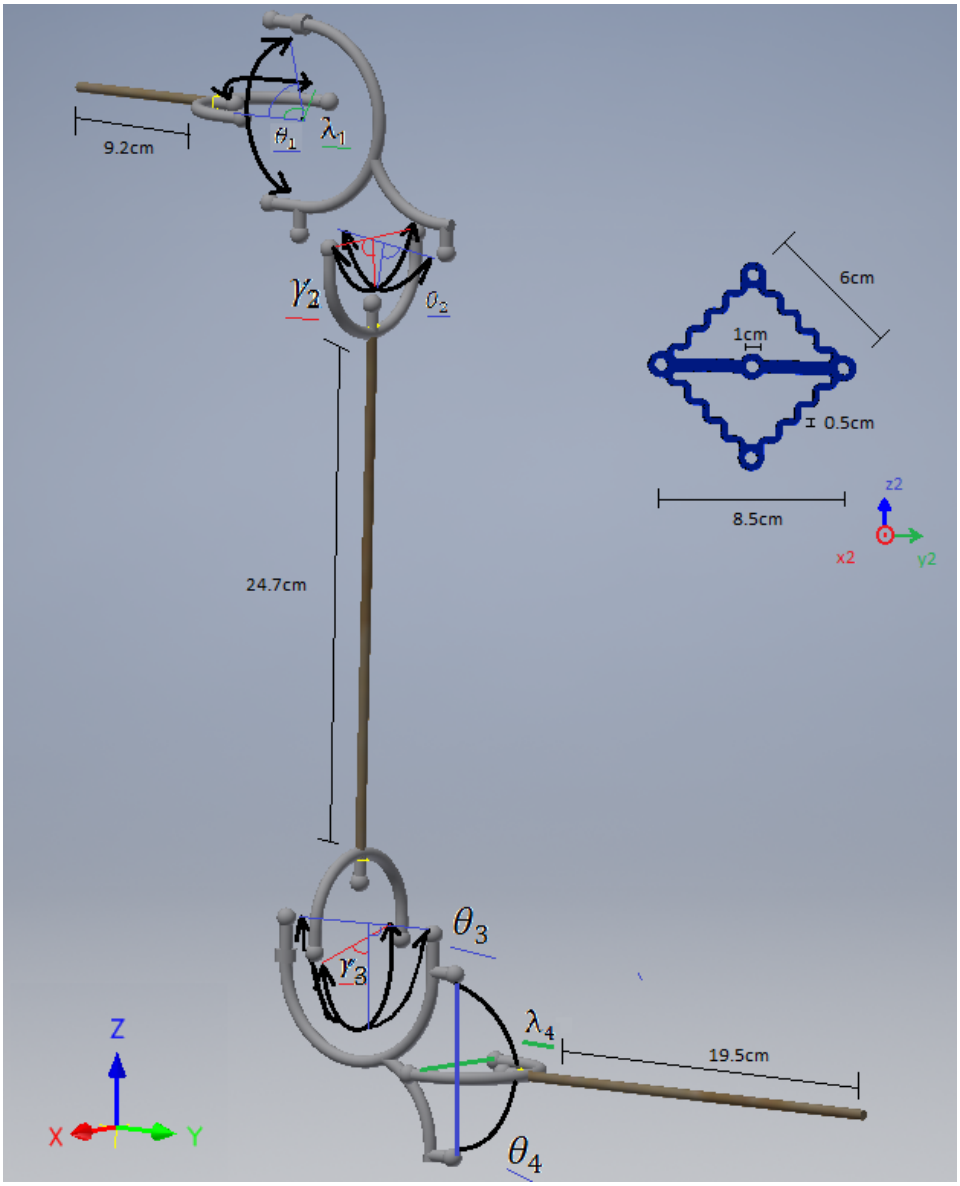

Figure 4.25: A tensegrity manipulator modeled using CAD. Although NTRT is an excellent simulator for tensegrity manipulators, CAD drawings of tensegrity robots allows for them to be more easily exported for manufacturing, as is the case in the robot depicted in Figure 4.23.

Structural Analysis of Compression Elements using FEA

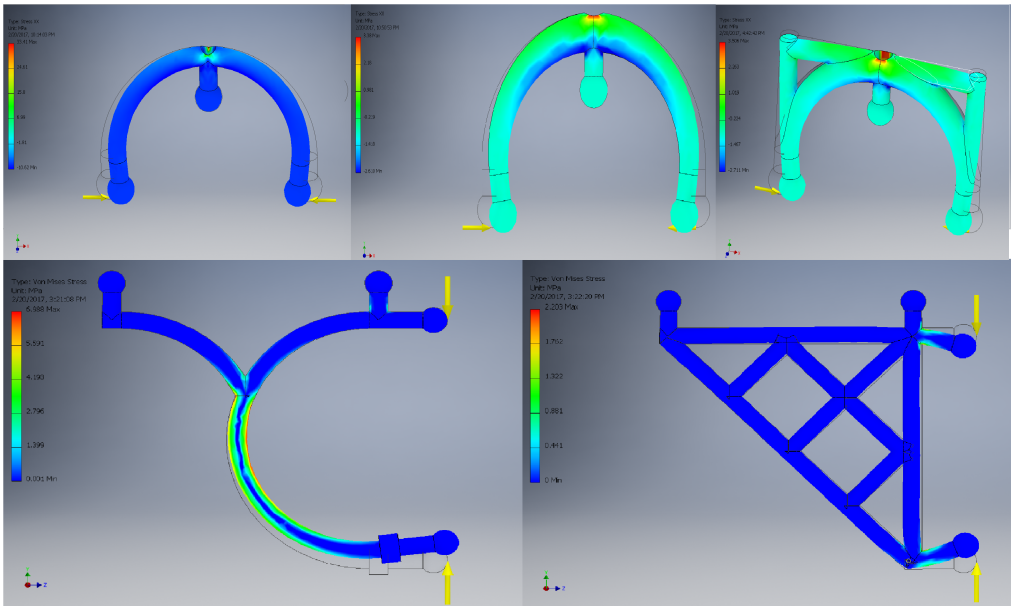

Figure 4.26: A compression element is analyzed within a CAD program, such as Autodesk Inventor or Solidworks, to determine its stress profile. We simulated 2 N of stress on the parts within the CAD program. In this plot, discolored parts receive more stress than the blue regions. Automated refining programs within the CAD studio optimize the structure to minimize these stress points.

Change in pitch per step as a function of Joint Insertion Angle

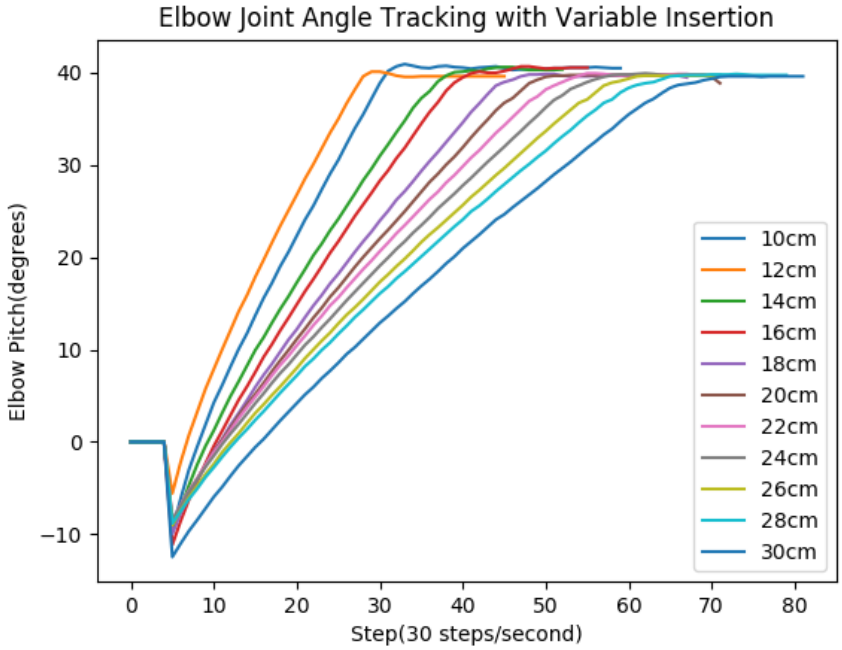

Figure 4.27: The effect of changing where a cable in the elbow joint is attached to its $\dot{\theta}$. Constructing the robotic joint to have a steeper angle yields a slower rate of change per step within the range of 10cm to 30cm.

Tensegrity Manipulator State over Time when Controlled via Reinforcement Learning

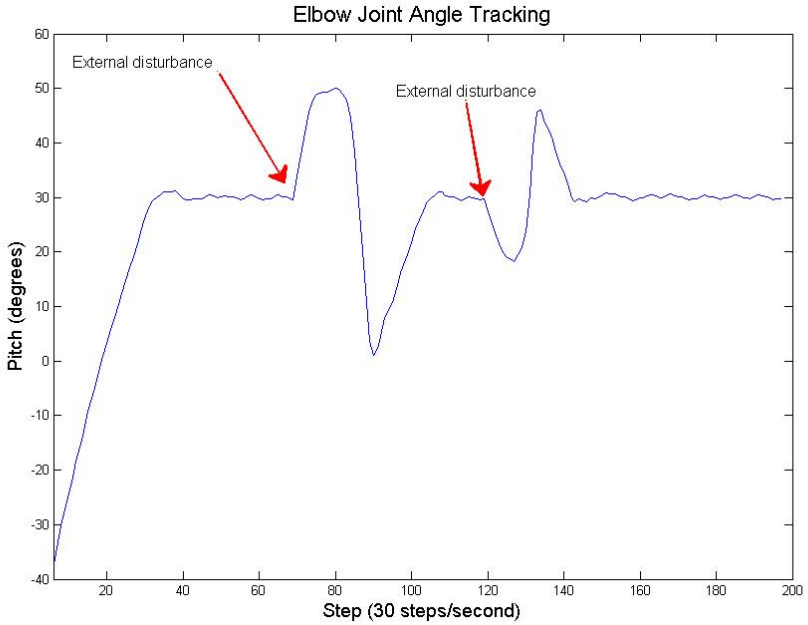

Figure 4.28: A learned response of the tensegrity manipulator when experiencing external disturbances. The manipulator returns to its initial state ($\theta = 30°$) after each disturbance through agent-based learning.

Chapter 5

SOFT EXOSKELETON SYSTEM

Tensegrity structures teach the value of hybrid soft-rigid structures. Through the study of combining rigid components with tension networks, we can create flexible robots that conform to the morphology and physiology of the human body. The traits that are characteristic to human compliance and flexibility are inherent to tensegrity structures. For that reason, the primary inspiration for our soft exoskeletons (also known as "exosuits") is tensegrity structures. Bio-inspired manipulators specifically illustrate novel solutions for combining rigid and flexible components to create and augment upper-extremity movement. In this chapter, we discuss our development of CRUX: the Compliant Robotic Upper-Extremity Exosuit. We describe how CRUX has evolved and improved with each design and prototype iteration. We conclude with a performance analysis and user evaluation which quantitatively and qualitatively measures the efficacy of our exosuit in performing tasks that involve upper-extremity augmentation, including physical therapy.

5.1 Modeling Human Motion

Tensegrity structures and robots, like the manipulators designed and tested in Chapter 4, provide novel mechanisms for understanding the fluid and flexible movement

characteristic to humans. Although these mechanisms prove useful when designing hybrid soft-rigid structures and robots, a more thorough analysis of biological and mimetic human motion further hones one's understanding of bio-mechanics. In pursuit of this knowledge, we examined the modeled bio-mechanics of the human arm via OpenSim. Using the MoBL-ARMS [86] OpenSim [7] simulation, we examine the antagonistic relationship between the biceps and triceps as they perform a reaching movement (Figure 5.1).

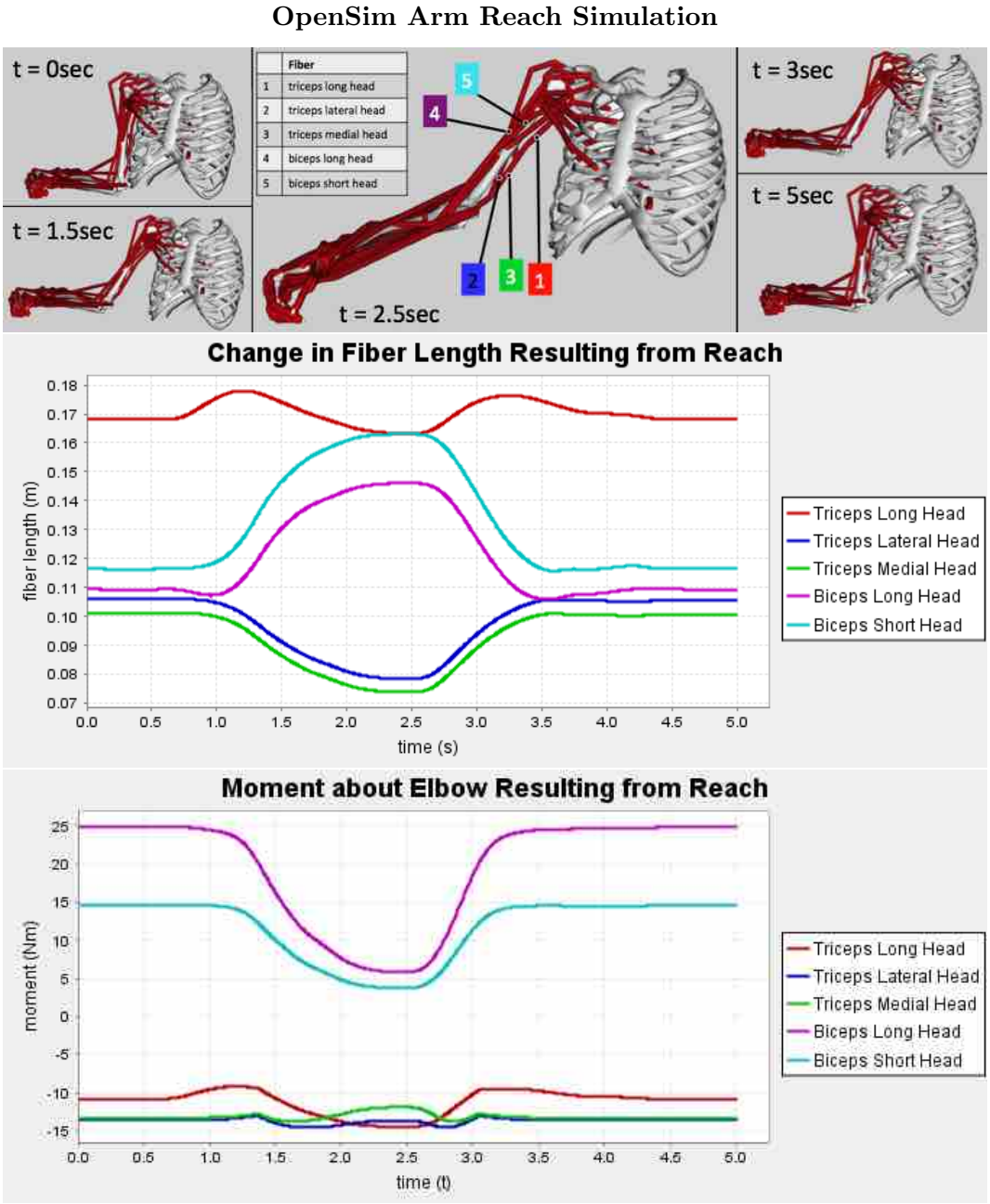

Figure 5.1: The fiber length and elbow moment of a human arm, modeled in OpenSim. By tracking the state and change of various muscles and joints in the human upper-extremity in real time, we can observe the convoluted harmony between each muscle and the arm's physiology as a whole [60].

This movement demonstrated in Figure 5.1 describes a user's arm mechanics and dynamics as they reach forward. The movement requires all major muscles in the upper extremity in order to execute and is therefore a great candidate to examine the interplay between these muscles. Both the deltoids and the triceps

must simultaneously engage to extend the hand forward. Examining just the elbow joint, we observe how the evolving moment influences the length of each muscle fiber in the biceps and triceps.

In Figures 5.2, 5.3, and 5.4, we observe the simulated results of a user performing a biceps curl. Figure 5.2 shows the fibers of the biceps and triceps at three different time steps during the exercise. The plots in Figure 5.3 illustrate the change in fiber lengths and the moment about the elbow required to execute a biceps curl. Figure 5.4 describes the activation energy spent by the arm, component by component and in aggregate as the muscle is provided energy to perform a biceps curl. We can be observe in these simulations that the biceps and triceps act inversely to each other and in fact form an antagonistic pair, consistent with the findings presented by Solomonow et al. and Gordon and Ghez[4]. The fiber length of the biceps decreases as the fiber length of the triceps increases. The moment about the elbow produced by the biceps is positive while the moment produced by the triceps about the elbow is negative. These results back up the findings from Figure 5.1 in how we characterize the antagonistic relationship between pairs of muscles like the biceps and triceps.

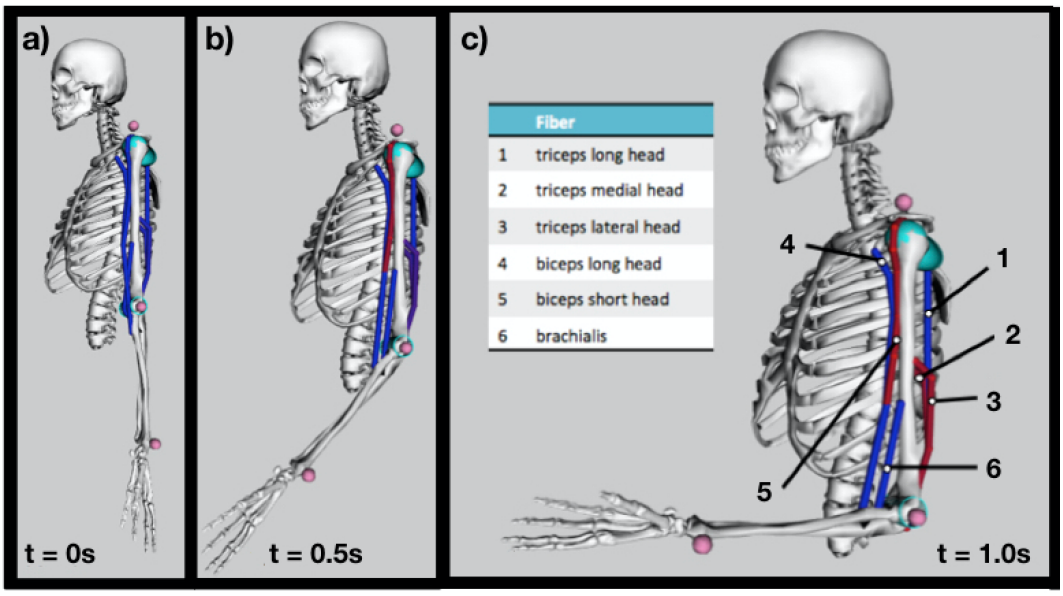

Figure 5.2: An OpenSim [7] simulation of a biceps curl. As the biceps contracts in length, the triceps elongates, due to the resulting moment about the elbow [62].

From these results, we can design an exosuit based upon similar principles. Studying antagonistic pairs in particular allows us to map tensegrity principles (i.e.

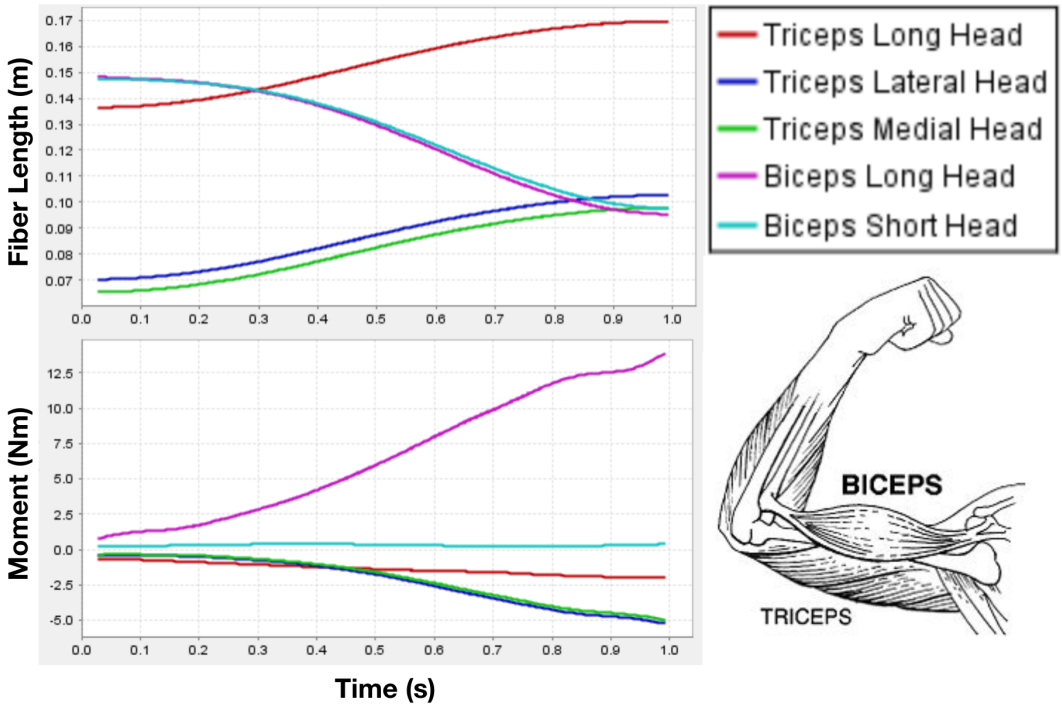

Figure 5.3: An OpenSim [7] simulation of the fiber length and moment of triceps and biceps from a biceps curl shown in Figure 5.2. This simulation describes the antagonistic nature of the biceps and triceps, an attribute common throughout the human upper-extremity where the contraction of one muscle yields an inversely proportional elongation of the other and vice versa [62].

tension networks providing compliance) to upper-extremity wearable devices. The implementation of this mapping is discussed in the remainder of the chapter.

5.2 Prototype 1: Basic Soft Exoskeleton

After performing an analysis of the tensegrity robots, we began designing a novel exosuit. We had two primary goals for our exosuit: to augment upper-extremity movement and to not impede user flexibility. Additionally, an ideal exosuit in our designs would be portable, easily to don, and comfortable. We also made sure that none of these goals sacrificed user safety. In our first prototype of CRUX, we created a simple, portable exosuit that could augment six separate motions (Figure 5.5).

This prototype features a neoprene base. Neoprene is a lightweight material that flexes well but also maintains its shape (unlike fabrics such as elastane). Six motors, located on a metal chassis on the back, pull cables attached to the exosuit's

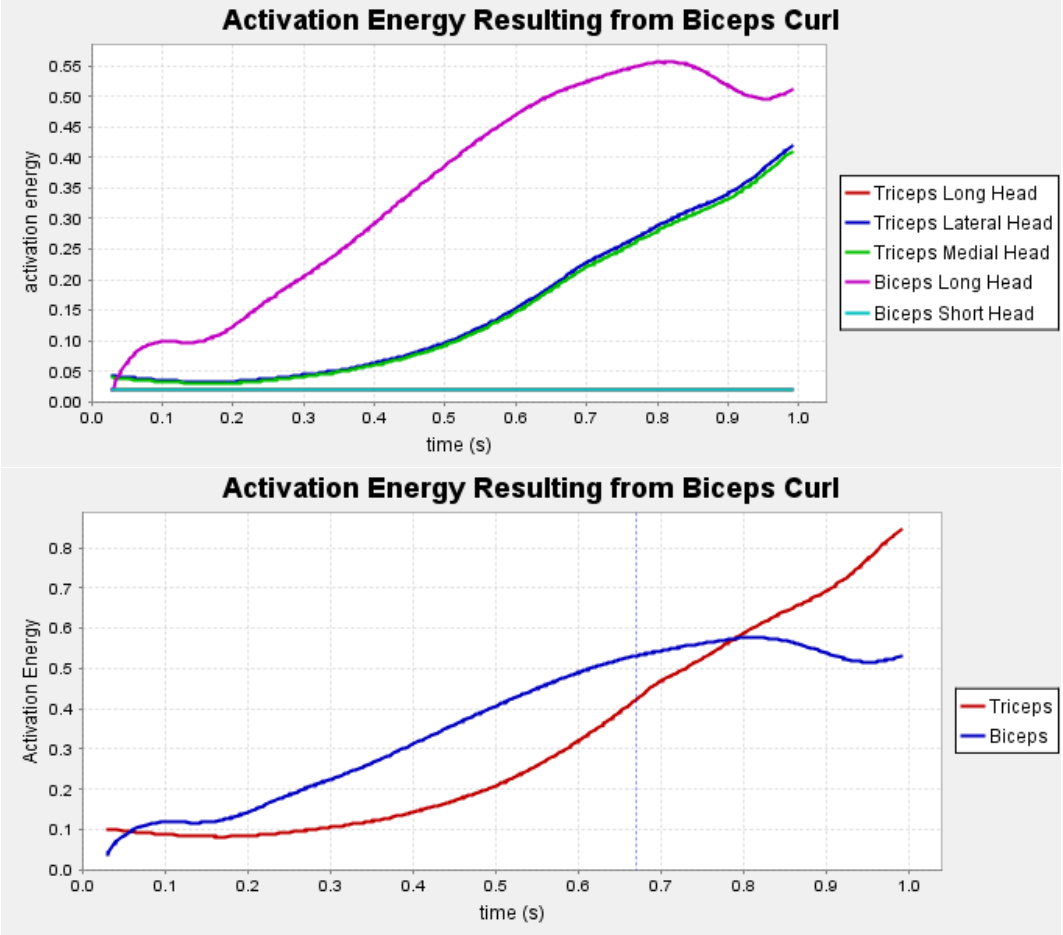

Figure 5.4: The activation energy of a biceps curl. The activation energy is the energy spent by the body to produce an action. In these two plots, we see the energy provided to each muscular component over time and then the sum of the related components (i.e. biceps and triceps) over time.

right arm. These cables are routed and attached along the arm such that they pull synchronously with a major muscle or muscle group in the upper-extremity. Specifically, these muscles are: the biceps, the triceps, the anterior deltoids, the medial deltoids, the posterior deltoids, the supinators, and the pronators. Cables are attached to the exosuit with metal anchors. These anchors are fastened to the exosuit with neoprene cement. Other methods of attachment may have unnecessarily increased the exosuit's rigidity.

This exosuit, the "proto-CRUX", was an interesting robot because it illustrated the tensegrity principles previously studied before on a wearable device. This exosuit exemplified basic augmentation for users through rudimentary, pre-programmed

open-loop control.

However, the construction and user testing of this exosuit demonstrated some draw-backs. Qualitatively, many users complained that the exosuit was too difficult to don. Likewise, the goal of unmitigated flexibility was not met since users had trouble moving their back and trapezius muscles. This inflexibility was attributed to the rigid metal chassis the mechatronic components were housed on. Users also agreed that the open-loop control had limited application. Since motions had to be pre-planned by the operator, a user could not spontaneously perform actions as one might expect with most upper-extremity activity. Additionally, this pre-planned action could only be programmed using a laptop and programming knowledge. Users also cited one concern to be that cables, especially around the shoulder, would often dig into the exosuit at awkward and unanticipated angles during an exercise, forcing them to compensate their movement accordingly. From a design perspective, this is not just a comfort issue, but a goal issue as well. Users who must inappropriately compensate their movement to use a device are likely to develop unhealthy habits, completely defeating the rehabilitative purpose of the exosuit. For these reasons and from our other observations of "proto-CRUX", we identified new design goals and carefully redesigned the exosuit into what is now CRUX [60, 62].

5.3 Identifying the Lines of Minimal Extension

The first step of the redesign of CRUX was ensuring that the exosuit properly conformed to the user's body. Although multiple people would be using the same exosuit for our user testing, we believed that if we used one characteristic user to design our exosuit, it could serve the other users well enough to complete performance based objectives, such as rehabilitative outcomes. For this reason, we sought to define users morphologically and physiologically with a unique identifier: their lines of minimal-extension.

5.3.1 Defining the Lines of Minimal Extension

Our definition of lines of minimal extension comes from a similar measurement, the lines of non-extension. Extensively studied originally by Iberall et al. in 1964 for extraterrestrial counter-pressure suits, lines of non-extension were defined as ellipses around the body where a person's skin would not stretch as he or she moves their body [9]. Further studies by Wessendorf and Newman explored lines of non-extension also for the use of extraterrestrial counter-pressure suits. These engineers developed novel ways to couple shape-memory allows, a very thin and powerful type of actuator, into fabrics. This gave their pressure suits a much less bulky, yet relatively flexible characteristic [8, 87]. While Iberall et al. manually tracked lines of non-extension, Wessendorf and Newman used speckled paint and motion capture to observe morphological changes in the skin.

For our designs, we differentiate our lines of minimal extension from lines of non-extension to account for differences between test subjects and the added overhead of wearable devices. The precise ellipses of skin that do not stretch vary from person to person so we account for this variability by looking for minimal stretching between users. Additionally, when a wearable device is donned, the wearer's morphology changes slightly, even for flexible devices such as ours. True lines of non-extension are inherent to the skin of the body and do not account for the aforementioned factors. As a result, lines that minimally extend when wearing an exosuit do not pedantically fit the definition of "non-extension". Although this definition is minor, it does emphasize the necessary consideration designers must make when designing a flexible wearable device. Lines of minimal extension are therefore useful when concessions must be made for a wearable device, especially if it is shared by multiple users. To account for this discrepancy, we perform our motion capture to identify lines of minimal extension with users wearing garments (Figure 5.6).

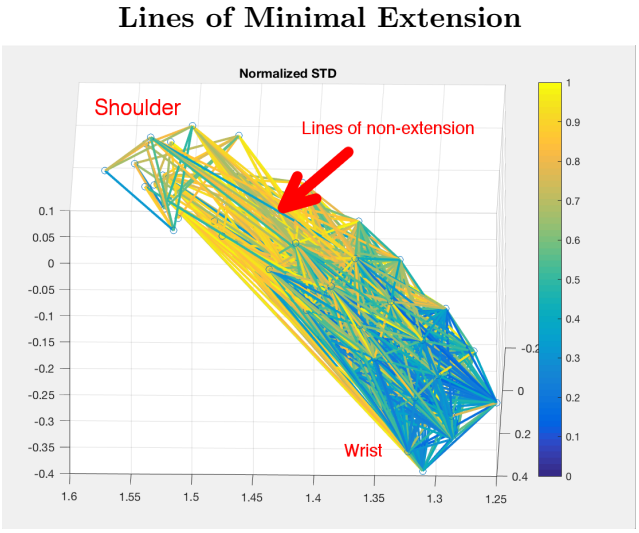

Figure 5.6: A subsection of a user's lines of minimal-extension. The gradient observed in this plot depicts the level of movement observed between the two end points of a particular drawn line The end points of these drawn lines are delimited on a user by IR-reflective dots which the CAVE cameras track in 3D space [60].

5.3.2 Motion Capture Process

To begin the motion capture process for identifying lines of minimal extension on users, we first created garments equipped with IR-reflective dots. Motion capture was performed in a Mechdyne CAVE (Cave Automatic Virtual Environment) (Figure 5.5). The CAVE is a 3x3 m^2 platform surrounded by three walls. These walls can have projected displays, but the features relevant to the four cameras located above these walls. These cameras display and capture at a 120 Hz refresh rate, ideal for virtual reality. They are also capable of precision within 2.0mm consistently and 0.3mm in ideal scenarios.

Users tracked in the CAVE are given one of two garments to wear. The first garment tracks the forearm from the elbow to the wrist (Figure 5.8A). The second garment tracks the upper-arm from the shoulder to the elbow. IR-reflective dots were attached uniformly across the surface of the entire garment at a rate of about one dot per 4 in^2. These dots, once tracked by the CAVE's cameras, produced trajectories as the wearer moved through space (Figure 5.8A). The precise movements performed by the wearer, listed in Table 5.1, were selected to fully test the range of motion in the shoulders, about the elbow, and in the forearm.

Table 5.1: Movements Performed during Motion Capture to Identify Lines of Minimal Extension

Movement	**Range of Motion (°)**
Shoulder Adduction and Abduction	200
Shoulder Extension and Flexion	200
Elbow Extension and Flexion	150
Wrist Pronation and Supination	160

Once the measurements were recorded, the precise results were studied. As shown in Figure 5.8, the plotting program measured movement between dots. The dots with the greatest movement between them rendered yellow and the dots with the least movement between them rendered darker. From this, we found which parts on the skin would move the least as a user exercised. These lines of minimal extension are then annotated on separate fabric (e.g. a neoprene base-layer) for later prototyping. On these parts, we would attach rigid on-suit elements, such as cable housing. To maintain overall flexibility in the exosuit, rigid elements should be forced to move as little as possible. Once the placement of the rigid elements is determined, a cable map can be produced.

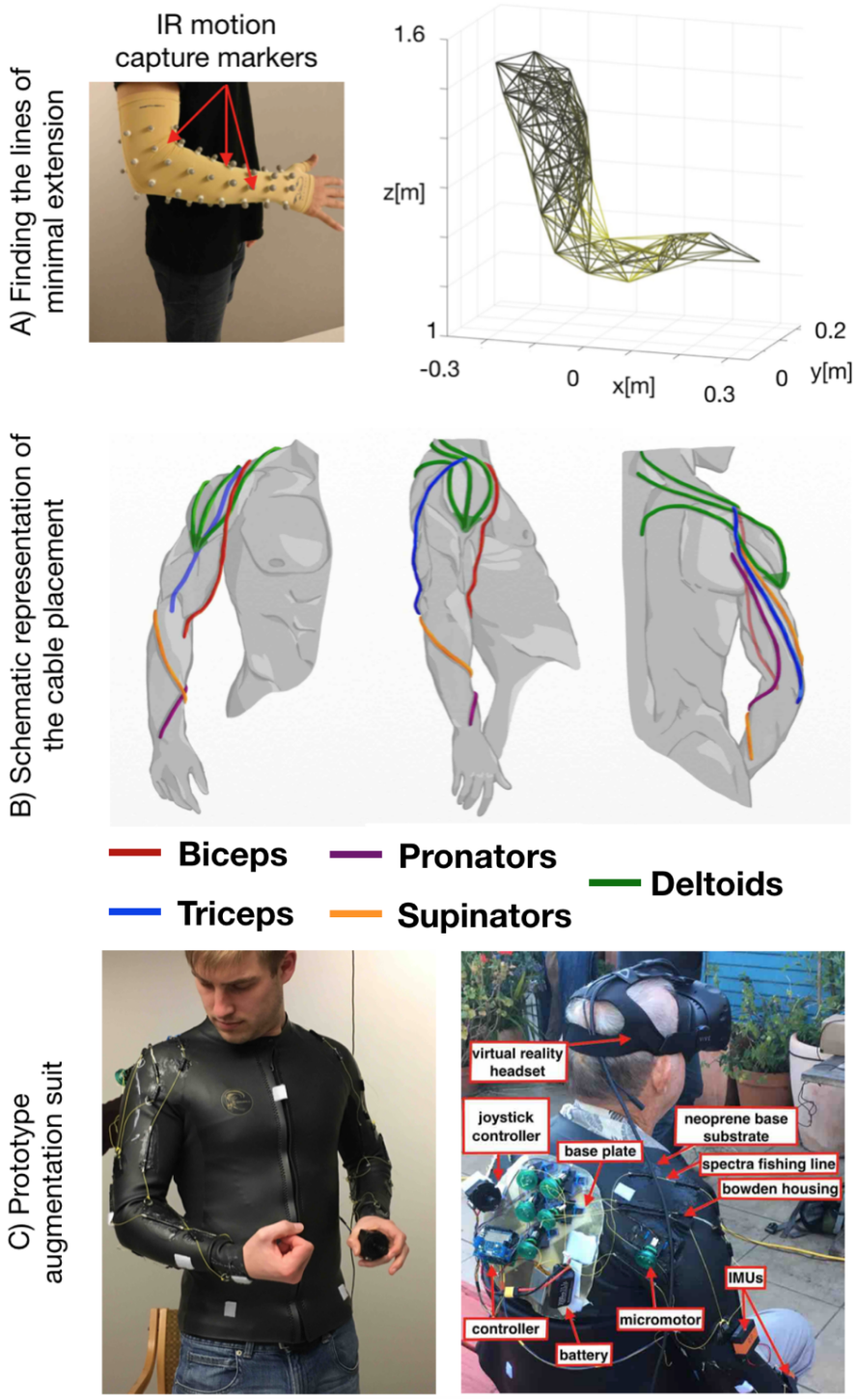

Figure 5.8: Designing CRUX in three stages [62]. In part A, we identify a user's lines of minimal extension via motion capture. In part B, we derive a cable map from the found lines of minimal extension. In part C, we produce the resulting prototype and test it on users.

5.3.3 Exosuit Customizability and Personalization

One interesting property to note about identifying the lines of minimal extension is that it can be repeated relatively quickly for any person who is studied under motion capture. This means that customizing exosuits for individuals can be streamlined and users' unique cable maps identified efficiently. One qualifying condition for producing these maps, however, is ensuring that the tracker garment fits the subject well. The greater the correlation between subject muscular movement and IR-reflective dot movement, the more accurate the produced lines of minimal extension. Just as one would not wear ill-fitting clothes, one should not produce a map of their lines of minimal extension with ill-fitting tracker garments.

5.4 Cable Map

From a lines of minimal extension analysis, we determined the optimal paths along which mechanical power should be transferred. The collection of the paths, the cable map, is bilaterally symmetrical since the upper-extremities are bilaterally symmetrical. To determine which muscles and muscle groups we would augment with a cable, we read previous studies on muscular strength indication. Ikai and Fukunaga observed in 1968 that muscular cross-sectional area is a sufficient determinator for muscle strength [88]. Principal component analysis and cluster analysis by Bohannon and Andrews also demonstrate the impact of stroke-induced paresis on upper-extremity movement [89]. Likewise Motricity Index, which measures motor function in muscles, indicates of paretic upper-extremity strength in stroke survivors as shown by Bohannon et al. [90].

From these findings, we then atomized arm movement into distinct sub-movements called motion primitives. Motion primitives are movements that are achieveable in one, unique degree of freedom. The motion primitives we chose to augment are: humeral rotation (in and out), elbow flexion and extension, wrist pronation and supination, lateral shoulder raise, and forward shoulder raise and lower. We explicitly chose not to augment lateral shoulder lowering since gravity already provides

enough force to achieve this motion when users are upright.

From these determined criteria, we outlined the following muscles and muscle groups for augmentation: the biceps, the triceps, the anterior, medial, and posterior deltoids, the pronators, and the supinators. Fortunately, these muscle groups were the same ones selected for the design of the "proto-CRUX". For that reason, we knew the cable map would be similar. The precise cable map chosen is depicted in Figure 5.8B. In this cable map, there are 14 total cable paths identified, 7 for each arm. Once the cable map was identified, we began construction on the prototype.

5.5 CRUX Prototype

The prototype of CRUX (Compliant Robotic Upper-extremity eXosuit) was constructed in a similar fashion as the "proto-CRUX", but with the additional analysis provided from user feedback on the "proto-CRUX" as well as the lines of minimal extension data.

5.5.1 Base layer

The base layer for CRUX, like its predecessor, is neoprene. The neoprene is 2mm thick around the torso and 1 mm thick on the arms. Unlike proto-CRUX, CRUX has a zipper on the ventral side of the base layer for easier donning and doffing. The purpose for the neoprene, like in the first prototype, is to provide a flexible base.

One downside that is common amongst upper-extremity exoskeletons is that they have trouble providing a foundation for the robot's structure. Lower-limb exoskeletons can use the pelvis and the ground to support movement, but upper-extremities cannot. For this reason, the tensegrity based construction of the exosuit serves an excellent purpose. As previously mentioned, tensegrity structures distribute forces throughout the entire network. This provides an anchor for augmentation generated by the in-network motors. Although this exosuit does not follow the dogmatic definition of traditional tensegrity structures (i.e. only rods for compression elements and only cables for tension elements), it still abides by using a network of tension members and compression members. Specifically, the base

layer itself serves as the primary tension member, linking all topical components directly to one another. The high modulus of elasticity in the neoprene thus mitigates extreme movement that isn't local to the portion of the exosuit being augmented.

5.5.2 Power-lines

To populate the proposed cable paths, we constructed power-lines (Figure 5.9). Power-lines are the cables that stretch from motor to anchor point as well as the housing that guides them. These power-lines are segments of Bowden housing serially spaced and separated along each cable path. As a result, there is one power-line per cable path. Power-line length is dependent on what proportion of the associated cable has been wound into the motor spools. This length, and consequently how much has been wound, should directly correlate to the augmented muscle's activity. Specifically, when one of the upper-extremity muscles is completely relaxed, it is fully elongated. The matching cable is then minimally wound in the spool. Another interesting observation is that that muscle or muscle group's antagonistic partner (if one exists) is inversely proportional in length. Since the antagonist cable must be inversely proportional to its agonist cable, the lengths of the antagonistic pairs can be summarized thus:

$$L = l + cx \tag{5.1}$$

$$0 \leq c \leq 1 \tag{5.2}$$

$$l = \Sigma h \tag{5.3}$$

In these equations, L is the expressed length of a power-line, l is the minimum length of the power-line, c is the percentage of contraction, x is the length of the exposed cable when the power-line is at maximum length, and h is each housing segment length. If the above properties in Equations 5.1, 5.2 hold, then for any pair

of antagonistic power-lines:

$$c_1 + c_2 = 1 \tag{5.4}$$

The construction of these power-lines consists of braided-aramid cable for the tension member and Shimano bike tubing for the housing. These two materials were chosen because both of them are designed to reduce friction as cable passes through the housing. The tensile strength of the cable is rated to 50 lbs-force (220 N), but due to other restrictions, this theoretical limit is never reached during expected use of the exosuit.

The segments of the housing, which can be described as a subset of the length of the power-line were placed reductively. Beginning with a power-line completely encased by housing, a user who fit CRUX's dimensions donned the exosuit. The housing was removed from the portions previously highlighted by the motion capture study. Next, the user moved their arms according to the same movements outlined in Table 5.1. Housing was removed in minor pieces at a time until the user could perform the movements without impediment from the housing. Just as before, these exercises were selected for flexibility measurements since they illustrated movement according to the aforementioned motion primitives. This iterative process produced the longest lengths of Bowden housing that are unnoticeable while still providing the necessary rigidity for cable guidance.

5.5.3 Back Plate

The largest rigid element on the exosuit is the back-plate. Back-plates are the component of the exosuit that primarily determine that exosuit's function. As shown in Figure 5.8C, the back-plate of CRUX can potentially host many components, so modifying proto-CRUX's design was essential to creating an improved exosuit. This component serves as the mounting plate for necessary mechatronic components, like the battery, the motors, and the controller. In proto-CRUX, the back-plate was a simple metal chassis. Due to complaints of users wearing proto-CRUX, we opted for a new, more flexible design (Figure 5.10). This particular back-plate Note that this back-plate's configuration is set to augment only the right arm of the user. CRUX's

back-plate can still be substituted for another back-plate to serve a different function.

The new back-plate is constructed out of a thin layer of fiber glass. This plate was molded into the shape of the upper back and attached to the neoprene via Velcro. We chose to use an easily detachable connection medium like Velcro for three reasons. The first was to keep the back-plate modular and provide the possibility of replacing this back-plate with a separate one for other uses. The second reason was to maintain a lightweight profile. Metal components are very dense and therefore add significant weight to the exosuit which both makes the exosuit bulkier and potentially unbalanced. The third reason is safety. In the event of a malfunctioning back-plate (e.g. a battery fire or out of control motor), being able to quickly detach the back-plate is crucial.

On board the back-plate chosen for CRUX, there are five micro-motors, a battery, a microcontroller, a joystick, and electrical wiring. Each micro-motor has a spool around which attached cable is spun. The micro-motors and their spools are situated on top of special mounts to mitigate cables tangling and cutting into the neoprene. These mounts were specifically designed considering the feedback received from users of proto-CRUX. Each mount is constructed out of 3D-printed PLA and is zip-tied into pre-punctured holes into the fiber glass back-plate.. Every micro-motor on the exosuit is a brushed DC micro-motor. The motors each have a stall torque of 88.3 Nm (125 oz-in) and a gear ratio of about 1000:1. Although five micro-motors are located on the back-plate, a sixth micro-motor is attached directly to the neoprene base layer at the shoulder. This single micro-motor performs the antagonistic augmentation of the pronation and supination of the forearms. Because these movements are both antagonistic to one another and require less force than the other augmented muscles and muscle groups, their function can be delegated to a single micro-motor.

To power the motors, a three-cell 3500 mAh lithium polymer battery is conjoined on the back plate. This power source provides between $11.1 - 12.6$ V and up to 50 A for the motors as well as the microcontroller.

The microcontroller used is an Arduino with two attached motor shields. The

motor driver modules are connected via I2C. The Arduino has 32 kB of memory, enough for some small programs and control functions.

Connected to the microcontroller (but technically held in hand) is the plunger. This device's function is used to help coordinate mimetic control, as explained in a future subsection.

The final attached component on the backboard is the joystick. Although not used for mimetic control (the primary function of this back-plate and exosuit), this interface allows for an alternative manually-controlled method. When the joystick is enabled, the user can manually control two motors simultaneously. The joystick affords the user the ability to augment two arbitrary pairs of antagonistic movements (e.g. biceps/triceps movement and pronation/supination). In the event of more than two movements requiring augmentation on CRUX, an external laptop could be used as a controller via USB attachment to the microcontroller on board.

Exoskeletal Back-plates

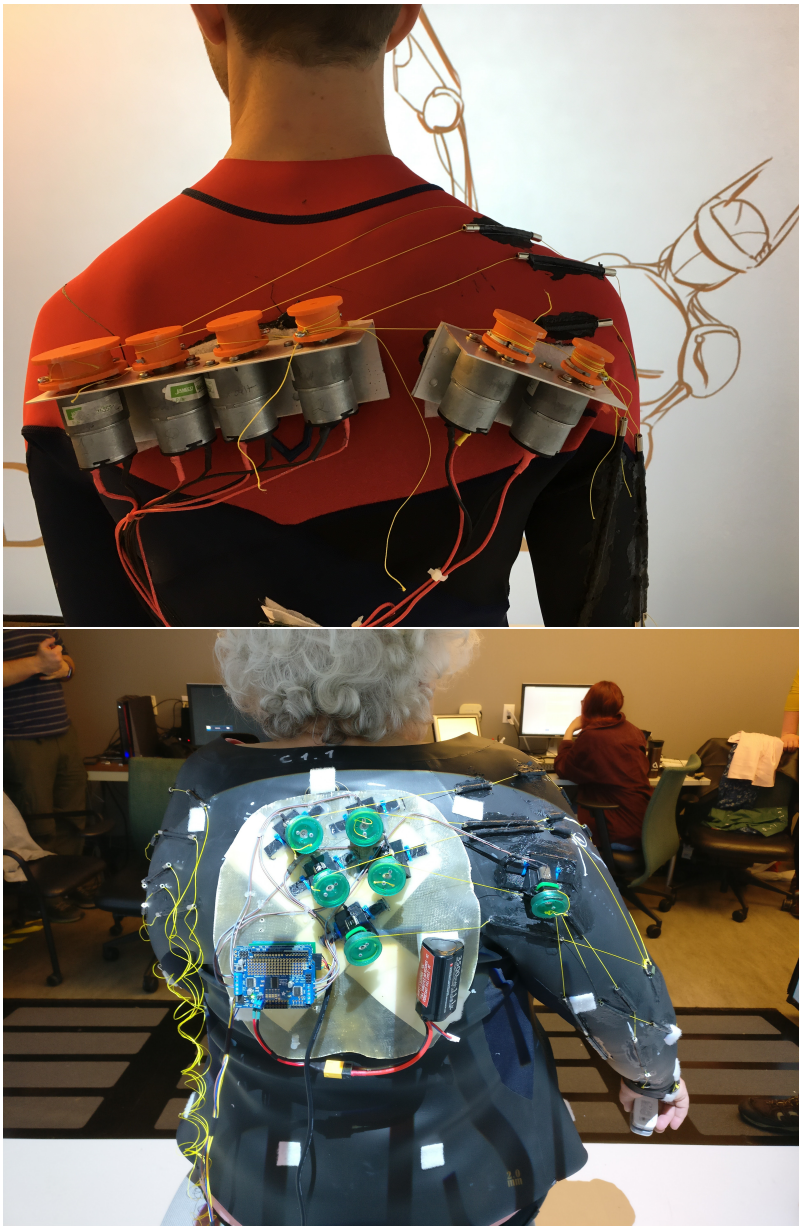

Figure 5.10: Exoskeletal Prototype 1 and 2 (CRUX) viewed from behind. The back-plate on CRUX is more flexible and has greater utility than that on the first prototype [62].

Table 5.2: Components on Prototype 2

Component	Location
Deltoid Motors	Back-plate
Biceps Motor	Back-plate
Triceps Motor	Back-plate
Pronator/Supinator Motor	Shoulder
Microcontroller	Back-plate
Battery	Back-plate
Plunger	Back-plate/Hand
Joystick (optional)	Back-plate/Hand
IMU's	Arms (see Figure 5.7)

5.5.4 IMU Network

To assist the control algorithm, IMUs on the exosuit provide pose data. The IMU uses Bosch Sensortec BN055's, each of which has a 3DoF accelerometer, a 3DoF gyroscope, and a 3DoF magnetometer. They output the pitch, yaw, and roll in quaternion format. Quaternion format is better than Euler angle format because the former avoids the mathematical pitfall of gimbal lock. The manufacturer of these IMUs guarantees that there is no more than 0.5° in alignment error at any time between the internal gyroscope and the provided label on each model.

Two IMUs are placed on each arm (Figure 5.11). Each of these IMUs is housed in a small module that is affixed to the neoprene base layer. Marking on the exosuit, the housing, and the IMU itself ensure that the devices remain oriented the same way each use. Additionally, the vertical profile of the module is minimized to keep the IMU's orientation and the orientation of the extremity as similar as possible. The modules are placed on the arms to best distinguish the pose of the forearm and the upper-arm. From the pose data of both of these halves, the pose of the arm as a whole can be reconstructed. For that reason, the arm's pose can be determined by a vector of six variables:

$$Q =< \theta_{upper}, \phi_{upper}, \psi_{upper}, \theta_{lower}, \phi_{lower}, \psi_{lower} > \tag{5.5}$$

where Q is the arm's pose (state) and θ, ϕ, and ψ are the pitch, roll and yaw respectively of the upper and lower arm.

The IMU nodes are connected via a wireless network. This ensures that the system can monitor the transmitted data via sniffing within the network without causing any interruptions or lag. Using DWM1000 wireless transceiver modules, the IMU network incorporates a feedback acquisition system. Proto-CRUX used IMUs in a similar fashion to this, but did not feature explicit attachment markings or housing that are necessary for the mimetic algorithm.

5.5.5 Mimetic Control

A joystick and even a laptop can be used to control CRUX manually, however this control interface can be challenging for users. As more focus is required from the user to manage the exosuit, they will struggle more to perform the necessary and often exhausting physical exercise. This challenge only becomes more daunting when one considers the lack of dexterity and operational experience to be expected in users with upper-limb impairment. To address this operational difficulty, we introduce a passive control mode for CRUX: the mimetic controller. From the pose data gathered using the IMU network, a mimetic controller can "think" for the user. As previously mentioned in the literature review, some forms of physical therapy like Graded Motor Imagery and mirror therapy involve a therapist helping a patient move an impaired arm according to their other, unimpaired arm. One manner for achieving this result is using an exosuit to augment a user's impaired arm as they attempt to relearn how to move it. An example of this is a user learning to change their elbow pitch (involving engagement from their biceps and triceps). If they move their unimpaired arm in this manner, the impaired arm would be assisted in doing the same. A mimetic controller can accomplish this so long as the goal pose is known from the IMUs and the actual pose of the impaired arm is known from the IMUs as well.

The precise state machine of this mimetic controller is outlined in Figure 5.12. This state machine consists of three states: off, ready, and mimic. This passive

algorithm synchronizes the position of one impaired arm to the measured position of the other unimpaired arm. The problem presented and solved by this mimetic controller, Robot position synchronization, is a form of consensus control. Previous systems implement such solutions to achieve exponential stability semi-globally [91, 92].

The foundation of this mimetic controller is a simple closed-loop controller. The leading state is tracked by finding the median of the previous five samples. This makes our measurement slightly more robust than simply taking the last reading. In a more complicated controller, like a Kalman filter, one can yield more accurate state tracking. We however determined that the added overhead and hardware necessary to support such an algorithm does not justify the relatively minor improvements in performance. Added hardware also physically burdens the back-plate and user as well.

In the case of CRUX, unilateral actuation means that the user's right arm is augmented while the left is free to move in the tests described in this paper. For this reason, the specific users meant for this iteration of CRUX are those with right-arm impairment. We represent the leader arm and the follower arm with the state vectors Q_l and Q_f. Q_l and Q_f are populated according to Equation 5.5. In either hand, the user can hold the plunger button to engage the algorithm. The top of the plunger has a red display LED which lights up when it is pressed. This provides visual feedback that alludes the user to the algorithm's state. The exosuit, when mimetically controlled, will not actuate if this plunger is not pressed. When the follower arm is not within the described threshold and the plunger is pressed, it moves until it mirrors the position of the leader arm, such that Q_f becomes equivalent to Q_l (with a tolerance of Th). We define the threshold as:

$$q_{Th} = |q_f - q_l|, \forall q \in Q \tag{5.6}$$

and the threshold signal will only be satisfied when:

$$L \leq q_{th} \leq H, \forall q \in Q \tag{5.7}$$

For this implementation, $L = 5°$ and $H = 40°$. This conservative threshold affords CRUX smoother and more calculated movements in the follower arm. Choosing a threshold of 40° sacrifices finer adjustments and movements during mimicry than a lower threshold would, but a high threshold ensures wary users in the exosuit's safety so that they can be confident when they use CRUX. This issue is discussed further in the "Safety" subsection.

5.5.6 External Applications

The outlined technology in our design for CRUX is what we consider to be the bare minimum for a functional exosuit. The addition of external applications and features can further enhance the user's experience. In Figure 5.8C, a user can be observed wearing a virtual reality (VR) headset that lets them to interact with a virtual environment. This feature can occur while CRUX simultaneously augments their arm movements. We discuss the use of peripheral equipment in greater detail in the Results chapter.

5.5.7 Safety

Human interfacing robots, especially wearable devices such as exosuits, must prioritize safety. Concerns for safety were in fact one of the top reasons potential recruits for the studies discussed any hesitation they had to try CRUX when introduced to the technology. CRUX involves explicit safety protocols at three different levels: the hardware, the software, and the user instruction.

Mechanical limitations are introduced into CRUX's design to avoid any physical danger. Motors are mechanically limited to never pull more than 88.3 N, as dictated by their maximum torque of 125 oz-in and spool radii of 1.0 cm. The back-plate can also be immediately detached in the event of an emergency, as can the battery on board in the event of overheating.

Software constraints implemented in the controller's source code act as a redundant safety protocol to prevent harmful behavior as well. Motors are purposefully limited to 80% power, which provides enough strength to meaningfully augment

users without completely neutralizing their efficacy. Additionally, the controller checks for extreme discrepancies between Q_l and Q_f. Any IMU-sensed angle pair with more than 40° difference between the two will stop the motors. IMUs that are inactive for more than 0.5 seconds also disable the whole exosuit. These motors are push-activated via an attached plunger. If a user is ever uncomfortable, simply disengaging the plunger stops all function.

Lastly, every user who wears CRUX is provided a safety briefing before they wear the robot to explain the functions of the exosuit and familiarize them with the necessary controls. Users must acknowledge that they both understand this briefing and that they are capable of exerting 10 lbs of force to overpower the exosuit in the event of an emergency.

First Exosuit Prototype

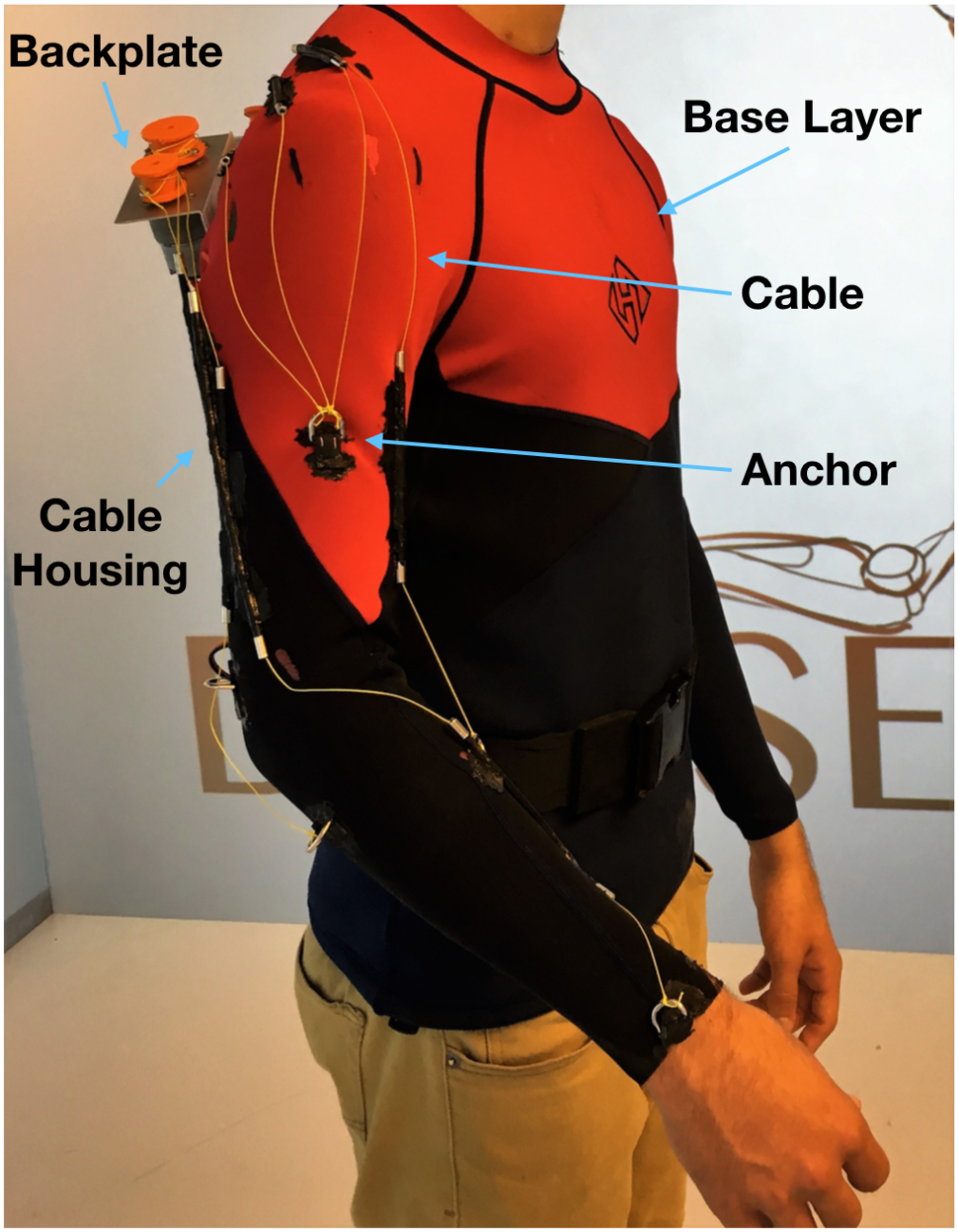

Figure 5.5: The first exosuit prototype. This preliminary exosuit exemplified augmentation with flexibility in a portable design. Future changes to the exosuit's design would improve on these features.

CAVE

Figure 5.7: The Cave Automatic Virtual Environment (CAVE) for 3D motion capture and virtual reality display. Four cameras in the CAVE track IR-reflective dots, which can be equipped to many materials, including garments.

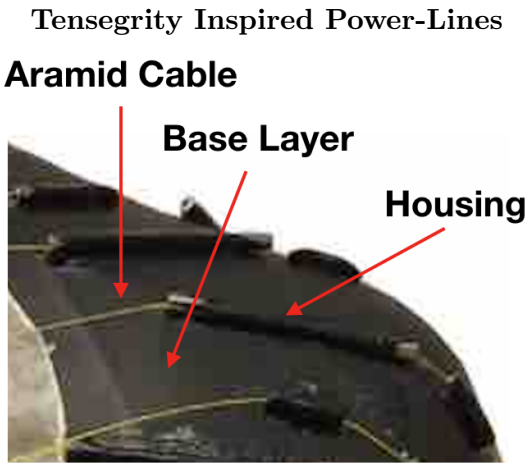

Figure 5.9: Power-lines, formed from flexible aramid cable are threaded through segments of rigid Bowden housing. These components are responsible for channeling power from the motors to actuate the exosuit. Seven power-lines on each arm assist user augmentation in the muscles highlighted in Figure 5.8B. The congregation of tension members (i.e. the aramid cables and the neoprene base layer) and compression members (e.g. housing segments) function similarly to tensegrity structures [62].

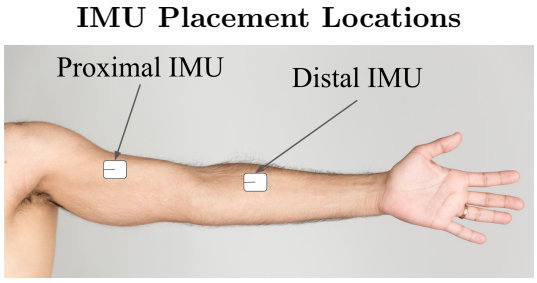

Figure 5.11: The locations of the IMUs on CRUX. The right arm locations mirror those of the left arm. To ensure consistent placement between uses, external markings on the IMU housing and the exosuit itself provide guidance for placement [62].

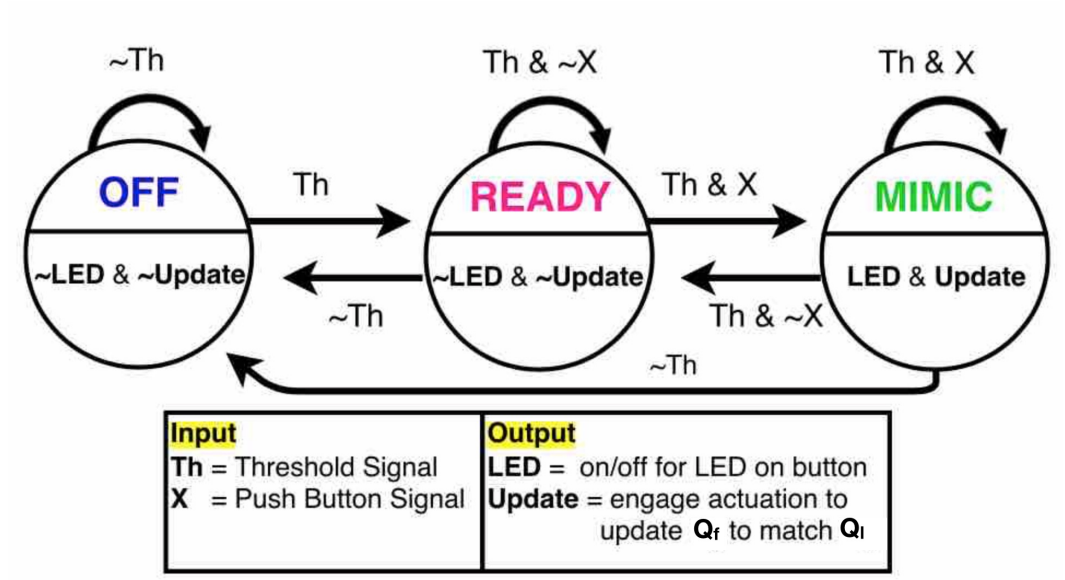

Figure 5.12: The state machine for CRUX's mimetic controller. When a difference in pose is noticed ($> Th$), the follower arm's motors actuate to match the leading arm. This activity can be suspended if the user takes their thumb off the plunger [62].

Chapter 6

USER EVALUATION RESULTS AND DISCUSSION

Once the prototype of CRUX was constructed, we proceeded to test its efficacy. We analyzed four aspects of CRUX: its mimetic controller, its structural flexibility and compliance, its ability to augment the user, and its ability to integrate into external applications. CRUX is a very complex device with numerous combinations of theoretical activities it can perform. Rather than studying all of these activities, which is intractable, we have instead decided to study fundamental activities which may be indicative of the device's performance as a whole. For this reason, we look back to the topic of motion primitives, single degree of freedom exercises which can combine with one another to produce all movement in the upper-extremity. The precise movements used in each study follow this theme and are discussed individually in their appropriate subsection.

6.1 Mimetic Control

The primary evaluation criteria of a satisfactory mimetic controller is the ability of new users to rapidly harmonize with the automatic adjustments performed by the exosuit to complete a mirrored exercise. To observe users' abilities to using CRUX to complete this task, we measured their arm's pose over time. This study focuses on

two aspects of mimetic control: the exosuit's ability to follow the stated algorithm and the user's ability to control the exosuit mimetically.

6.1.1 Study Demographic

For this study, we recruited a total of 4 unimpaired participants. These participants had a median age of 26. 3 participants were male and 1 was female. We chose to examine unimpaired participants for this study for two primary reasons. First, these participants can express a larger range of motion and operate more flexibly. This means that exosuit users can better test the full capability of the exosuit and will not be inhibited by their own physical limitations. Subsequently, the exosuit as a device is tested more thoroughly. Second, observing only unimpaired users for this study meant that the results from impaired subjects could be reserved for the far more pertinent studies on augmentation and VR applications. Recruiting impaired subjects with inclusion criteria as strict as what we defined is challenging, so to ensure that the augmentation study's results are as statistically significant as possible, we reserved all impaired recruits for the final study.

6.1.2 Protocol

In this study, each user dons CRUX and is instructed on how to use the mimetic controller. Specifically, the user is told the controller rules outlined by the mimetic algorithm (Figure 5.11). The user is also handed the plunger to be held in their left hand throughout both exercises. The precise exercises chosen to test users were lateral shoulder abduction and adduction (Figure 6.1) and biceps curls (Figure 6.2). These two exercises (and the motion primitive pairs they reflect) do not fully express the capability of the human upper-extremity or exosuit, but they do illustrate two fundamental movements one would associate with physical therapy. A physical therapist is likely to prescribe these movements or movements involving them in order to reduce the impairment in that user's arm. By strengthening these movements, full arm well-being can be theoretically improved.

After the two exercises and control algorithm were explained to the subject and

the subject confirmed they understood, subjects were equipped with CRUX and the additional four IMUs, attached as outlined in the System Design section. Once the full exosuit had been donned, the user was instructed to perform the lateral arm raise as described in Figure 6.1. To keep trails consistent, every user was to to place their arms flat against their sides, palms in, and then lift their leading arm laterally until their hand was level with their shoulder. Their arm was outstretched the whole time to reduce the impact of accidental elbow movement. The subject then asked to perform a biceps curl, beginning in the same initial pose as before. The biceps curl, the subject was told, should have their leading forearm elevating, bringing their hand towards their shoulder (Figure 6.2). To better learn how the mimetic controller worked, the user was told to move their follower extremity as little as possible, thus maximizing the impact of the exosuit's augmentation. One example of a user learning this process is visible in Figure 6.3. Once that user begins using CRUX to perform a mirrored exercise, we track their arm pose over time.

6.1.3 Results and Discussion

During each performed exercise, CRUX measured and output the pitch, roll, and yaw of each extremity (i.e. Q_l and Q_s). These twelve readings and the plunger state (i.e. pressed or not) constituted the control signal of the exosuit.

In Figure 6.3, we observe the pitch of two of the four IMUs on CRUX ($\theta_{leader,lower}$ $\theta_{follower,lower}$) during a lateral arm raise. Each pair of plots (labeled T_1, T_2, and T_3) illustrates a consecutive 17s time period. These particular 17s periods were chosen because each one illustrates a particular stage in that user's learning. Selected time periods were chosen to be 17 seconds because 17s was the shortest time period during which a lesson was concisely demonstrated. The three time periods occur in quick succession such that the end of T_3 occurs roughly one minute after the start of T_1. For each time period, we couple illustrated quantitative data with qualitative data acquired when discussing the mimetic process with users as they perform the exercises.

In T_1, the user wears and operates CRUX for the first time. Unfamiliar with the new sensation of wearing augmentative technology, the user reactively resists movement in their follower arm as they move their leading arm. Upon realizing their involuntary response, the user overcompensates and consciously forces their follower arm to the precise pose of the leader arm at roughly $t = 10s$.

In T_2 from $t = 2$s to $t = 6$s, the user manually overrides the exosuit's motors to move their follower arm. At $t = 6$s, the user recognizes their action and immediately re-corrects their follower arm manually to be within the threshold for mimetic augmentation. Since the follower and leader arms differ by more than 40° (the threshold for mimetic augmentation), the user had to manually intervene. The precise rule followed by the exosuit's mimetic controller is to engage the motors attached to the follower arm power-lines until that arm reaches the pose of the leader arm (with a tolerance of 5°). This rule, however, does not take effect until there is a difference in pose between both arms by less than 40°. Although 40° is a large threshold for practical applications, this threshold further ensures safety in this prototypical design and reassured otherwise intimidated users. By $t = 8s$, the user has relaxed

their control slightly and begun to trust the exosuit more. They can recognize the pulling sensation of CRUX in their upper-arm (proximally) unlike during T_1. After a few seconds of acclimating to the tension force from CRUX's power-lines, the user demonstrates very rudimentary augmentation movement, enough to demonstrate some degree of control when assisting their follower arm.

In T_3, the user demonstrates the greatest degree of control when using CRUX thus far. The user illustrates their leader arm (left) controlling the follower arm (right) almost perfectly with a 1s delay. The user operates in a relatively voluminous workspace (around 20° in proximal pitch and 60° in distal pitch) An operational workspace that large is necessary for many arm movements during mirror therapy. At $t = 12$s, we observe one interesting phenomenon: the user's leader arm rapidly moves unexpectedly (perhaps to scratch their nose) but the follower arm does not mimic the movement. This inaction can be attributed to the built-in safety feature in the controller's design that prevents unintended movement of the follower arm. In a hypothetical case with stronger motors and a weaker user, this movement could potentially damage the user, so CRUX correctly intervenes during this unexpected movement and halts augmentation.

The data in Figure 6.3 illustrate the proof-of-concept that CRUX can augment upper-extremity movement in users who have learned to mimetically control the exosuit. In approximately one minute of using CRUX, the subject featured in Figure 6.3 learned to operate CRUX at satisfactory level for mirror therapy based upper-extremity movements. Although formally measuring behavior as complex as device mastery is challenging, we can confidently say that every user tested was able to comfortably operate CRUX within minutes. Sometimes, users would become momentarily stuck on how to proceed in using CRUX, but after quick verbal assistance from a study proctor, these users were able to resume operation of the exosuit as intended. Future testing can focus on methods that reduce the learning curve even further for operating exosuits such as CRUX.

6.2 Flexibility and Compliance

One of the most prominent differences between CRUX, an exosuit, and other exoskeletons is its claim to be more flexible and structurally compliant. These attributes can be measured by the change in user range of motion with and without CRUX worn.

6.2.1 Study Demographic

For this study, we recruited the same 4 subjects as in the mimetic control study, each of which identified as highly-flexible. We chose to study the flexibility and compliance of CRUX on unimpaired users in order to reserve impaired users for the metabolic study. Because of this, impaired users do not have to perform as many exercises as otherwise (which can potentially injure their arms) and their data does not inappropriately influence future studies. Additionally, since unimpaired users are more flexible, they can further stress test the mechanical properties, the true phenomenon being studied in this test, better than less flexible unimpaired users.

6.2.2 Protocol

The four subjects each performed five iterations of both exercises while wearing reflective tracking dots on their arms similar to those in Figure 5.8A. The subjects then repeated the same series of exercises while wearing CRUX, which was also covered with reflective dots for motion capture. To study the flexibility and compliance of CRUX, we chose two arm movements, shoulder circles and biceps curls to measure. Although forearm flexibility cannot be observed in these exercises, shoulder circles and biceps curls still exemplify the necessary flexibility to perform the aforementioned mimetic control tests and the metabolic tests described in the next section. More specifically, biceps curls demonstrate the full range of motion of the elbow joint in one movement. Similarly, shoulder circles combine both shoulder flexion/extension movement and shoulder abduction/adduction into a single movement that demonstrates the flexibility of the shoulder joint. During the study, range of motion was tracked via a 3D infrared camera system using a CAVE (Figure 5.6) to

evaluate and compare range of motion with and without CRUX being worn.

The user was told to stand in the CAVE and perform each iteration of the first exercise at a constant tempo. For arm circles, the user swung their arms forwards and backwards (for a total of ten repetitions without wearing CRUX and then another ten while wearing CRUX). To keep results consistent among subjects, every exercise was performed with the user standing as still as possible. This also ensured that the IR cameras had the clearest view of the subject.

6.2.3 Results and Discussion

The exercises observed with and without CRUX appear to differ from one another minimally (Figure 6.4). We should observe a theoretical restriction due to wearing an additional layer and the slight mismatch between the red and green trajectories can be attributed to a combination of this and minor noise in measuring. This theory also explains why we notice in the shoulder range of motion plot that users wearing CRUX appear to be more flexible at times than without the exosuit, which is improbable given that neoprene of CRUX is objectively more restrictive than the baseline elastane garment. The observed results of Figure 6.4 are consistent with our hypothesis that CRUX will not impede users significantly.

Since all four users wore the same exosuit (i.e. CRUX) throughout this study, they all fit the exosuit slightly differently than one another and none of them to the precise dimensions. CRUX had been modeled based upon a member of the target demographic (i.e. upper-extremity impairment) and so the fit in these studies was imperfect. Although this concession created a sub-optimal fit for the users, we fortunately found that there was no significant impedance in user flexibility when wearing this exosuit.

Post-study surveys of both the impaired and unimpaired users also yielded qualitative results that the exosuit did not hinder perceived user flexibility or compliance in most subjects. Two of the thirteen impaired users reported that they felt that the exosuit marginally inhibited their range of motion. However, both of these users also mentioned in their post-study interviews that this inhibition was due to the neo-

prene base layer being too tight for their stature (which differed from the user whose template provided the dimensions for CRUX). The other eleven impaired users did not mentioned any issues with the flexibility or compliance of the exosuit.

This confirms that our iterative design process (outlined in the previous chapter) for reducing rigid, constrictive Bowden housing produces a sufficiently flexible design. We then conclude From these findings that CRUX's fabric-based structure does not inhibit user movement significantly enough to restrict movements central to mirror therapy and upper-extremity rehabilitation.

6.3 Metabolic Impact

Critical to Graded Motor Imagery and mirror therapy is the visual and kinetic feedback patients receive as they perform an exercise [93]. Without exosuits, this reinforcement is provided by practitioners in the form of physical assistance or optical illusion. One example of this feedback is a patient seeing their arm move as they attempt to move it themselves. The underlying mechanism in this traditional example is either the practitioner moving their arm for them or the image of the arm moving simultaneously in the mirror. The therapeutic result is that the user experiences the neural response of moving their arm while expending less energy than otherwise required, reinforcing their neurological recovery. Reducing the metabolic barrier necessary to recover this physiological ability is the primary purpose of mirror therapy and Graded Motor Imagery.

To provide this feedback, CRUX must mechanically augment the user's movements during the exercise, ideally without any added metabolic cost. We measure users' heart rate increases in this study to serve as a proxy measurement for metabolic expenditure. Specifically, we record starting and ending heart rates of users as they perform biceps curls without and then with CRUX assisting them.

Heart rate and metabolic expenditure have previously been shown to correlate closely to one another. A study by Dowd. et al in 2018 discusses and compares various methods of measuring physical activity in humans across 63 different studies[94]. Of these discussed methods, heart rate is highlighted by Dowd et al. as a good in-

dicator of metabolic expenditure. Although this paper concedes that every metric discussed therein is imperfect for observing metabolic cost, the authors agree that objective and quantitative metrics like heart rate are better than subjective and qualitative metrics like self-reporting. The metabolic cost of physical activities like biceps curls are therefore (relatively) accurately measured by examining the heart rates of subjects.

6.3.1 Study Demographic

For the metabolic study, we recruited 13 users. Of these 13, 9 had suffered some degree of upper-extremity impairment and 4 were unimpaired control group from before. The unimpaired subjects served as a control group. To minimize the impact of confounding variables, we used very precise inclusion criteria during recruitment. We searched for users who had single-arm weakness or neglect, but not paralysis. This criterion selected for users who described themselves as functional enough to use CRUX and potentially benefit from its therapeutic use. Additionally, the recruitment message ensures that we do not violate HIPAA laws.

Of the impaired users, 4 users were men and 5 users were women. Of the unimpaired users, 3 were men and 1 was a woman. The median age of our impaired users was 65 and the median age of our unimpaired users was 26. Of the 9 impaired users, 7 had previously gone to physical therapy. When surveyed how much they agreed with the statement "My physical therapy was helpful.", all 7 relevant users chose "Agree" or "Strongly Agree" on a five-point Likert scale. The metabolic study was performed in our lab for 8 participants, and at the homes of the remaining 5 participants. All 5 participants who performed the metabolic test in their homes were impaired.

6.3.2 Protocol

To study CRUX's metabolic impact, we chose to observe subjects performing biceps curls. Biceps curls were chosen as a characteristic exercise to exemplify CRUX's effect on users for two reasons. First, isolating a single motor's metabolic effect on one

muscle group demonstrates the capability of the exosuit with the fewest confounding variables. Second, biceps curls are an exercise explicitly mentioned by licensed physical therapists we spoke with when discussing the necessity of strengthening upper-extremity during stroke rehabilitation due to their prevalence in the majority of patients' day-to-day arm movement.

During the study, users were instructed to lift a dumbbell that they judged would fatigue them after 10 repetitions according to the same motion outlined in Figure 6.2. For each trial, the user's heart rate was recorded at rest, while wearing CRUX. Heart rate measurements were conducted using a heart rate monitor that fit over the user's index finger. After the ten repetitions, the user's heart rate was recorded again. The user took a five minute break to allow their heart rate to reach resting again. After this rest, the procedure was repeated but with CRUX powered on and augmenting their biceps curl.

6.3.3 Results and Discussion

After aggregating the results of our study, we determined that CRUX was able to augment biceps strength by reducing the increase in user heart rate after exercise (Figure 6.5, Tables 6.1, 6.2).

Table 6.1: Mean Heart Rate Percent Increases after Exercising

	Impaired	**Unimpaired**
Unassisted	12.4	27.6
Assisted	3.03	29.3

Table 6.2: Median Heart Rate Percent Increases after Exercising

	Impaired	**Unimpaired**
Unassisted	7.7	12.7
Assisted	1.6	19.0

The results of the metabolic study show that users saw less of an increase in heart rate while CRUX was actively augmenting the user than without the exosuit powered. For impaired users, CRUX profoundly improved their metabolic efficiency.

The mean heart rate increase in impaired users was 12.4% without assistance and 3.03% with assistance. Similarly, the median increase was 7.7% without assistance and 1.6% with assistance. When compared to unimpaired users, this improvement was quite significant. Unimpaired users did not experience the same level of improvement as the impaired subject pool. The mean heart rate increase in unimpaired users was 27.6% without assistance and 29.3% with assistance. The median increase was 1.6% without assistance and 19.0% with assistance.

The result for unimpaired users was surprising, so we investigated the outcome further. Post-study surveys yielded that all four users reported a decrease in effort required to perform the biceps curls when assisted by CRUX. Potential anomalies in these data could have been caused by failing to provide enough rest for these unimpaired users before their assisted trials. This claim is supported by two of the unimpaired users, whose starting heart rates for the assisted trial were higher than their respective initial unassisted resting heart rate. Additionally, decreases in performed tempo were observed in video recordings for all four users by their second round of exercise (i.e. assisted by CRUX). This reduction can be the result of a user selecting a test dumbbell that is too heavy for 20 lifts (10 per trial). This reason explains both the decrease in tempo and the abnormal higher starting heart rates and heart rate increases for the unimpaired demographic. One possible reason, we hypothesize, that impaired users did not experience these same issues is because impaired users may have been more reluctant to lift a heavier weight with their conditions. As a result, these users were pushed too less of their cardiological limits than unimpaired users. We also observe some slight increases and outliers in heart rate increase among particular users. In at least one case, an impaired user commented in their pre-study survey that they suffered from PTSD, a condition that is known to cause great variance in starting heart rate and heart rate increase when compared to people without PTSD [95].

The results from the post-study surveys support the hypothesis that CRUX successfully augments users, both impaired and unimpaired. When presented with a five-point Likert scale, 8 impaired users and 3 unimpaired users said that they

"Agree" or "Strongly Agree" that the exosuit assisted them with their biceps curls. The remaining 2 users said that they "Neither Agree nor Disagree" that the exosuit assisted them during this exercise. No user, impaired or unimpaired, stated that they would "Disagree" or "Strongly Disagree" that the exosuit helped them during the exercises. Of the 7 users who had previously completed some physical therapy, all 7 of them stated that they "Agree" or "Strongly Agree" that CRUX or something similar would have been useful during their therapy. Multiple users mentioned during an open-ended question about CRUX's wearability that they did not feel the exosuit weighing them down during the tests. The two most common complaints among the 16 subjects were confusion when using the controller interface while simultaneously exercising and overheating due to movement while wearing the exosuit.

When participants in a lab setting were compared against participants at their own homes, we found no significant change in metabolic efficiency. Subjects in labs had a 0.5 percentage point average increase in heart rate over users at their own homes when accounting for both unassisted and assisted biceps curls. This is an intriguing outcome because it justifies the claim that CRUX is a portable exosuit. An exosuit that is not influenced by where it is used can be used without regard to location, including outside of a physical therapist's office. For this reason, we justify merging the two data sets into one and examining the cumulative results of both.

To determine the statistical validity of the impaired users' performances, we conducted a lower-tailed paired t-test (Equation 6.1 —6.5). We chose to test the significance of only the impaired users because they are the primary demographic for which the study is designed. Additionally, the unimpaired subject pool features a small sample size in which there is a significant outlier. The test uses the following parameters:

$$H_0 : \mu_{unassisted,impaired} = \mu_{assisted,impaired} \tag{6.1}$$

$$H_1 : \mu_{unassisted,impaired} > \mu_{assisted,impaired} \tag{6.2}$$

$$n = 9 \tag{6.3}$$

$$t - value = 1.79 \tag{6.4}$$

$$p = 0.046 \tag{6.5}$$

The test concluded that the results were significant at a p-value of 0.05. From this result, we can be 95% confident that active assistance from CRUX increases the heart rate of a user by less than when not actively assisting that user.

These quantitative and qualitative data demonstrate CRUX's ability to augment users and satisfy the need required of an exosuit for Graded Motor Imagery and mirror therapy. The ability to mechanically assist the user and provide positive kinesthetic reinforcement has been observed across multiple demographics and in both a lab as well as participants' homes. Testing both more impaired and unimpaired subjects can elucidate the hypotheses formed after this study.

6.4 External Applications: Virtual Reality

As discussed in the System Design chapter, CRUX is designed to function as a standalone assistive robot. The exosuit can also be incorporated into other technological applications. To demonstrate CRUX's potential as a rehabilitative device, we built a virtual-reality (VR) environment and game to be used in conjunction with an exosuit. This VR application, titled "Project Butterfly" (PBF), is an immersive tool that allows users to interact with lifelike events and objects that are programmed by us to serve a rehabilitative goal (Figure 6.6).

6.4.1 Protocol

Users access Project Butterfly through an HTC Vive (Figure 6.7). The HTC Vive is a proprietary head-mounted display that provides users with a binocular, full field-

of-view (110°) of their virtual setting (Figure 5.8C). The HTC Vive's projections of the virtual setting are refreshed at a rate of 90 Hz. Users are also provided two handheld controllers they can use to interact with their environment. Virtual environments are illustrated in the headset via an attached cable which physically connects the HTC Vive to a computer where the virtual environment is rendered. The handheld controllers transmit their data wirelessly to the the render computer. On this computer, the virtual environment is simulated. User actions (i.e. their position within the real space and their controller input and position) are taken in as input and factored into the environment's response.

In PBF, the user has the option to play multiple mini-games each of which serves a specific rehabilitative function. Each mini-game encourages a user to perform a real exercise according to a pre-defined motion primitive (Figure 6.8). For example, one mini-game is played by a user who attempts to avoid virtual objects (e.g. rocks) that approach them in their simulated environment with their handheld controller.

By avoiding more of these objects, the user accrues a higher score. This mini-game is programmed by us to ensure that the objects approaching the user form a path that coincides with a specific arm movement. In the example of the approaching rocks, the user must perform biceps curls to successfully avoid every rock encountered. A second example is a game where users control an umbrella to protect a butterfly from rain. The butterfly flies in an orbital path, forcing users to perform arm circles to successfully protect the butterfly.

6.4.2 Study Demographic

We recruited four users to play-test PBF and provide their feedback on the games as well as CRUX. These four users were recruited according to the same criteria for the metabolic study: single arm impairment to a moderate degree. All four users were over the age of 60. Two users were men and two were women. None of the four users had any previous experience with virtual reality or video games.

6.4.3 Results and Discussion

Quantitative Data

To study the compounded effects of exosuit-based augmentation and VR gaming on rehabilitative outcomes, we tracked users movements and achievements throughout their playtime. At the start of each trial, the video game was tailored to measurements specific to that particular trial's subject (Figure 6.9). This ensures that no in-game goal is too easy or too difficult to achieve. Appropriately balanced challenge in the game maximizes user engagement and motivation.

Four quantitative metrics related to user movement were observed: arm movement, hand position, hand velocity (via controller), and head rotation. In Figure 6.10, we observe users performing biceps curls during a mini-game. The four users produce similar trajectories with their arms, illustrating the mini-game's ability to influence user movement in a specific manner. In traditional physical therapy, a patient may not know the ideal, precise movement they should be performing. This can lead to inconsistency between physical therapy sessions for patients. In a scenario where users are separated from physical therapists (as in the hypothetical case of using an augmentative exosuit at their own home), such consistency is extremely important in preventing the development of poor habits.

The measurements of hand extension in Figure 6.11 also provide a manner for tracking user ability. Without the use of computational devices, qualitative judgments and human error often yield challenges in precisely articulating user capability. By improving the methods by which we measure user ability, such errors can be mitigated. Users can also track their own progress objectively and can be provided literal reach goals to obtain throughout the course of their exercise.

The data illustrated in Figures 6.12 and 6.13 also yield valuable insight into user intention. With the development of VR games, understanding user intent and focus is significantly easier than without. By tracking user metadata, like where they look or how quickly they reach towards something, we can glean an objective measurement in regards to that user's engagement level and the ability of the game to successfully motivate players. User scores are also a good metric for measuring

an individual's progress within a specific game. Scores are a function of a subject's ability to conform to the goals we outlined within PBF. The better we encapsulate and reward the motion-primitive movement in the games, the better of an indicator the scores will be.

Qualitative Data

In addition to the quantitative data collected during these trials, we also conducted post-study surveys that allowed users to openly discuss their thoughts and concerns with the game design. All four users "Agreed" or "Strongly Agreed" that the games played were enjoyable. All four users also "Agreed" or "Strongly Agreed" that PBF was an effective tool for moving their arms and provided some distraction from the otherwise focused effort required to do so. The median score of users' ratings of whether or not they felt confident in using PBF and CRUX as a combined rehabilitative suite was 1 with a 1 being "Strongly Agree" and a 5 being "Strongly Disagree". This is an important insight because it verifies PBF as a means of motivating users to complete the associated rehabilitative exercises.

One key issue we observed during user playtime was that two in-game mechanics were positioned too low for the users. This accidental positioning forced the users to lean forward in order to play the game successfully. This was a poor feature because users slouching forward could strain their backs or, in extreme cases, tip users over. Given that all four users were over the age of 60, such a hazard could prohibit game-play without a caretaker or assistant to watch over them. Postural stability is important for full body health [97], including that of the upper-extremities, so mitigating this behavior was critical to creating a rehabilitative game. Once the slouching was accommodated for in the game design, all four subjects agreed that the games were appropriately challenging. This confirms that our ability to adjust the game based upon the person and their body size is successful to a satisfactory degree.

One interesting observation we discovered was that the use of a realistic avatar and game objects assisted users greatly. One user explicitly commented in their

post-study survey that they "knew the goal was to always protect the butterfly" just from looking at the screen. This is a very encouraging result; when game-play feels intuitive and fewer explicit instructions are required to play the game, players have one fewer mechanic to distract them. Such features are especially important in the elderly demographic (who our users fell under) due to their tendency to be unfamiliar with video games or virtual reality.

Through observation and commentary during the study, no subject seemed displeased with the aesthetics of the mini-games. In fact, three subjects complimented the game's aesthetics. One user, in their post-study survey explained that the VR-experience coupled with the exosuit allowed them to "escape into a world where [I am] mobile" and that was "a positive thing." A second user commented that game objectives like saving the butterfly "to feel protected, to feel safe, that felt really good." This second user further discussed the issue by explaining "the thing that I felt the most related to it was when I had a sense of compassion. If there is anything that could be tailored to a particular person it would trigger their sense of compassion. I think that would have a tremendous effect." This is a particularly exciting discovery because many people unfamiliar with video games and virtual reality are often intimidated or dissuaded from immersive nature of these environments. The first user even mentioned how their pre-conception of video games was that they were "totally turned off" but this new experience changed with PBF because they "liked what we were doing", referring to the game's objective. If users are psychologically comfortable with a system, they may be more likely to benefit from it.

One important discovery we draw from these data are the progression observed in each subject. All four subjects learned over time not just two new assistive technologies, virtual reality gaming and exosuit operation, but they did so in an enjoyable manner. Each user developed an intuition for playing and exercising simultaneously, as observed by our quantitative and qualitative data. The plots produced by these users indicate that each user was actively engaging and focusing on the virtual tasks with which they were presented. The quantitative data demonstrated that as users played the game more, they not only performed the specified exercises more con-

sistently, but they were able to score higher, thus completing the task with greater efficacy. A user might begin the game as a cautious and confused user, but interactive game-play transformed them into an engaged, exercising individual who independently performed the various exercises correctly.

Our analysis of CRUX and PBF combined yields the conclusion that these two technologies blend into one harmonious exercise experience. The small case study examined demonstrated players' willingness to complete movement-based objectives in a new setting. Despite unfamiliarity with both exosuits and virtual reality, users quickly adopted PBF and CRUX and responded positively to the experience as a whole. Future testing should focus on investigating a larger sample size and comparing success from PBF and CRUX to CRUX alone.

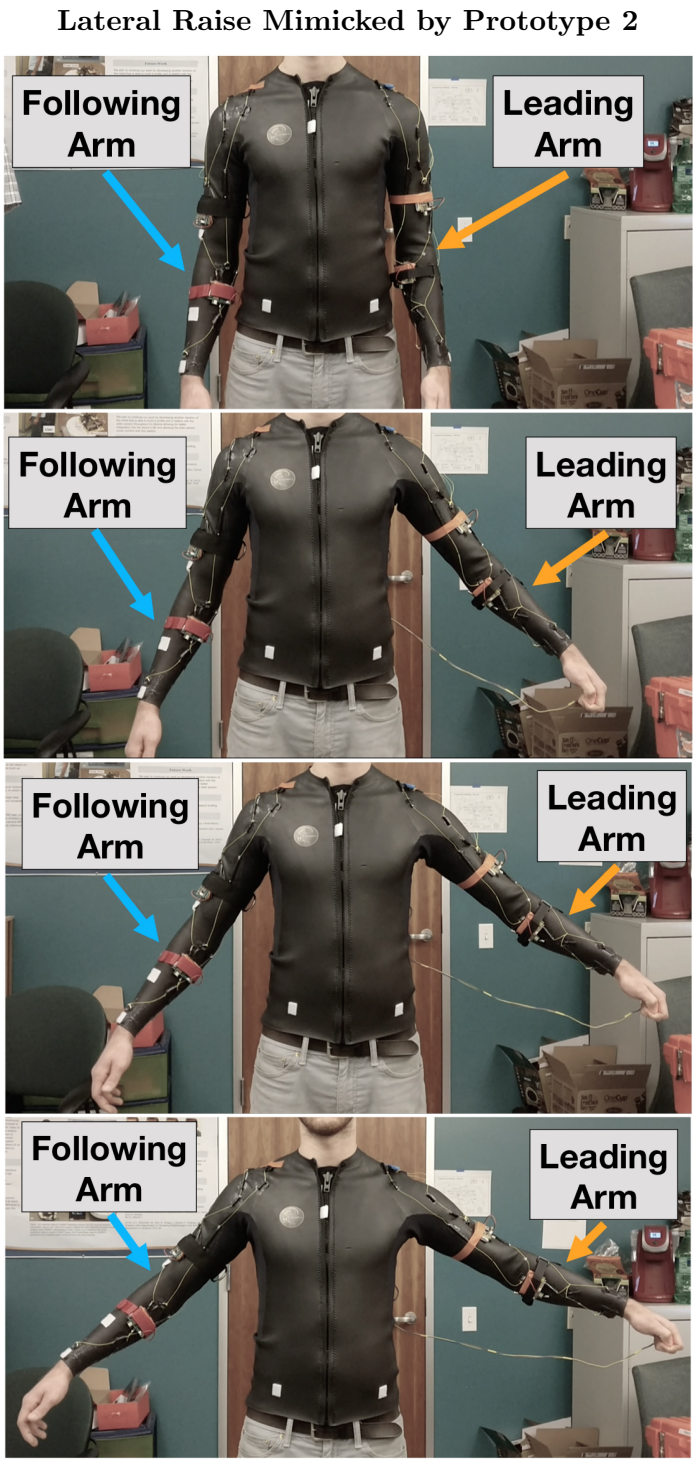

Figure 6.1: A user performs a lateral arm raise while wearing CRUX. The user's leading arm (left) dictates the motion of their following arm (right). The following arm, which lags behind the leading arm slightly, updates its pose to match that of the leading arm. The mimetic controller determines these poses from the IMU network [62].

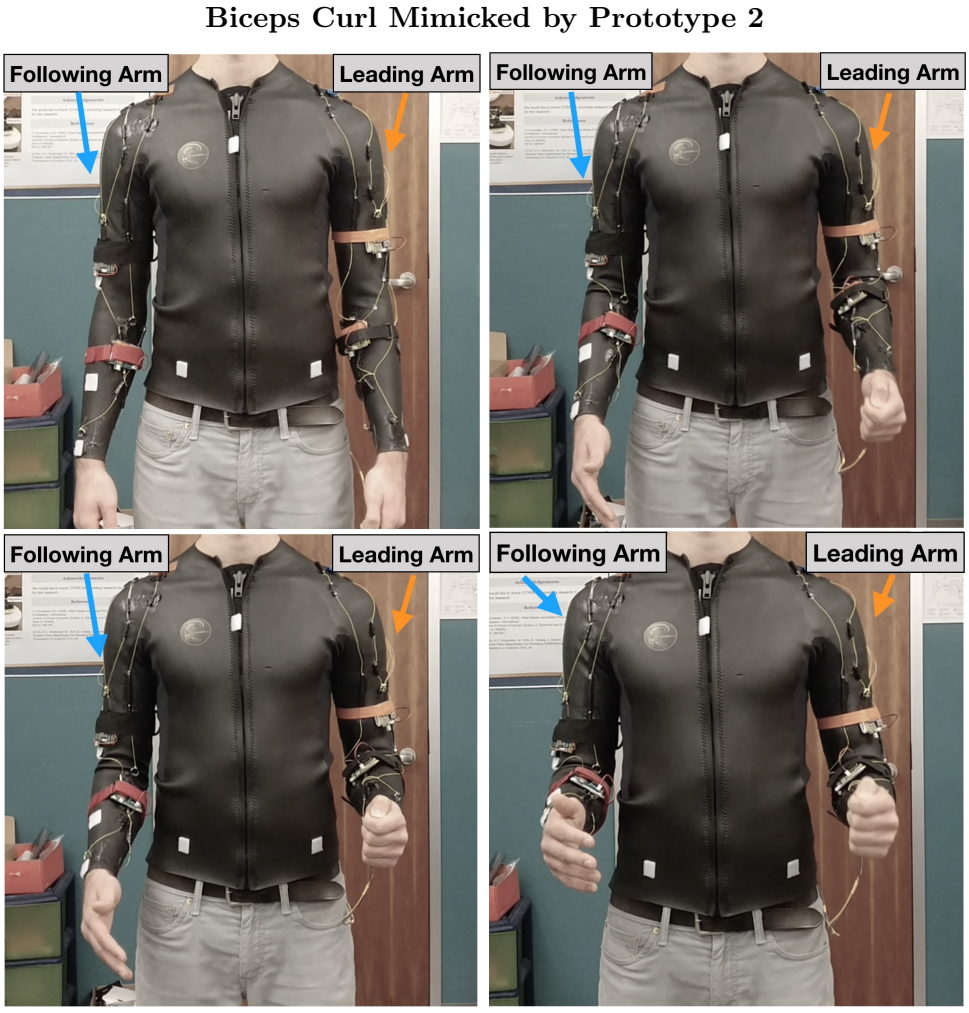

Figure 6.2: A user performs a biceps curl while wearing CRUX (left to right, top to bottom). The user's leading arm (left) dictates the motion of their following arm (right). The following arm, which lags behind the leading arm slightly, updates its pose to match that of the leading arm. The mimetic controller determines these poses from the IMU network [62].

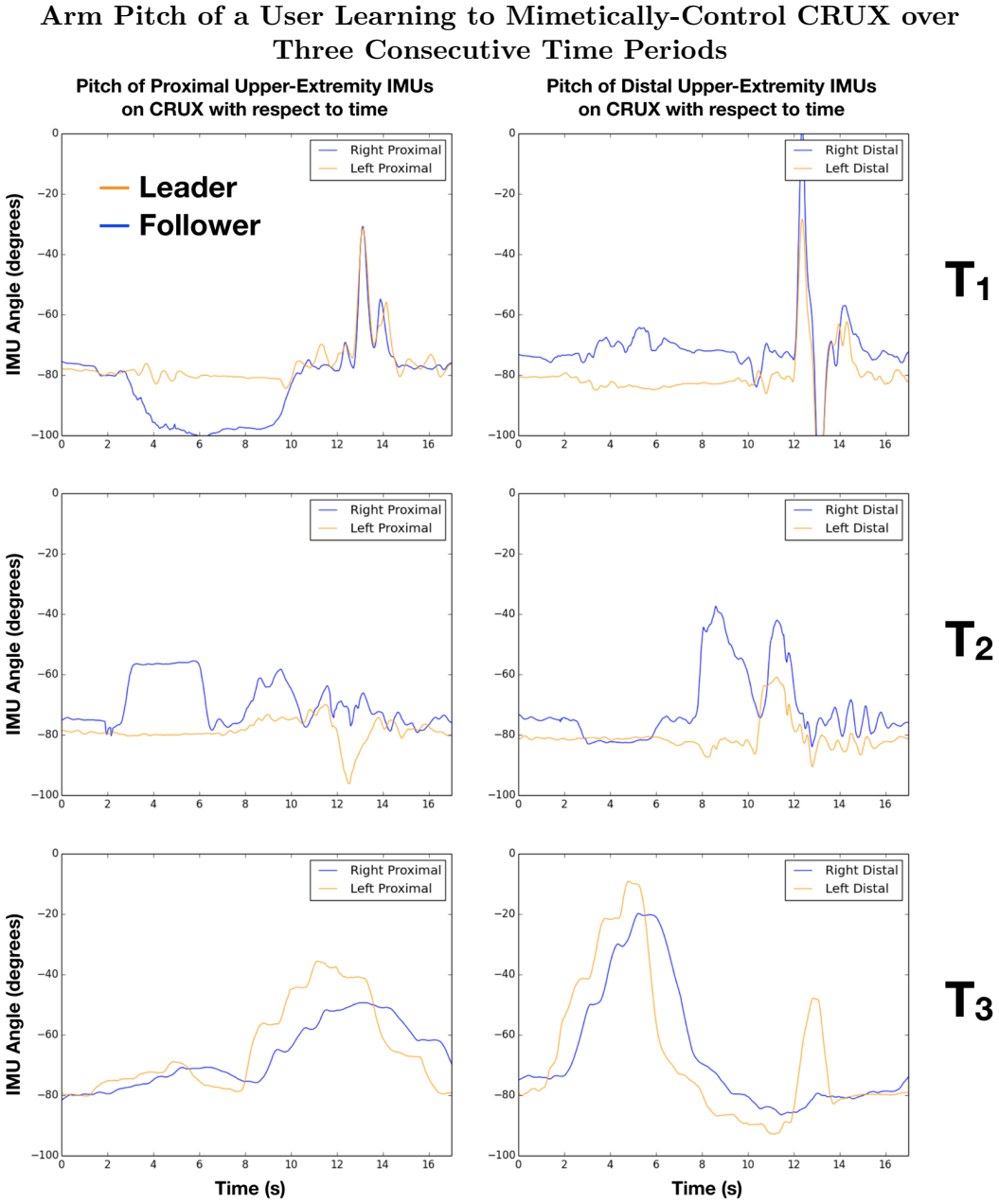

Figure 6.3: The pitch (θ) of two of the four IMUs on CRUX, measured in degrees with respect to time (accurate within 0.01°). The three pairs of plots represent three consecutive time periods (T_1, T_2, and T_3) of $17s$ each where a user mimetically controls CRUX. Here, the left arm (orange) leads the movement of the right arm (blue) of one user during a lateral arm raise and lateral arm lower. These function according to the state machine outlined in Figure 5.11 and the movement described in Figure 6.1. This figure illustrates the improvement of a characteristic user in leveraging CRUX to augment right arm movements from one time period to the next [62].

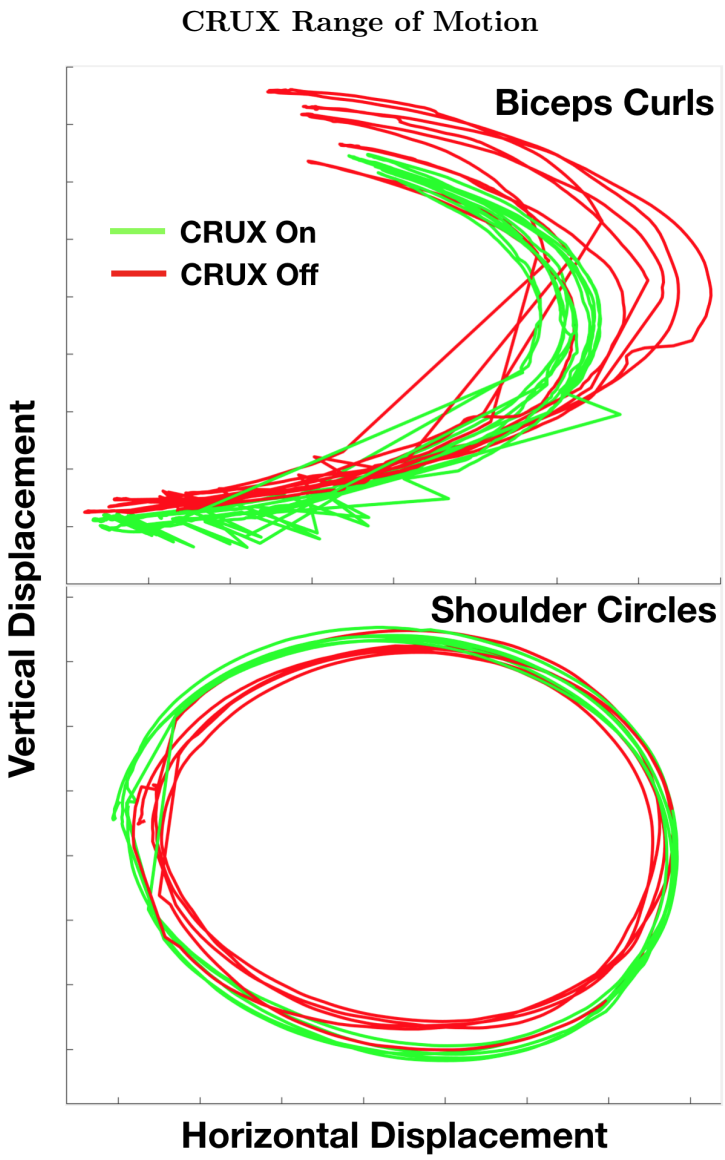

Figure 6.4: A pair of plots that illustrate the normalized 2D projection of wrists that moved through space. User flexibility is most apparent at the distal points of the upper-extremity (i.e. the wrists and hands) where one's range of motion is most pronounced. The particular exercises that produced these plots were chosen to study because they express extreme movement a CRUX user could experience. Red trajectories are those without CRUX worn and green trajectories are those with CRUX worn [62].

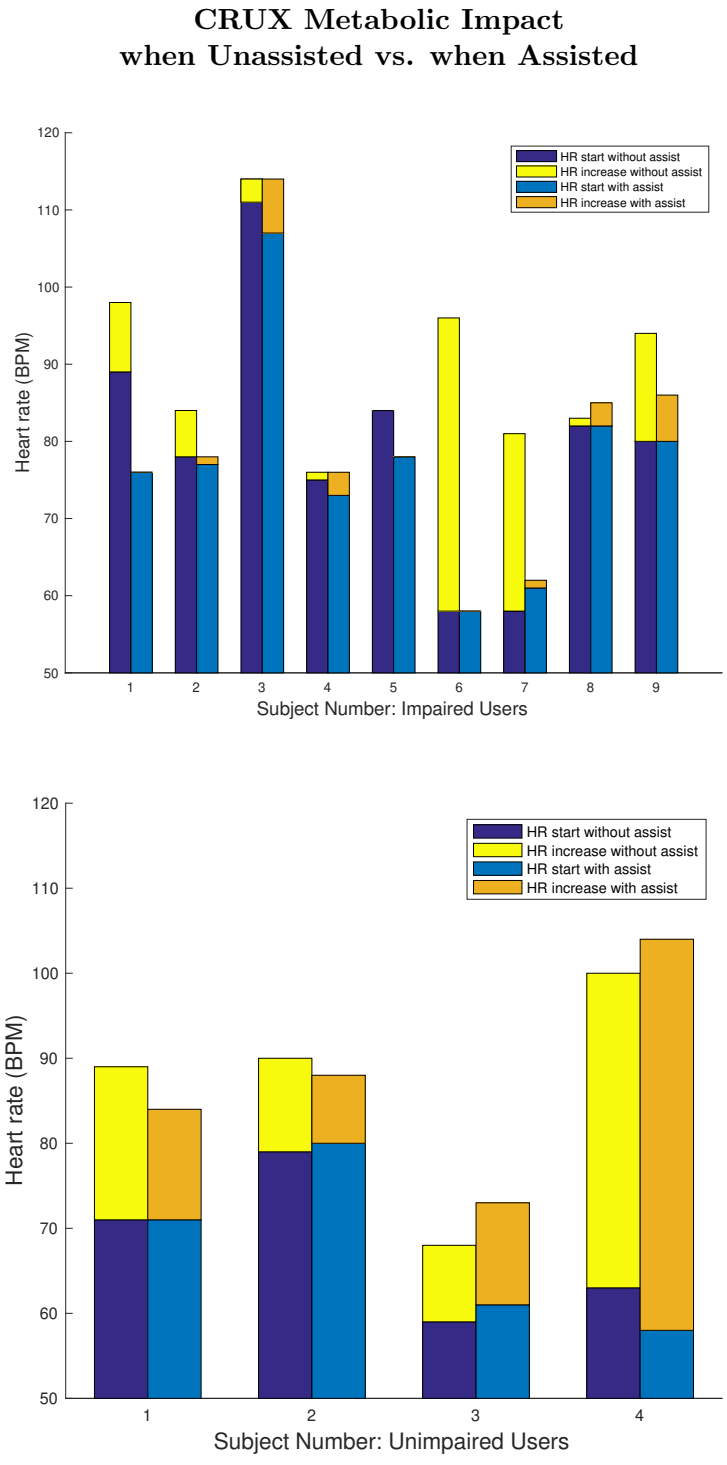

Figure 6.5: CRUX's impact on heart rate on impaired and unimpaired users, with and without exercise assistance [62]. Users completed 10 repetitions of biceps curls without assistance from CRUX and then after resting, 10 more with assistance. Mean and median heart rate increases for impaired/unimpaired and assisted/unassisted subjects are presented in Tables 6.1 and 6.2.

2D Projection of a Project Butterfly View

Figure 6.6: Project Butterfly is a suite of virtual reality games designed to test users' abilities to exhibit upper-extremity function [96]. Each game focuses on a specific motion primitive for the sake of isolating upper-extremity rehabilitation by its atomized movements.

Lateral Raise Augmentation by CRUX during a VR Game

Figure 6.7: A subject playing a game from Project Butterfly in virtual reality. By combining CRUX and VR, a user can more feel more motivated and engaged when completing physical therapy [96].

A User and their View of PBF during an Exercise

Figure 6.8: A user's perception and the test proctor's perception of the lateral raise mini-game. By observing both the real actions and the virtual consequences of a user playing a VR game, physical therapy can be optimized with greater insight than otherwise.

User Evaluator Interface

Figure 6.9: A virtual menu used by study proctors to tailor each VR experience towards the specific player [96]. Since player have different dimensions than one another, the game must be adaptable to these differences in order to provide meaningful challenges, irrespective of the user's difference between prior players.

User Arm Position during a VR Exercise

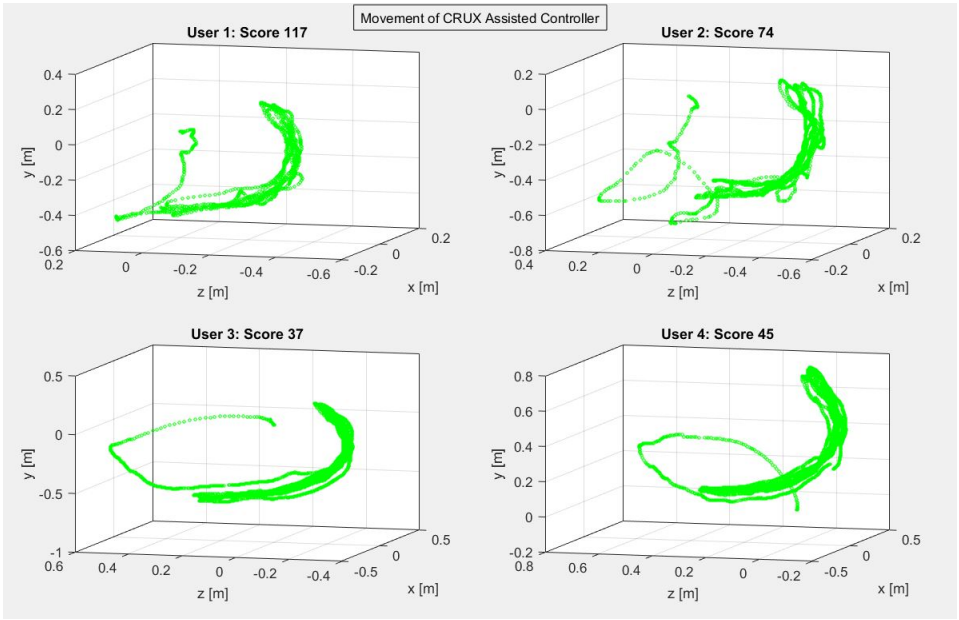

Figure 6.10: Arm position of a user in 3D space as they complete a mini-game requiring biceps curling [96]. Scores indicate the result of that particular round of the game and are not meant to be compared between users.

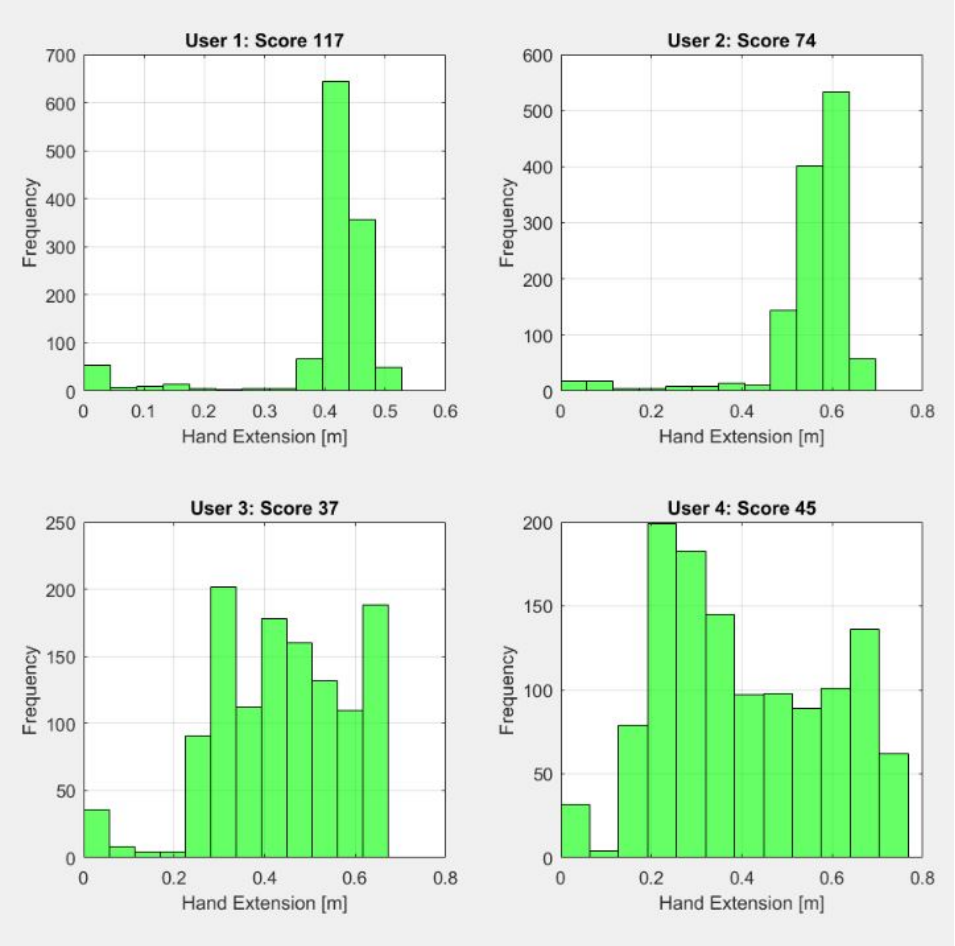

Figure 6.11: User hand extension in meters. Quantitative metrics like physical improvements in capability are hard to measure without computer aided assistance. PBF demonstrates one manner in which this metric can be tracked and recorded for various purposes, including predicting user movement, observing improvement between trials, and incentivizing improvement [96]. Scores indicate the result of that particular round of the game and are not meant to be compared between users.

Handheld Controller Velocity during a VR Exercise

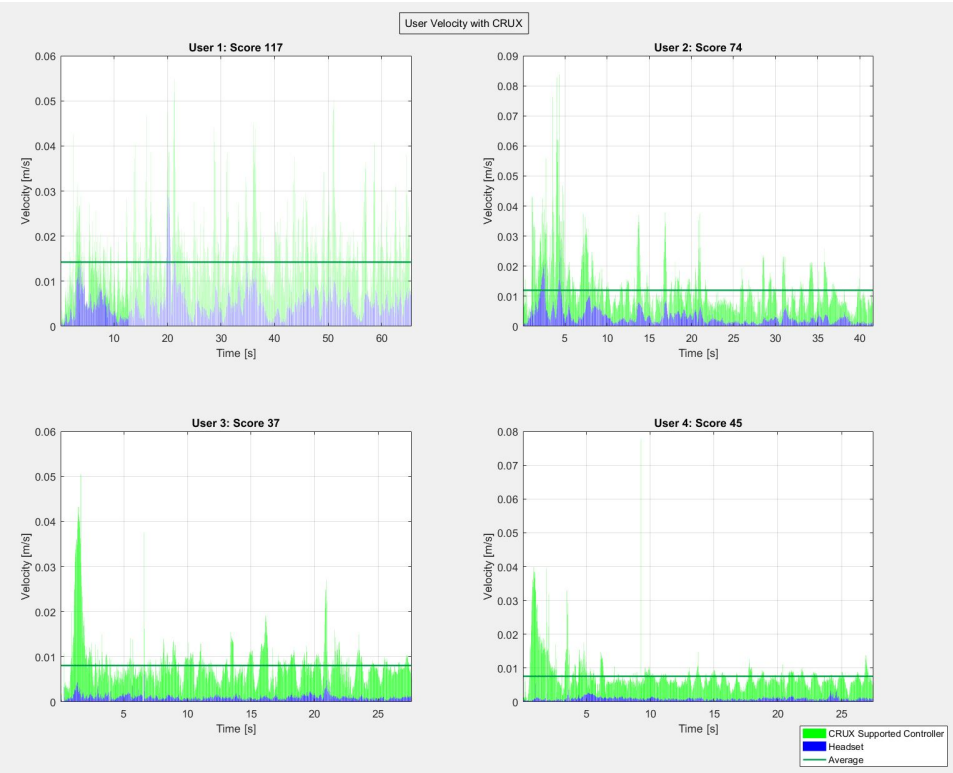

Figure 6.12: Handheld controller velocity in m/s. This metric is indicative of hand velocity and illustrates both capability in meeting the necessary physiological criteria to score well in PBF as well as the user's intention and focus. Both of these purposes influence our understanding of the player/game dynamic and how successful PBF is in exercising users [96].

Headset Rotation during a VR Exercise

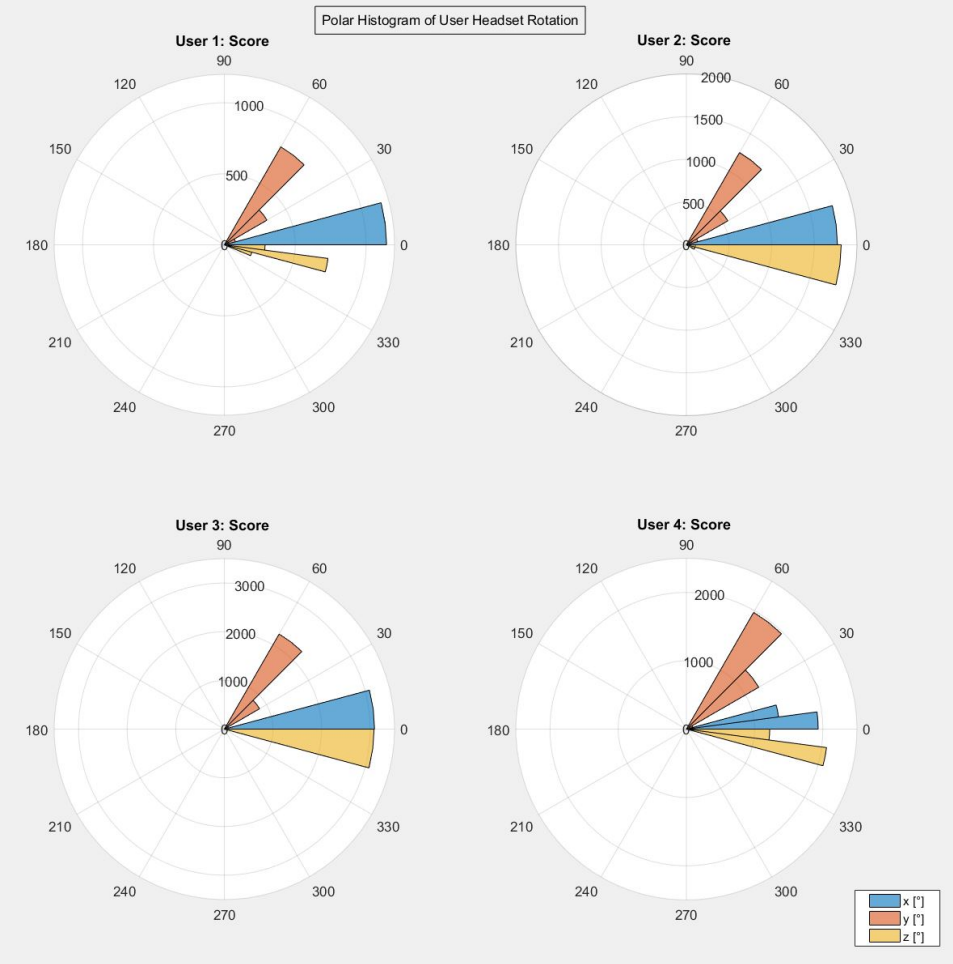

Figure 6.13: A frequency histogram of headset rotation in 3D. The user's head pose indicates what they are looking at in virtual reality. These data are useful for determining which environmental factors they need to watch and focus on in order to complete their task [96]. Ideally, the user focuses mostly on in-game objectives and not their own impairments when playing.

Chapter 7

CONCLUSION

CRUX, the Compliant Robotic Upper-Extremity eXosuit, is a wearable device that affords users upper-extremity augmentation without sacrificing flexibility or structural compliance. The study of bio-inspired tensegrity robotics has illustrated methods that compliant upper-extremity motion can be produced in lightweight structures. By studying individual tensegrity joints and the concatenation of multiple joints in series, we discovered the necessary criteria for using a robot's own morphology to actuate itself. These capabilities have been applied towards the tensegrity-inspired base in CRUX. This created tension network provides a foundation upon which external disturbances and augmentative counter-balances can be applied and distributed safely.

Physical therapy techniques, such as Graded Motor Imagery and mirror therapy, focus on bridging the gap between user capability and user perception. CRUX has demonstrated the ability to do that through four studies.

The first study exemplified a mimetic controller that produces bilaterally-symmetrical movement using a leader arm and a follower arm. Subjects were able to quickly learn, oftentimes within a minute, how to control their follower arm through dictation provided by their leader arm. The most common issues that arose during mimetic control, like over-compensation and acclimation towards the augmentation sensation, were typically resolved by the user within tens of seconds. Being able to rapidly learn how to operate CRUX while still performing movement central to

mirror therapy and Graded Motor Imagery is a critical obstacle in developing a rehabilitative exosuit.

The second study examined user's flexibility in the exosuit compared to no exosuit at all. We found that CRUX minimally impeded users as they performed arm circles and biceps curls. CRUX must minimally interfere with user movements if it is to augment and rehabilitate those movements. If a user did not exercise their full range of motion during physical therapy, rehabilitation outcomes would prove limited. This study illustrates CRUX's capability in remaining a flexible exosuit, even during exercise.

The third study examined user's augmentation as a function of heart rate increase. Heart rate increase has been shown to a relatively accurate indicator of metabolic cost, the necessary energy spent by a person to complete an exercise. CRUX produced an over 9 percentage point improvement for impaired users when it actively augmented their movements than when it did not. Users across multiple demographics, such as impaired and unimpaired, in-lab subjects and at-home subjects, almost universally agreed that the exosuit assisted them successfully with the exercises. Two users in our metabolic studies reported that CRUX neither helped nor hindered them and no user reported that CRUX hindered them. The central goal of all augmentative exosuits and exoskeletons is to reduce the necessary energy to perform an action and CRUX succeeded in this regard.

The fourth major study conducted combined CRUX with Project Butterfly (PBF), a virtual-reality based set of games. These games promoted upper-extremity movement and rehabilitation through in-game incentives and goals. A quantitative and qualitative analysis showed that users were satisfied with their VR experience, despite being initially unfamiliar with both exosuit technology and virtual reality. Lowering the barrier for people with upper-extremity impairment to engage in interactive and novel rehabilitative methods is critical for widespread adoption of this technology among users who would otherwise avoid the unknown and intimidating experience of trying these technologies.

Our development of CRUX, the virtual reality applications, the tensegrity robots,

and all of the other studies and discoveries will hopefully pave the way for more capable soft robots and wearable devices in the future.

Bibliography

[1] Tetsuo Fukunaga, Yasuo Kawakami, Shinya Kuno, Kazuo Funato, and Senshi Fukashiro. Muscle architecture and function in humans. *Journal of biomechanics*, 30(5):457–463, 1997.

[2] RD Herbert and SC Gandevia. Changes in pennation with joint angle and muscle torque: in vivo measurements in human brachialis muscle. *The Journal of Physiology*, 484(2):523–532, 1995.

[3] M Solomonow, AL Guzzi, R Baratta, H Shoji, and R d'Ambrosia. Emg-force model of the elbows antagonistic muscle pair. the effect of joint position, gravity and recruitment. *American journal of physical medicine*, 65(5):223–244, 1986.

[4] J Gordon and C Ghez. Emg patterns in antagonist muscles during isometric contraction in man: relations to response dynamics. *Experimental Brain Research*, 55(1):167–171, 1984.

[5] Yuan-cheng Fung. *Biomechanics: mechanical properties of living tissues.* Springer Science & Business Media, 2013.

[6] Archibald Vivian Hill. The heat of shortening and the dynamic constants of muscle. *Proc. R. Soc. Lond. B*, 126(843):136–195, 1938.

[7] Scott L Delp, Frank C Anderson, Allison S Arnold, Peter Loan, Ayman Habib, Chand T John, Eran Guendelman, and Darryl G Thelen. Opensim: open-source software to create and analyze dynamic simulations of movement. *IEEE transactions on biomedical engineering*, 54(11):1940–1950, 2007.

[8] Ashley M Wessendorf and Dava J Newman. Dynamic understanding of human-skin movement and strain-field analysis. *IEEE Transactions on Biomedical Engineering*, 59(12):3432–3438, 2012.

[9] Arthur S Iberall. The use of lines of nonextension to improve mobility in full-pressure suits. Technical report, DTIC Document, 1964.

[10] Michael Jäntsch, Steffen Wittmeier, Konstantinos Dalamagkidis, Alexander Panos, Fabian Volkart, and Alois Knoll. Anthrob–a printed anthropomimetic robot. In *Proc. IEEE-RAS International Conference on Humanoid Robots (Humanoids)*, 2013.

[11] Yoichiro Nakanishi, Yuji Asano, Toyotaka Kozuki, Hiroshi Mizoguchi, Yotaro Motegi, Masahiko Osada, Tokimasa Shirai, Junichi Urata, Kenichi Okada, and Masayuki Inaba. Design concept of detail musculoskeletal humanoid kenshiro-toward a real human body musculoskeletal simulator. In *Humanoid Robots (Humanoids), 2012 12th IEEE-RAS International Conference on*, pages 1–6. IEEE, 2012.

[12] Veljko Potkonjak, Bratislav Svetozarevic, Kosta Jovanovic, and Owen Holland. Anthropomimetic robot with passive compliance-contact dynamics and control. In *Control & automation (med), 2011 19th mediterranean conference on*, pages 1059–1064. IEEE, 2011.

[13] Nancy S Pollard, Jessica K Hodgins, Marcia J Riley, and Christopher G Atkeson. Adapting human motion for the control of a humanoid robot. In *Robotics and Automation, 2002. Proceedings. ICRA'02. IEEE International Conference on*, volume 2, pages 1390–1397. IEEE, 2002.

[14] Andrea Maria Zanchettin, Paolo Rocco, Luca Bascetta, Ioannis Symeonidis, and Steffen Peldschus. Kinematic analysis and synthesis of the human arm motion during a manipulation task. In *Robotics and Automation (ICRA), 2011 IEEE International Conference on*, pages 2692–2697. IEEE, 2011.

[15] David Lau, Denny Oetomo, and Saman K Halgamuge. Generalized modeling of multilink cable-driven manipulators with arbitrary routing using the cable-routing matrix. *Robotics, IEEE Transactions on*, 29(5):1102–1113, 2013.

[16] Thomas Lens, Jürgen Kunz, and Oskar Von Stryk. Dynamic modeling of the 4 dof biorob series elastic robot arm for simulation and control. In *International Conference on Simulation, Modeling, and Programming for Autonomous Robots*, pages 411–422. Springer, 2010.

[17] Yu-Feng Lee, Cheng-Yu Chu, Jia-You Xu, and Chao-Chieh Lan. A humanoid robotic wrist with two-dimensional series elastic actuation for accurate force/torque interaction. *IEEE/ASME Transactions on Mechatronics*, 21(3): 1315–1325, 2016.

[18] Bertrand Tondu. Modelling of the mckibben artificial muscle: A review. *Journal of Intelligent Material Systems and Structures*, 23(3):225–253, 2012.

[19] Ron Pelrine, Roy D Kornbluh, Qibing Pei, Scott Stanford, Seajin Oh, Joseph Eckerle, Robert J Full, Marcus A Rosenthal, and Kenneth Meijer. Dielectric elastomer artificial muscle actuators: toward biomimetic motion. In *SPIE's 9th Annual International Symposium on Smart Structures and Materials*, pages 126–137. International Society for Optics and Photonics, 2002.

[20] Robert J Anderson and Mark W Spong. Hybrid impedance control of robotic manipulators. *IEEE Journal on Robotics and Automation*, 4(5):549–556, 1988.

[21] Cecilia Laschi, Matteo Cianchetti, Barbara Mazzolai, Laura Margheri, Maurizio Follador, and Paolo Dario. Soft robot arm inspired by the octopus. *Advanced Robotics*, 26(7):709–727, 2012.

[22] Sangok Seok, Cagdas Denizel Onal, Kyu-Jin Cho, Robert J Wood, Daniela Rus, and Sangbae Kim. Meshworm: a peristaltic soft robot with antagonistic nickel titanium coil actuators. *IEEE/ASME Transactions on mechatronics*, 18 (5):1485–1497, 2013.

[23] Sangbae Kim, Cecilia Laschi, and Barry Trimmer. Soft robotics: a bioinspired evolution in robotics. *Trends in biotechnology*, 31(5):287–294, 2013.

[24] Michael Wehner, Ryan L Truby, Daniel J Fitzgerald, Bobak Mosadegh, George M Whitesides, Jennifer A Lewis, and Robert J Wood. An integrated design and fabrication strategy for entirely soft, autonomous robots. *Nature*, 536(7617):451, 2016.

[25] Donald Ruffatto III, Paul Glick, Michael T Tolley, and Aaron Parness. Long duration surface anchoring with a hybrid electrostatic and gecko-inspired adhesive. *IEEE Robotics and Automation Letters*, 2018.

[26] Paul Glick, Srinivasan A Suresh, Donald Ruffatto, Mark Cutkosky, Michael T Tolley, and Aaron Parness. A soft robotic gripper with gecko-inspired adhesive. *IEEE Robotics and Automation Letters*, 3(2):903–910, 2018.

[27] Jun Shintake, Vito Cacucciolo, Herbert Shea, and Dario Floreano. Soft biomimetic fish robot made of dielectric elastomer actuators. *Soft robotics*, 2018.

[28] Tom Flemons. The bones of tensegrity. *http://www.intensiondesigns.com/bones_of_tensegrity*, 2012.

[29] Stephen Levin. The tensegrity-truss as a model for spine mechanics: Biotensegrity. *Journal of Mechanics in Medicine and Biology*, 2:375–388, 2002. doi: 10.1142/S0219519402000472.

[30] Graham Scarr. A consideration of the elbow as a tensegrity structure. *International Journal of Osteopathic Medicine*, 15(2):53–65, 2012.

[31] Stephen Levin, Susan Lowell de Solórzano, and Graham Scarr. The significance of closed kinematic chains to biological movement and dynamic stability. *Journal of bodywork and movement therapies*, 21(3):664–672, 2017.

[32] B Mirletz, In-Won Park, Thomas E Flemons, Adrian K Agogino, Roger D Quinn, and Vytas SunSpiral. Design and control of modular spine-like tensegrity

structures. In *The 6th World Conference of the International Association for Structural Control and Monitoring (6WCSCM)*, 2014.

[33] Jonathan Bruce, A Sabelhaus, Yangxin Chen, Dizhou Lu, Kyle Morse, Sophie Milam, Ken Caluwaerts, A Agogino, and Vytas SunSpiral. SUPERball: Exploring tensegrities for planetary probes. In *12th International Symposium on Artificial Intelligence, Robotics and Automation in Space (i-SAIRAS)*, 2014.

[34] Jeffrey M Friesen, Paul Glick, Michael Fanton, Pavlo Manovi, Alexander Xydes, Thomas Bewley, and Vytas Sunspiral. The second generation prototype of a duct climbing tensegrity robot, ducttv2. In *Robotics and Automation (ICRA), 2016 IEEE International Conference on*, pages 2123–2128. IEEE, 2016.

[35] Dawn Hustig-Schultz, Vytas SunSpiral, and Mircea Teodorescu. Morphological design for controlled tensegrity quadruped locomotion. In *Intelligent Robots and Systems (IROS), 2016 IEEE/RSJ International Conference on*, pages 4714–4719. IEEE, 2016.

[36] Andrew P Sabelhaus, Abishek K Akella, Zeerek A Ahmad, and Vytas SunSpiral. Model-predictive control of a flexible spine robot. In *American Control Conference (ACC), 2017*, pages 5051–5057. IEEE, 2017.

[37] Andrew P Sabelhaus, Huajing Zhao, Edward L Zhu, Adrian K Agogino, and Alice M Agogino. Model-predictive control with reference input tracking for tensegrity spine robots. *arXiv preprint arXiv:1806.08868*, 2018.

[38] Steven Lessard, Jonathan Bruce, Erik Jung, Vytas SunSpiral, Mircea Teodorescu, and Adrian Agogino. A Lightweight, Multi-axis Compliant Tensegrity Joint. In *Proceedings of 2016 IEEE International Conference on Robotics and Automation, (ICRA), May 2016, Stockholm, Sweden*, 2016.

[39] Steven Lessard, Dennis Castro, William Asper, Shaurya Deep Chopra, Leya Breanna Baltaxe-Admony, Mircea Teodorescu, Vytas SunSpiral, and Adrian Agogino. A bio-inspired tensegrity manipulator with multi-dof, struc-

turally compliant joints. In *Intelligent Robots and Systems (IROS), 2016 IEEE/RSJ International Conference on*, pages 5515–5520. IEEE, 2016.

[40] Erik Jung, Victoria Ly, Nicholas Cessna, Lawrence Ngo, Dennis Castro, Vytas SunSpiral, and Mircea Teodorescu. Bio-inspired tensegrity flexural joints. 2018.

[41] Shaurya Chopra, Mircea Teodorescu, Steven Lessard, Vytas SunSpiral, and Adrian Agogino. Tensegrity Heat Shield for Atmospheric Entry through Celestial Bodies. In *Proceedings of ASME 2016 International Design Engineering Technical Conferences & Computers and Information in Engineering Conference (IDETC/CIE), August 21-August 24, 2016, Charlotte, NC, USA.*, 2016.

[42] Kalyanmoy Deb. *Multi-objective optimization using evolutionary algorithms*, volume 16. John Wiley & Sons, 2001.

[43] Richard A Watson, Sevan G Ficici, and Jordan B Pollack. Embodied evolution: Distributing an evolutionary algorithm in a population of robots. *Robotics and Autonomous Systems*, 39(1):1–18, 2002.

[44] Richard S Sutton and Andrew G Barto. *Reinforcement learning: An introduction*, volume 1. MIT press Cambridge, 1998.

[45] Maja J Matarić. Reinforcement learning in the multi-robot domain. In *Robot colonies*, pages 73–83. Springer, 1997.

[46] RARC Gopura, DSV Bandara, Kazuo Kiguchi, and GKI Mann. Developments in hardware systems of active upper-limb exoskeleton robots: A review. *Robotics and Autonomous Systems*, 75:203–220, 2016.

[47] Jacob Rosen and Joel C Perry. Upper limb powered exoskeleton. *International Journal of Humanoid Robotics*, 4(03):529–548, 2007.

[48] Ying Mao and Sunil Kumar Agrawal. Design of a cable-driven arm exoskeleton (carex) for neural rehabilitation. *IEEE Transactions on Robotics*, 28(4):922–931, 2012.

[49] Khurram Nasir. Heart disease and stroke statistics-2015 update: A report from the american heart association. 2014.

[50] John R Marler, BC Tilley, M Lu, Thomas G Brott, PC Lyden, JC Grotta, JP Broderick, SR Levine, MP Frankel, SH Horowitz, et al. Early stroke treatment associated with better outcome the ninds rt-pa stroke study. *Neurology*, 55(11):1649–1655, 2000.

[51] R Jay Turner and Samuel Noh. Physical disability and depression: A longitudinal analysis. *Journal of health and social behavior*, pages 23–37, 1988.

[52] Joke Kokkonen, Arnold G Nelson, Carol Eldredge, and Jason B Winchester. Chronic static stretching improves exercise performance. *Medicine & Science in Sports & Exercise*, 39(10):1825–1831, 2007.

[53] Roy David Kornbluh, Alexander Steele Kernbaum, Thomas Low, Katherine Goss Witherspoon, Brian Keith McCoy, Adam Arnold Edward Ziemba, Paul Michael Birkmeyer, and Richard M Mahoney. Exosuit system, February 23 2016. US Patent 9,266,233.

[54] Saul Griffith, Pete Lynn, Della Shea, Kevin Albert, and Tim Swift. Pneumatic exomuscle system and method, October 15 2015. US Patent 20,150,290,794.

[55] Michael Wehner, Brendan Quinlivan, Patrick M Aubin, Ernesto Martinez-Villalpando, Michael Baumann, Leia Stirling, Kenneth Holt, Robert Wood, and Conor Walsh. A lightweight soft exosuit for gait assistance. In *Robotics and Automation (ICRA), 2013 IEEE International Conference on*, pages 3362–3369. IEEE, 2013.

[56] Darwin G Caldwell, Nikolaos G Tsagarakis, Sophia Kousidou, Nelson Costa, and Ioannis Sarakoglou. "soft" exoskeletons for upper and lower body rehabilitationdesign, control and testing. *International Journal of Humanoid Robotics*, 4(03):549–573, 2007.

[57] Hyunki In, Brian Byunghyun Kang, MinKi Sin, and Kyu-Jin Cho. Exo-glove: a

wearable robot for the hand with a soft tendon routing system. *IEEE Robotics & Automation Magazine*, 22(1):97–105, 2015.

[58] Hong Kai Yap, Jeong Hoon Lim, Fatima Nasrallah, James CH Goh, and Raye CH Yeow. A soft exoskeleton for hand assistive and rehabilitation application using pneumatic actuators with variable stiffness. In *Robotics and Automation (ICRA), 2015 IEEE International Conference on*, pages 4967–4972. IEEE, 2015.

[59] Cole S Simpson, Allison M Okamura, and Elliot W Hawkes. Exomuscle: An inflatable device for shoulder abduction support. In *Robotics and Automation (ICRA), 2017 IEEE International Conference on*, pages 6651–6657. IEEE, 2017.

[60] Steven Lessard, Pattawong Pansodtee, Ash Robbins, Leya Breanna Baltaxe-Admony, James M Trombadore, Mircea Teodorescu, Adrian Agogino, and Sri Kurniawan. Crux: A compliant robotic upper-extremity exosuit for lightweight, portable, multi-joint muscular augmentation. In *Rehabilitation Robotics (ICORR), 2017 International Conference on*, pages 1633–1638. IEEE, 2017.

[61] Ciarán T O'Neill, Nathan S Phipps, Leonardo Cappello, Sabrina Paganoni, and Conor J Walsh. A soft wearable robot for the shoulder: Design, characterization, and preliminary testing. In *Rehabilitation Robotics (ICORR), 2017 International Conference on*, pages 1672–1678. IEEE, 2017.

[62] S Lessard, P Pansodtee, A Robbins, JM Trombadore, S Kurniawan, and M Teodorescu. A soft exosuit for flexible upper-extremity rehabilitation. *IEEE transactions on neural systems and rehabilitation engineering: a publication of the IEEE Engineering in Medicine and Biology Society*, 2018.

[63] Ranathunga Arachchilage Ruwan Chandra Gopura, Kazuo Kiguchi, and Yang Li. Sueful-7: A 7dof upper-limb exoskeleton robot with muscle-model-oriented

emg-based control. In *2009 IEEE/RSJ International Conference on Intelligent Robots and Systems*, pages 1126–1131. IEEE, 2009.

[64] Yong-Lae Park, Carmel Majidi, Rebecca Kramer, Phillipe Bérard, and Robert J Wood. Hyperelastic pressure sensing with a liquid-embedded elastomer. *Journal of Micromechanics and Microengineering*, 20(12):125029, 2010.

[65] Yiğit Mengüç, Yong-Lae Park, Ernesto Martinez-Villalpando, Patrick Aubin, Miriam Zisook, Leia Stirling, Robert J Wood, and Conor J Walsh. Soft wearable motion sensing suit for lower limb biomechanics measurements. In *Robotics and Automation (ICRA), 2013 IEEE International Conference on*, pages 5309–5316. IEEE, 2013.

[66] Sai K Banala, Suni K Agrawal, and John P Scholz. Active leg exoskeleton (alex) for gait rehabilitation of motor-impaired patients. In *2007 IEEE 10th International Conference on Rehabilitation Robotics*, pages 401–407. IEEE, 2007.

[67] Jacob Rosen, Moshe Brand, Moshe B Fuchs, and Mircea Arcan. A myosignal-based powered exoskeleton system. *IEEE Transactions on systems, Man, and Cybernetics-part A: Systems and humans*, 31(3):210–222, 2001.

[68] Conor Walsh, Alan Thomas Asbeck, Ignacio Galiana Bujanda, Ye Ding, Robert Joseph Dyer, Arnar Freyr Larusson, Brendan Thomas Quinlivan, Kai Schmidt, Diana Wagner, Michael Wehner, et al. Soft exosuit for assistance with human motion, May 31 2016. US Patent 9,351,900.

[69] Centers for Disease Control, Prevention (CDC, and others). Prevalence of stroke–united states, 2006-2010. *MMWR. Morbidity and mortality weekly report*, 61(20):379, 2012.

[70] Valery L Feigin, Bo Norrving, and George A Mensah. Global burden of stroke. *Circulation research*, 120(3):439–448, 2017.

[71] G Lorimer Moseley. Graded motor imagery for pathologic pain: a randomized controlled trial. *Neurology*, 67(12):2129–2134, 2006.

[72] Victoria W Priganc and Susan W Stralka. Graded motor imagery. *Journal of Hand Therapy*, 24(2):164–169, 2011.

[73] K Jane Bowering, Neil E O'Connell, Abby Tabor, Mark J Catley, Hayley B Leake, G Lorimer Moseley, and Tasha R Stanton. The effects of graded motor imagery and its components on chronic pain: a systematic review and meta-analysis. *The Journal of Pain*, 14(1):3–13, 2013.

[74] Edmund Frank Lopresti, Alex Mihailidis, and Ned Kirsch. Assistive technology for cognitive rehabilitation: State of the art. *Neuropsychological rehabilitation*, 14(1-2):5–39, 2004.

[75] Mitchell P LaPlante et al. Assistive technology devices and home accessibility features: prevalence, payment, need, and trends. *Advance data from vital and health statistics*, 1992.

[76] BulletPhysicsEngine. http://www.bulletphysics.org/, 2013.

[77] Brian T Mirletz, Roger D Quinn, and Vytas SunSpiral. Cpgs for adaptive control of spine-like tensegrity structures.

[78] Steven Lessard, Jonathan Bruce, Adrian Agogino, Vytas SunSpiral, and Mircea Teodorescu. Robust Monte Carlo Control Policies to Maneuver Tensegrity Robots out of Obstacles. In *Proceedings of Autonomous Robots and Multirobot Systems (ARMS), May 2015, Istanbul, Turkey*, 2015.

[79] Glenn K Klute, Carol F Kallfelz, and Joseph M Czerniecki. Mechanical properties of prosthetic limbs: Adapting to the patient. *Journal of Rehabilitation Research & Development*, 38(3), 2001.

[80] H Henrik Ehrsson, Birgitta Rosén, Anita Stockselius, Christina Ragnö, Peter Köhler, and Göran Lundborg. Upper limb amputees can be induced to experience a rubber hand as their own. *Brain*, 131(12):3443–3452, 2008.

[81] Jeffrey Friesen, Alexandra Pogue, Thomas Bewley, Mauricio de Oliveira, Robert Skelton, and Vytas SunSpiral. DuCTT: A tensegrity robot for exploring duct

systems. In *ICRA*, pages 4222–4228, May 2014. doi: 10.1109/ICRA.2014.6907473.

[82] Leya Breanna Baltaxe-Admony, Ash Robbins, Erik Jung, Steven Lessard, Mircea Teodorescu, Vytas SunSpiral, and Adrian Agogino. Simulating the Human Shoulder through Active Tensegrity Structures. In *Proceedings of ASME 2016 International Design Engineering Technical Conferences & Computers and Information in Engineering Conference (IDETC/CIE), August 21-August 24, 2016, Charlotte, NC, USA.*, 2016.

[83] O. Orki. *A Model Of Caterpillar Locomotion Based On Assur Tensegrity Structures*. PhD thesis, Tel Aviv University, 2012.

[84] Brian R Tietz, Ross W Carnahan, Richard J Bachmann, Roger D Quinn, and Vytas SunSpiral. Tetraspine: Robust terrain handling on a tensegrity robot using central pattern generators. In *AIM*, pages 261–267, 2013. doi: 10.1109/AIM.2013.6584102.

[85] Jeffrey Friesen, Alexandra Pogue, Thomas Bewley, Mauricio de Oliveira, Robert Skelton, and Vytas Sunspiral. Ductt: a tensegrity robot for exploring duct systems. In *Robotics and Automation (ICRA), 2014 IEEE International Conference on*, pages 4222–4228. IEEE, 2014.

[86] Katherine R Saul, Xiao Hu, Craig M Goehler, Meghan E Vidt, Melissa Daly, Anca Velisar, and Wendy M Murray. Benchmarking of dynamic simulation predictions in two software platforms using an upper limb musculoskeletal model. *Computer methods in biomechanics and biomedical engineering*, 18(13):1445–1458, 2015.

[87] Dava Newman, Jeff Hoffman, Kristen Bethke, Joaquin Blaya, Christopher Carr, and Bradley Pitts. Astronaut bio-suit system for exploration class missions. *NIAC Phase II Final Report*, 2005.

[88] Michio Ikai and Tetsuo Fukunaga. Calculation of muscle strength per unit cross-sectional area of human muscle by means of ultrasonic measurement. *In-*

ternationale Zeitschrift für Angewandte Physiologie Einschliesslich Arbeitsphysiologie, 26(1):26–32, 1968.

[89] Richard W Bohannon and A Williams Andrews. Relationships between impairments in strength of limb muscle actions following stroke. *Perceptual and motor skills*, 87(3_suppl):1327–1330, 1998.

[90] Richard W Bohannon. Motricity index scores are valid indicators of paretic upper extremity strength following stroke. *Journal of Physical Therapy Science*, 11(2):59–61, 2001.

[91] Wei Ren, Randal W Beard, and Ella M Atkins. A survey of consensus problems in multi-agent coordination. In *American Control Conference, 2005. Proceedings of the 2005*, pages 1859–1864. IEEE, 2005.

[92] A Rodriguez-Angeles and H Nijmeijer. Cooperative synchronization of robots via estimated state feedback. In *Decision and Control, 2003. Proceedings. 42nd IEEE Conference on*, volume 2, pages 1514–1519. IEEE, 2003.

[93] Daniëlle Ezendam, Raoul M Bongers, and Michiel JA Jannink. Systematic review of the effectiveness of mirror therapy in upper extremity function. *Disability and rehabilitation*, 31(26):2135–2149, 2009.

[94] Kieran P Dowd, Robert Szeklicki, Marco Alessandro Minetto, Marie H Murphy, Angela Polito, Ezio Ghigo, Hidde van der Ploeg, Ulf Ekelund, Janusz Maciaszek, Rafal Stemplewski, et al. A systematic literature review of reviews on techniques for physical activity measurement in adults: a dedipac study. *International Journal of Behavioral Nutrition and Physical Activity*, 15(1):15, 2018.

[95] Hagit Cohen, Jonathan Benjamin, Amir B Geva, Mike A Matar, Zeev Kaplan, and Moshe Kotler. Autonomic dysregulation in panic disorder and in post-traumatic stress disorder: application of power spectrum analysis of heart rate variability at rest and in response to recollection of trauma or panic attacks. *Psychiatry research*, 96(1):1–13, 2000.

[96] Aviv Elor, Steven Lessard, John McIntyre, Pattawong Pansodtee, Ocean hurd, Mircea Teodorescu, and Sri Kurniawan. Combining a soft exosuit and virtual reality for upper-extremity physical therapy. In *review.*, 2018.

[97] Nataliya Shkuratova, Meg E Morris, and Frances Huxham. Effects of age on balance control during walking. *Archives of physical medicine and rehabilitation*, 85(4):582–588, 2004.